CORRELATION BETWEEN THE VOLUMES OF SLURRY AND THE VOLUME OF FRACTURE IN BARNETT SHALE

…………………………………………………...

A Thesis

Presented to

the Faculty of the Department of Earth and Atmospheric Sciences

University of Houston

…………………………………………………

In Partial Fulfillment

of the Requirements for the Degree

Master of Science

…………………………………………………

By

Olawale John Adejuyigbe

August 2013

CORRELATION BETWEEN THE VOLUMES OF SLURRY AND THE VOLUME OF FRACTURE IN BARNETT SHALE

____

Olawale Adejuyigbe

APPROVED BY:

____

Dr. Evgeni M. Chesnokov, Professor
(Committee Chair)
Department of Earth and Atmospheric Sciences
University of Houston

____

Dr. Gennady M. Goloshubin, Professor
Department of Earth and Atmospheric Sciences
University of Houston

____

Renato Leite, Ph.D.
Senior Petrophysicist II
Petrobras America, Inc.

____

Dean
College of Natural Sciences and Mathematics

Dedication

This work is dedicated to my mother, the late Bosede Adejuyigbe who stood by me and offered invaluable moral and financial support all through my life.

Acknowledgements

I sincerely acknowledge and thank my project supervisor, Dr. Evgeny Chesnokov, who allowed me to pursue this research, for his immeasurable input and guidance which helped in the completion of this work. The lessons learned from him will be an invaluable asset in my career. It would have been impossible to complete this work without his helpful supervision.

My appreciation also goes to the other members of my thesis committee, Dr. Gennady Goloshubin and Dr.Renato Leite, for reading through this work. Dr. Yasser Mohammed helped me understand the microseismic activities of the study area and I also remain eternally grateful for his assistance.

The following friends have also contributed in different ways towards the successful completion of this thesis: Arnold Oyem, Abdul Moshudi, Michael Macdonalds, and Aloisio Pellon. I say a big thank you to you all. Finally, I will want to thank my father and my sister Bola for their endless support.

CORRELATION BETWEEN THE VOLUMES OF SLURRY AND THE VOLUME OF FRACTURE IN BARNETT SHALE

…………………………………………………………...

An Abstract of a Thesis

Presented to

the Faculty of the Department of Earth and Atmospheric Sciences

University of Houston

…………………………………………………………

In Partial Fulfillment

of the Requirements for the Degree

Master of Science

…………………………………………………………

By

Olawale Adejuyigbe

August 2013

Abstract

Microseismic fracture mapping has revealed that large fracture networks can be generated in many shale reservoirs and create multiple of plan complex structure. The ultra-low permeability in Barnett shale requires hydraulic fracturing to generate wellbore contact with the reservoir in order to achieve economic gas rates by the concept of a single fracture half-length. This is the reason for using fracture half-length of the hydraulic fracture area dimensions through the total fracture network length to estimate the volume of hydraulic fracture from a Dollie Thorell IV well in Barnett Shale. All data were released by Devon Energy for the purpose of this study.

As a way to better evaluate the effective producing network of the shale reservoir, Surfer VI and discrete bin method were used to estimate of the volume of hydraulic fracture. The results of the analyses from Surfer VI were from (i) Trapezoidal rule; and (ii) Simpson's rules, which gave an average result of 6.7×10^{10} cubic ft, the discrete bin method was calculated from the equation of fracture network half-length where length ($2x_f$) and width (x_n) represented the fracture spacing in the shale reservoir. The discrete bin method analysis gave a total result of 6.7×10^{10} cubic ft; this is the estimated figure for the volume of hydraulic fracture in very tight reservoirs. The correlation between the volume of slurry and the volume of the hydraulic fracture will establish the crack density. The graphic result of the correlation between the volume of slurry and the estimated volume of fracture showed that the crack density increases when the volume of the fracture increases. The crack density is always less than 1 due to leak-off of fracturing fluid into the reservoir during the hydraulic fracturing treatment.

Table of Contents

CHAPTER 1: INTRODUCTION

Studies of the volume of hydraulic fractures provide information about the untreated reservoir sections that can be targeted on subsequent treatments, as well as see whether a fracture intersects an aquifer or other geo-hazard. The volume of hydraulic fractures keeps the fracture propped open throughout the created fracture area and provides sufficient conductivity contrast to accelerate flow to the wellbore through the permeable pathway. This study focuses on the best method to calculate the volume of hydraulic fractures by comparing the volume of the slurry to the volume of the fracture. The micro-seismic location data and fracture treatment data from Dollie Thorell well in the Barnett Shale were integrated to calculate the volume of hydraulic fracture.

The Barnett Shale is among the most important onshore natural gas fields in North America and also the biggest in Texas. Billions of cubic feet of natural gas are produced from a great number of wells each year. The advancement in techniques for gas recovery and substantial gas value has caused recovery activity to increase dramatically within the last decades. The Barnett Shale is an ultra-low permeability reservoir that should be comfortably fracture-stimulated in an effort to achieve commercial production. Major fracture network operations are required for virtually any ultra-low permeability shale reservoirs with the purpose of improving the well performance. Microseismic fracture mapping is the main process that normally monitors the development of the fracture network.

1.1 Geologic Setting

The Barnett Shale of the Fort Worth Basin is classified as a homogenous undifferentiated black shale. Marine shale serves as the source for many different conventional clastic and carbonate reservoirs, which include the Pennsylvanian Bend and Strawn groups of the Fort Worth Basin (Pollastro et al. 2007). The Barnett Shale is now assumed to be a completely self-contained petroleum system, in which it serves as the source, seal and reservoir rock (Jarvie 2005). The Barnett Shale is known as one of the most prolific shale gas plays with unconventional resources. It produced more than 2.6 TCF (trillion cubic feet) of gas in 1987 (Durham 2007). Research on wireline logs as well as cores focuses on the sedimentology, internal geometry, and cyclical depositional patterns in the Fort Worth Basin (Figure 1.1) (Frantz and Jochen 2005). The Fort Worth basin is a north-south elongated Basin in north-central Texas, encompassing roughly 15,000 square miles (24,100 sq km). It is one of seven late Paleozoic basins associated with the Ouachita fold and overthrust belt (Meckel, et al. 1992). The basin is bordered on the north by the Red River Arch and on the south by the Llano Uplift and toward northeast by the Muenster Arch see (Figure 1.2). The complete history of the Fort Worth Basin reflects the Wilson cycle of the opening and subsequent closing of an ocean basin (Walper, 1982). The continental breakup of the North American part of Laurentia in the early Paleozoic gave

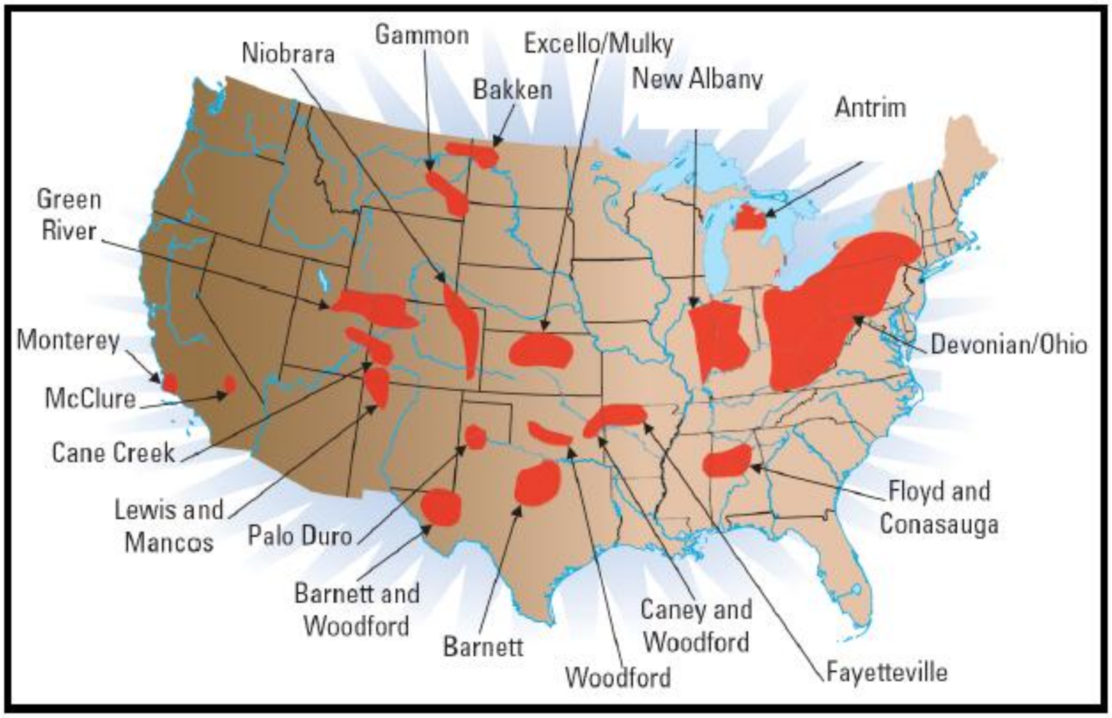

Figure 1.1 Major gas shale basins in the United States (After Frantz and Jochen, 2005)

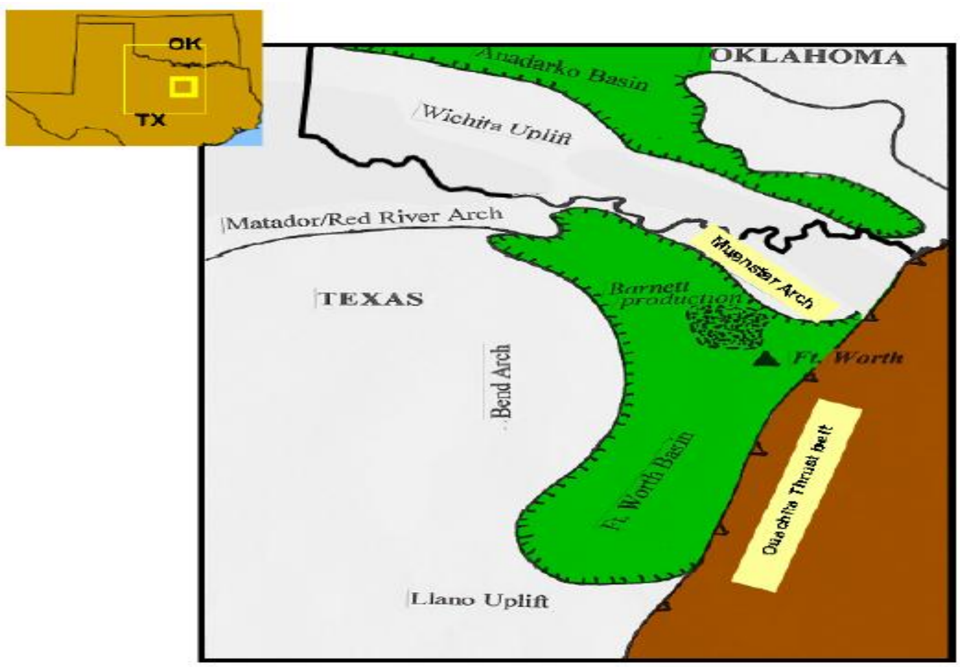

Figure 1.2 Regional setting of Fort Worth Basin modified (after Bawker, 2008)

rise to several aulacogens in nearby areas (Walper, 1977). As the margin of southern North America subsided and retreated from a spreading ridge, the Paleozoic sea, the Iapetus Ocean advanced. This invasion of the warm tropical sea is marked by widespread carbonate shelf deposition such as the Ellenburger Group of rocks. By Early Ordovician time the Iapetus Oceanic lithosphere began to subduct beneath the eastern margin of North America to form a marginal ocean basin between them (Walper, 1982).

In the Middle Paleozic, there was a period of tectonic activity that resulted in erosion in the Fort Worth basin area marking the onset of the closure of the marginal ocean basin and reversal of the subduction polarity. With the onset of closure of the continents to form Pangaea, the formation of the Ouachita fold belt began, which represents the suture zone of the collision of the North America and the Afro-South American plates. The Ouachita foldthrust belt grew and evolved as the subduction complex - composed of the Ouachita facies strata which were deposited in the marginal ocean basin - was scraped from the subducting oceanic crust (Walper, 1982).

The subduction complex continued to be underthrust by the North American plate which made the outer arch migrate westward to make the hinge line to continue to retreat in the cratonic interior. A widespread marine transgression resulted in the formation of younger strandlines towards the craton suggesting that dormant aulacogens (zones of structural weakness) were reactivated by the subsequent collision of the North and South American plates, to eventually subside and become inundated by the sea (Hoffman, et al. 1974). By late Paleozoic time, the Fort Worth foreland basin formed in front of the advancing Ouachita structural belt. The basin was submerged and the Barnett

Shale and Comyn Limestone formations were deposited over the area of the Fort Worth basin (Walper, 1982). (Figure 1.3).

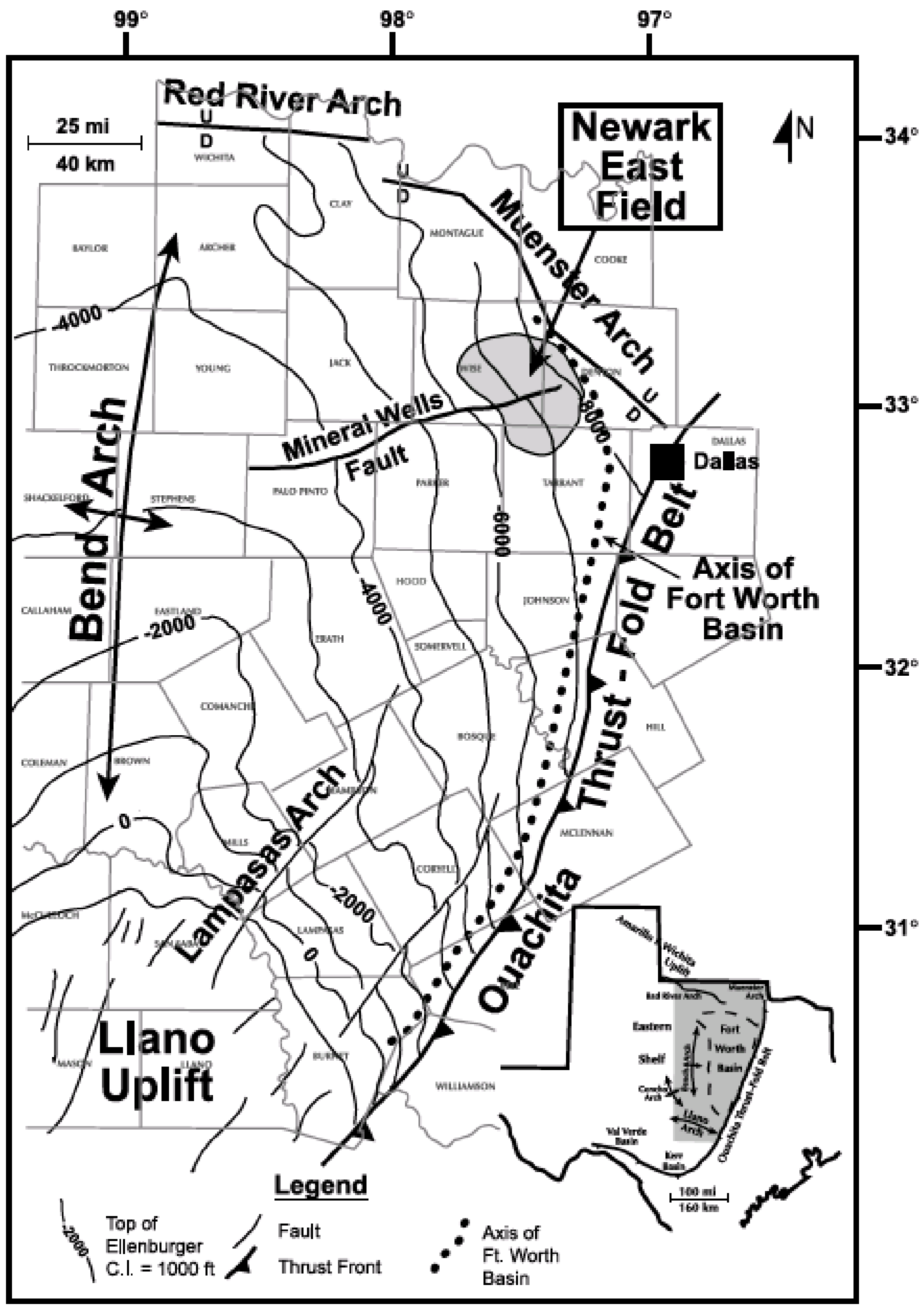

Figure 1.3 Regional setting and structure contour map of the Fort Worth basin, north-central Texas (Scott et al. 2005)

1.2 Scope of Work and Objectives

The aim of this thesis is to estimate the volume of hydraulic fractures by using micro-seismic events. The volume of hydraulic fractures is expressed in terms of the number, size and orientation of micro-seimic events. Knowing the volume of hydraulic fractures is good for correlation parameters for well performance. However, an important fracture is not the only parameter that drives well performance. There are other parameters such as fracture spacing for a given conductivity which can affect production acceleration and ultimate recovery (Fisher, et al. 2002). The largest fracture networks in the Barnett Shale show initial relationships between treatment size, network size, shape, and production response (Fisher, Maxwell and Urbancic, 2002).

Our results from micro-seismic fracture mapping show that network size is related to stimulation treatment volume. Figure 1.4 shows the large network which implies

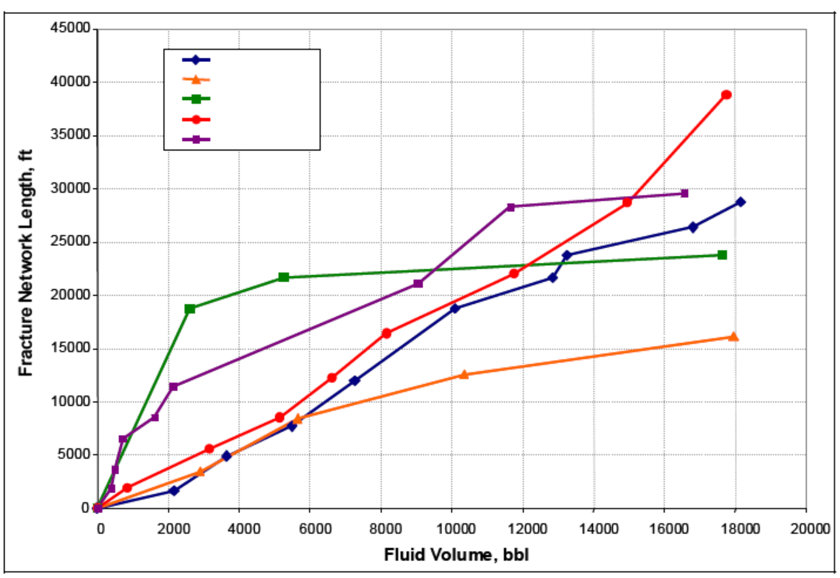

Figure 1.4 Relationship of total fracture network length as a function of total job fluid volume pumped (from Mayerhofer and Warpinski, 2008).

multiple fractures prompts the relationship between treatment volume and fracture network size. Millions of dollars are spent for fracture stimulation, but it has been difficult to evaluate and design stimulation treatment.

1.3 Previous Work

This study is part of an ongoing work aimed at better understanding the volume of hydraulic fractures as a correlation parameter for well performance. The size of the created fracture network, as indicated by the volume of hydraulic fractures, can be approximated as the 3-D volume of the micro-seismic event cloud. The estimation from micro-seismic mapping data is related to total injected fluid volume and well performance. A fluid mixed with chemicals called a "pad" is pumped to initiate the fracture and to establish propagation. This is followed by a slurry of fluid mixed with a propping agent which continues to extend the fracture and carry the proppant deeply into the fractures. After the materials are pumped, the fluid chemically "breaks back" to a lower viscosity and flows back out of the well, leaving a highly conductive propped fracture for oil and/or gas to flow easily from the extremities of the formation into the well (Gidley et al., 1989).

CHAPTER 2: HYDRAULIC FRACTURING AND MICROSEISMIC PRINCIPLES

2.1 History and Development of Hydraulic Fracturing

The first research to increase the production of commercial gas was performed in the Hugoton Gas Area in 1947 on Kelpper Well 1. As a fracturing fluid, a gasoline-based napalm-gel was used. However, these unpropped treatments did not increase production, leading to the belief that hydraulic fracturing did not represent any improvement in well performance (Gidley, et al., 1989). In 1949, 11 out of 23 wells where hydraulic fracturing treatments had been applied a reported a significant increase in productivity in fields located in Wyoming, Colorado, Oklahoma and Texas (Clark, 1949). In 1952, the use of refined and crude oils as fracturing fluids gained popularity. Due to the lower cost, greater volumes per job were achieved. Nevertheless, a gradual change began in 1953 when aqueous-base fluids began being used, and by the end of 1963 up to 60 per cent of the fracturing jobs used this type of fluid (Hassebroek and Waters, 1964). The regular cost for a hydraulic fracturing treatment method ranged from $2500 to $3500 per well. Wells that had been hydraulically fractured proved to be more productive in comparison with those in which acid treatments had been used. (Patterson 1957)

In 1957, mathematical connections between overall fracturing performance, injection rate, and pumping time, as well as fracture size, were designed to predict fracture length. This provided the reason why some fluids were more effective and even why some pumping rates produced more effective end results. From this period on, fracturing treatments transformed from an experiential basis to technically- based perspective (Hassenbroek and Waters, 1964). In the 1970's high tech massive hydraulic fracturing (MHF) treatments making use of great volumes of water started to be used. During these treatments as much as 1 million gallons of water and 3 million pounds of proppant were utilized. At that time, MHF was the main technique to economically improve tight reservoirs (Veatch, 1983). The earliest commercial vertical Barnett Shale well was the C .W. Slay No .1 drilled and stimulated in 1981 by Mitchell Energy. The initial fracturing productivity consisted of titanium, and zirconium-based crosslinkers with hydroxypropyl guar (HPG) and carboxymethyl hydroxypropyl guar (CMHPG). Treatments varied greatly: from 650-750 gallons of fracturing fluid to one million gallons and nearly about three million pounds of propping agent, at that time 25-30% of the whole U .S. oil reserves had been economically produced using this method (Veatch, 1983).

Hydraulic fracturing was preferred as a technique to optimize productivity in low-permeability reservoirs as well as to overcome damage in moderate- and high-permeability reservoirs. Hydraulic fracturing furnishes increased control of fines in unconsolidated formations; pressure decreases because of production is distributed over the surface area of the created surface, as opposed to the surface texture of the wellbore or gravel pack radius. This circulation of pressure generates a reduction in flow rate per unit area, which decreases flow velocity. A reducing of flow velocity will reduce formation fines movement (Parker, et al. 1994). In 1995, Union Pacific Resources (UPR) carried out the first "waterfrac" in the Cotton Valley Formation. A waterfrac is implemented by pumping large volumes of water with minimal amount of chemicals such as surfactants and friction reducers. Normally 20/40 Ottawa sand is blended at 0.5 ppg. Early results showed a very similar production compared to that generated by former fracturing techniques but with 30-70% less fracturing costs. In 1997, using this technique represented about $4.5 million in savings (Walker et al., 1998). After the effective usage of waterfracs in the Cotton Valley Formation, Mitchel Energy commenced experimenting in 1997 with waterfracs in the Barnett Shale. It was thoughht that similar accomplishments would be obtained with this particular treatment, and therefore different types of the treatment were implemented until a working design was reached. A current average fracturing job in the Barnett Shale only requires 750,000 gallons of slick water and 80,000 pounds of proppant pumped at 60 bpm with proppant concentrations from 0 .1 to 0.5 ppg (Fisher, et al. 2002).

2.2 Microseosmicity

Microseismic theory is analogous to that used in earthquakes; when fluid is injected into the formation causing changes in pore pressure, those changes affect the stability of planes of weakness, such as natural fractures and bedding planes. Shear slippages are produced in planes of weakness leading to failure and these are known as microseismic events. Microseismic activity in field applications has moment magnitudes which are measured based of the strength of the source from 3.5Ms to 2.5Ms. An earthquake usually needs to have a moment magnitude of starting time (t_3) to be felt at the surface (Warpinski, 2009). The receivers that record these events are an array of sensors located either on the surface or down-hole in an observation cell (Warpinski, 1998).

Analysis is performed to locate the source of each microseism and map the geometry and orientation of hydraulic fractures. There are two approaches to analyze the recorded data. The first approach uses the arrival time of P, and S-waves and formation velocities at different receivers located at different observation wells. The location of the microseismic event is then triangulated until the calculated location matches the observed arrival times. The second method involves the use of a single observation well with a multilevel array of receivers. Since more information is required, this technique requires higher-level technology receivers. The arrival times from the P- and S- waves, and the particle motion of the P-wave are required to estimate the azimuth of the microseismic event with respect to the position of the receiver (Warpinski, 1998).

2.2.1 Microseismicity Development

Microseismicity study has its origins in the 1930's when L. Obert and W.I. Duval discovered that a stressed rock pillar emitted microlevel sounds at a deep hard rock's mine (Obert, 1975). Since then several researchers have performed laboratory and field experiments to develop this technique; Obert and Duvall (1942, 1945-a, 1945-b) performed several experiments both in the lab and in the field, where they showed that different types of rock under compressive load generate acoustic emissions. Acoustic emission (AE) rate increased as the load was increased. The results of laboratory experiments on metals known as the Kaiser effect, noticed the effect of sample stress history on the production of acoustic emissions (Tam and Weng, 1995). Goodman (1963) also observed the relationship of stress state and AE rate during cyclic loading experiments that were performed on sandstone and quartz diorite samples. Other researchers performed experiments under uniaxial and triaxial compressive stresses and found that the acoustic emission rate increased significantly as the compressive failure stress was reached (Barron, 1969, 1970; Mogi, 1962; Suzuki, et al. 1964; Mae and Nakao, 1968; Scholz,1968a, 1968b).

During the 1970's, AE studies were underway in several geo-technical areas. Barron (1970) used a device to detect microseismic activity in specimens under triaxial load conditions. Haimson and Kim (1977) and Khair (1977) performed cycling uniaxial and triaxial compressive experiments in which AE were used to study fatigue mechanisms. Byerlee and Lockner (1977b) carried out hydraulic fracturing experiments in which AE was used to map the fractures; Lockner and Byerlee (1977a) also used AE to map fractures created during deformation of rocks under confining stress. During the 1980's and 1990's several researchers performed many laboratory experiments in which different materials were hydraulically fractured and AE was used to map the created fractures and study the fracture mechanisms (Majer and Doe,1986; Matsunaga, et al.1993; Van Dam, et al.1998; Groenenboom, et al. 1999; Kranz, et al.1990) Microseismic data have also been used more recently to estimate formation permeability, as reported by Shapiro, et al. (2006), Dinske, et al. (2010), and Grechka, et al. (2010).

2.2.2 Microseismicity Tools

Transducers used in microseismic applications are devices consisting of a coil around a mass hanging on a spring surrounding fixed magnets (Figure 2.1). Whenever the case (housing) moves, the coil moves with regards to the permanent magnet. The relative velocity is converted into an electromagnetic field. This magnetic field generates power voltages that can be measured. Three-component receivers, where each axis is perpendicular to the opposite two, are used to record the polarization details from the P- and S-waves. Before actual recording can be attained, calibration of the receivers is performed with the intention of identifying the orientation and polarity response of the transducers; calibration is carried out by generating a source at a known location: this is known as a perforation shot. Generally, two of the axes are placed in sideways positions while the third is aligned in a vertical direction. Orientation of the receiver is achieved by using the location of the “artificial” source and the signals recorded by the two horizontal channels and the corresponding hodogram, which is a plot of the polarization of the signal (Sleefe, et al., 1995).

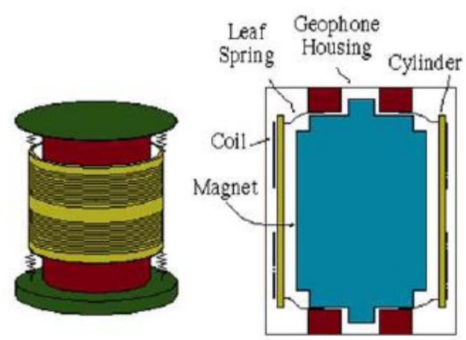

Figure 2.1 Schematics of Transducers (Barzilai, et al. 1998)

In microseismic applications, accelerometers are more suitable than geophones because of the many limitations of geophones. Geophones provide unsubstantial coupling to the borehole over an entire frequency band. Geophones are paired to the borehole via a locking arm that runs and clamps the unit to the borehole. The conventional swing-arm clamp typically includes a resonance around 200-400 Hz (Warpinski, et al., 1998); this implies that at those frequencies the motions of the clamping unit usually do not go along with the motions of the borehole wall structure, causing a weakened coupling. Also, geophones present spurious modes at frequencies about 25 times higher than the natural frequency of the geophone. This is caused when the spring reaches a resonant frequency in the direction perpendicular to the axis of the geophone (Faber and Maxwell, 1996). Accelerometers, however, are built to have resonances above 2000 Hz, and they never contain spurious resonances.

Accelerometers are usually responsive, in comparison with geophones, at higher seismic frequencies because of their smaller electric noise (Sleefe, et al., 1995). Another essential criterion in selecting the best tool is the noise options; the signal-to-noise ratio (SNR) should be as large as possible in an effort to pick up weaker signals. When the intensity of the event cannot be enhanced, the noise should be decreased to attain a satisfactory SNR. According to Warpinski, et al. (1998), there are basically two forms of noise: cultural and electrical. Cultural noise includes that which forms as a result of gas bubbling via perforations from a region below the receivers, as well as truck and pumping activity. It is difficult to decrease this noise, although restorative action may be carried out to mitigate it. Electrical noise, on the other hand, is due to the transducers, electronic components, noise in the power supply, and pickup over unshielded components and wires (Warpinski, et al., 1998). The electrical-noise floor of the accelerometers is more advanced than geophones at frequencies challenged in microseismic services. This implies electrical noise of accelerometers is substantially lower than that of the geophones at high frequencies (above 1000 Hz), allowing accelerometers to detect weak signals even at those frequencies (Sleefe, et al., 1995).

2.2.3 Microseismic Event Location

Microseismic events produce acoustic waves that travel throughout the earth. The location of a microseismic event is referred to as an inverse problem where the data are the arrival times recorded by different sensors, and the unknowns are the spatial coordinates (x, y, z) and the origin time of the microseismic event (Stein and Wyssesion, 2003).

To describe how the inverse problem technique is used, let us imagine a MS event with unknown position x= (x, y, z) and unknown origin time $t_{o;}$ the arrival time varies between the travel time and the origin time:

$$d_i = t_0 + t_i \text{.} \qquad \text{Eq. 2.1}$$

t_i = the travel time, and this can be expressed as functions of spatial coordinate the sensor and the source:

$$t_1 = \sqrt{\frac{(x_i - x)^2 + (y_i - y)^2 (z_i - z)^2}{v}} \quad , \qquad \text{Eq. 2.2}$$

where v is the velocity. The arrival time can be written in the simplest case of constant velocity as

$$d_i = t_o + \sqrt{\frac{(x_i - x)^2 + (y_i - y)^2 (z_i - z)^2}{v}} \, , \qquad \text{Eq.2.3}$$

This issue can be stated as data vector d which is from the function, A, acting on a vector m which represents the model factors, or unknowns

$$d = A(m)\text{.} \qquad \text{Eq. 2.4}$$

Simply, the inverse problem can be seen as given observed arrival times, and a model must be constructed to suit the observation. The procedure begins with a preliminary guess of the model (spatial coordinates and origin time). The initial guess will allow determining information, or appearance times, which we evaluate with the real noticed data, *m*. Usually the starting model generated wrong results; therefore, changes in the beginning style are necessary to arrive at a better remedy.

$$m_j^1 = m_j^o + \Delta m_j\text{.} \qquad \text{Eq.2.5}$$

Here Δm_j is the difference of the *j*th model parameter modification which makes a better fit of the recorded data. The information does not rely linearly on the model parameters; therefore, a linearization of the issue is necessary. This is acquired by expanding the data in a Taylor series about the starting model m^o and maintaining only the linear term.

$$\Delta d_i^o \approx d_i^o + \Sigma_j \frac{\partial d_1}{\partial m_j} \Delta m_j\text{.} \qquad \text{Eq. 2.6}$$

Therefore, the vector d_i^o contains arrival time calculations by using the initial guess of the model. Equation 2.6 is expressed in terms of the difference between the noticed data (arrival times) and those expected by the model.

$$\Delta d_i^o \approx \Sigma_j \frac{\partial d_1}{\partial m_j} \Delta m_j\text{.} \qquad \text{Eq.2.7}$$

The term $\frac{\partial d_1}{\partial m_j}$ is determined as the partial mixture matrix, *Gij*; therefore, the change between the observed and calculated arrive time at a given model can be

$$\Delta d_i^o \approx \Sigma_j G_{ij} \Delta m_j. \qquad \text{Eq. 2.8}$$

The model vector has four unknowns: source time to the three spatial coordinates; therefore, *j* varies from 1 to 4. However, i varies from 1 to *n*, where *n* is the variety of number of arrival time record by *n* sensors, which is usually greater than 4. Since the variety of lines and the variety of content in *G* are not equivalent, the matrix is not square, so it cannot be inverted. To resolve this issue equation, 2.8 has to be multiplied by *GT*, or the transposed of the partially derivative matrix, leading to

$$G^T \Delta d = G^T G \Delta m, \qquad \text{Eq. 2.9}$$

and

$$\Delta m = (G^T G)^{-1} G^T \Delta d. \qquad \text{Eq. 2.10}$$

This is the least square solution to modify in the model so the spatial coordinate and the origin time approach the observed data. We begin with an initial model m^0, which is made up by an initial guess of the spatial coordinate and the source time. The recently expected arrival times are calculated and compared to the observed ones. The complete squared misfit is then measured as,

$$\sum (\Delta d_i^o)^2 = \sum (d_i - d_i^o)^2. \qquad \text{Eq. 2.11}$$

The first model usually does not provide an excellent fit to the observed data; therefore, a further modification is necessary. The partially derivative matrix around the starting model can be approximated as

$$G_{ij} = \frac{\partial d_1}{\partial m_j}_{m^o} .$$ Eq. 2.12

Once the partial derivative matrix is calculated, the change in the model Δ*mo* and a new model can be estimated to repeat the process:

$$m^1 = m^0 + \Delta m^0 .$$ Eq. 2.13

The procedure recurs until the complete squared misfit is acceptably small.

Some signals have a low signal-to-noise rate due to the noise environment. This requires a solution so each sensor is given a certain significance according to its quality. This solution is known as the weighted least square and is expressed as

$$\Delta m = (G^T W_d G)^{-1} G^T W \Delta d .$$ Eq.2.14

Where W_d is the data weighting matrix and is obtained by inverting the variance-covariance matrix of the data, or vector.

2.3 Importance of Hydraulic Fracturing Technology

Study of the tracking of the fracture provides us with better knowledge of the fracture geometry, azimuth, connection, solidity, and length. This allows upgrades to be made to the fracture system in real-time, such as variations to push stress and rate or proppant capability. Moreover, the operator can recognize fluid activity patterns, fracture growth, connection, compaction, and whether the fracture and proppant are remaining "in zone" or "out of location." These crucial ideas allow the stimulation treatment plan to be enhanced, and provide ideas useful for long-term upgrades to the well space strategy, the well design, and the completion design. Ultimately, hydraulic fracture mapping applied through microseismic tracking helps to boost the stimulated reservoir volume while enabling enhanced production rates and bookable supplies. Seismic waves go through attenuation (a decrease in the wave amplitude due to loss in energy), dropping, refraction, expression and function alterations by the time they are recorded by the receptors. The immediate compressional trend (P-wave) is the first stage to reach the indicator.

Fracture mechanisms and the frequency content of each signal help in understanding the fracture morphology. However, under similar conditions, tensile, compressive and more complex failure mechanisms have been observed in hydraulic fractures (Matsunaga, et al., 1993; Sasaki, 1998; Ishida, et al. 2004b). Microseisms do not map exactly where individual hydraulic fracture planes are located, but rather form an ellipsoid around the fracture, outlining the length, height, and azimuth of the fracture (Warpinski, 1994). Because microseisms may happen several feet off to one side of the fracture, no details on fracture size are accessible. The reason for this is most certainly the errors associated with hypocenter locations.

2.3.1 Hydraulic fracturing experiments at laboratory scale

Many researchers in recent years have performed hydraulic fracturing analysis at the laboratory scale. Haimson and Fairhurst (1969) tested hydrostone samples loaded polyaxially to simulate the three tectonic stresses encountered in the subsurface. They determined the type of fracture, its inclination and orientation and correlated those to the stress state in every sample. In addition, they determined the pressures at which the fracture triggered at different pressurization rates and different borehole sizes and compared those values with those generated from theoretical criteria. Solberg, et al. (1977) conducted hydraulic fracture studies on triaxially stressed samples of oil shale and Westerly Granite. They obtained results from those samples with different stresses: higher than 29000 psi failed by shear, while samples with different stress lower than 29000 psi failed in tension.

Lockner and Byerlee (1977) performed many hydraulic fracturing experiments in Weber sandstone samples in which they used AE to locate the microseismic events. The samples were put through various stresses and fluid injection rates. Medlin and Masse (1979) chose four different varieties of limestone quarry rocks (Carthage, Indiana, Lueders, and Austin) for hydraulic fracturing laboratory experiments with the purpose of calculating fracture initiation pressure and orientation. Both cylindrical and spherical cavities were tried. Fracture initiation pressure was determined for each rock category making use of different injection fluids (non-penetrating grease and penetrating vacuum pump oil) under different conditions (hydrostatic stress and ambient) to monitor the effect of each parameter. End results of fracture initiation pressure were measured against those estimated by poroelasticity theory. Fracture initiation pressures produced from laboratory experiments are based on the poroelasticity theory over several ranges of hydrostatic stress, and vary depending on the rock properties. Medlin and Masse (1984) chose the Mesaverde sandstone, and the Carthage, and Lueders limestones for laboratory hydraulic fracturing analysis. They fractured the rock samples applying distinct injection fluids, injection rates, and confined stress state to estimate additional variables, including fracture width, fracture length, and propagation pressure to calculate crack propagation theories.

Majer and Doe (1986) hydraulically fractured 300x300x450 mm salt blocks triaxially filled to compare the impact of confining pressure on breakdown pressure and the time dependency of breakdown pressure. Also, they applied AE to locate the microseismic events, as well as to investigate the behavior of the hydrofracture process. Cheung and Haimson (1989) conducted laboratory hydraulic fracturing experiments on fractured Niagara dolomite under a triaxial conditions. They investigated the conditions that regulate whether newer hydraulic fractures are produced or whether pre-existing fractures are reopened every time fluid is injected into the sample, and checked the results with values obtained theoretically. The results suggested that generation of new fractures or the reopening of pre-existing ones might be estimated in most circumstances, especially once the penetration of the injection fluid into the rock is considered.

Haimson and Zhao (1991) carried out many experiments hoping to explain the effect of borehole size and injection rate on the hydraulic fracturing break pressure, using granite and limestone samples. They concluded that borehole size and pumping rate influence breakdown pressure in the laboratory, but that impacts are insignificant in the field scale. Matsunaga, et al. (1993) performed laboratory hydraulic fracturing experiments in acrylic resin blocks, Inada granite, Komatsu andesite and Akiyoshi marble samples, using both water and oil as fracturing fluids. AE monitoring was used to interpret the fracturing mechanism during the fracturing process and the reaction of the fluid used. From focal mechanisms analysis, it was noted that events for all three rock samples were the result of shear failure, while fractures in the acrylic resin blocks was the result of tensile failure. Masuda, et al. (1993) performed laboratory experiments on Inada granite samples in which they monitored the AE generated when fluid was injected into the samples. They planned two different experiments: one in which the sample was dried out and subjected to hydrostatic stress, and the second in which the sample was saturated and put through a differential stress. In the first experiment no AE was observed; however, in the second experiment, from the moment the water pressure was increased microfracturing was induced.

Van Dam, et al. (1998) performed hydraulic fracturing experiments on 30 mm (1 inch) cubic blocks of various substances. They made use of plaster, cement paste, and diatomite. Every single block was triaxially loaded to simulate in-situ stresses. AE was helpful to calculate the fracture radius as well as size of the non-penetrated area. They concluded that the variety of fracture radii after shut-in induces the leak-off volume. Song, et al. (2001) carried out hydraulic fracturing experiments on Table rock sandstone. They set out to identify whether this particular treatment (hydraulic fracturing) was easy for calculating in-situ stresses in highly permeable rocks. After assessing a couple of samples and several experimental parameters they saw a relationship between breakdown pressure and far-field stress. Song and Haimson (2001) researched the end results of pressurization rate and pore pressure on breakdown pressure using Table rock sandstone, and confirmed a relationship between breakdown pressure and the far-field stresses. Good agreement between experimental results and theoretical prediction of breakdown pressure was found in the case of variable pressurization rates (Detournay and Cheng, 1992).

However, if pore pressure varied, the equivalent theoretical concept required some modification. Lhomme, et al. (2002) conducted hydraulic fracturing experiments at laboratory scale on Colton sandstone samples. A variety of fluid viscosities and injections rates were normally used to study fracture propagation fracture observations. In contrast to previous studies, they noticed that initiation pressure and breakdown pressure are not controlled by rates of pressurization or fluid viscosity. When they used high viscosity fluid and low injection rates they discovered a monotonic pressure drop after breakdown; whenever low viscosity fluid was used and injected at high rates, numerous fluid pressure rises were detected after the first pressure maximum. De Pater and Dong (2007) conducted several laboratory experiments to investigate the effects of confining stress and fluid rheology on hydraulic fracturing treatments using loose sand samples. The injection fluids used in the experiments were highly viscous Newtonian fluids (500 Poise), a bentonite slurry, a cross-linked gel, and the related cross-linked gel with fine quartz particles. Confining stresses, starting from 29 to 29000 psi, were used. Only when cross-linked gel with quartz particles was applied as the injection fluid was a hydraulic fracture created at all confining stresses used, and at any pumping rate.

Surdi, et al. (2010) conducted hydraulic fracturing experiments on a pair of identical quartz-rich, Carbon Tan sandstones, and observed the acoustic activity. To simplify fracture initiation two diametrically opposed slits ¼-inch in length were cut. They also modeled the distribution of stress focusing in the sample within well pressurization; they associated stress concentration during loading and fracturing with the localization of acoustic emissions in space and time. It is most evident that many researchers have tried to understand the hydraulic fracturing process through controlled experimental results.

2.3.2 Current Status of Hydraulic Fracturing Technology

Hydraulic fracturing was first established as a strategy to prevent well damage and increase production in conventional and tight gas reservoirs. However, growth in interest in unconventional reservoirs has taken hydraulic fracturing to new technological frontiers. The prospective advantages of refracturing have found the interest of oil and gas operators for more than five decades. If an original treatment is inadequate or the existing proppant deteriorates over the time, re-fracturing the well re-establishes linear flow into the wellbore (Dozier et al., 2003). Wells with effective initial treatment can be re-stimulated by creating a new fracture that propagates along a different azimuth than the original fracture which exposes more net pay to the wellbore (Dozier, et al., 2003). The key to successful development of an unconventional gas reservoir is to create complex fracture networks that contact a large reservoir volume (Mayerhofer, et al., 2006). However, the nature and degree of the fracture complexity must be understood in order to select the best stimulation strategy (Cipolla, et al., 2010).

Enhanced hydraulic fracturing techniques attempt to make the stimulation process more effective. One of these is hydraulic fracturing using carbon dioxide (CO_2). Verdon et al. (2010) studied a hydraulic fracturing field case in which water and supercritical CO_2 were injected under similar conditions. Microseismicity was used to observe performance variations. The microseismic event location showed similar styles in both cases, but in the case of water injection the fracture extended further laterally. When CO_2 was injected, microseismic activity appeared far above the injection factor, indicating that its higher buoyancy permitted CO_2 to move from top to bottom. The magnitude of the events caused in both situations is identical. Verdon et al., (2010) determined that despite the change in compressibility, solidity and viscosity, both liquids (water and CO_2) have identical styles of caused seismicity.

2.4 Considering Anisotropy

Isotropic, linear, elastic materials are completely characterized by two independent constants, usually Young's modulus and Poisson's ratio. Therefore, calculation of both P-wave and S-wave velocities becomes independent of the direction of wave propagation (Mavko et al., 2003). In anisotropic rocks, elastic characterization is not as simple as the isotropic case; up to 21 elastic constants are needed to describe the elastic behavior of anisotropic rocks. We often encounter two types of anisotropy: transverse isotropy and azimuthal anisotropy. The former has a hexagonal symmetry with five independent elastic constants, where the symmetry axis is normally perpendicular to the bedding. The latter is caused by stress anisotropy. Azimuthally anisotropic rocks may have 5, 9 or 13 independent elastic constants, depending on stress orientation and the intrinsic properties of the rock (Wang, 2002).

Most crustal rocks are found experimentally to be transversely isotropic as a result of the preferred orientations of anisotropic mineral grains, the shapes of isotropic mineral and those of cracks or thin bedding of isotropic or anisotropic layers (Thomsen, 1986).

Thomsen further pointed out that in most cases of interest to geophysicists, the anisotropy is weak (<10 percent). He indicated that a weak transverse isotropic formation can be characterized by three anisotropic parameters (ε, δ, and γ) and two velocities. The equations of the phase velocity variation as function of the angle are as follows:

$$V_p(\theta) = \alpha_0(1 + \delta \sin^2\theta \cos^2\theta + \varepsilon \sin^4\theta) \text{ ,} \qquad \text{Eq. 2.15}$$

$$V_{SV}(\theta) = \beta_0(1 + \frac{\alpha_0^2}{\beta_0^2}(\varepsilon - \delta)\sin^2\theta\cos^2\theta) \text{ ,} \qquad \text{Eq. 2.16}$$

$$V_{sh}(\theta) = \beta_0(1 + \gamma \sin^2\theta) \text{ .} \qquad \text{Eq. 2.17}$$

The angle between the wave front normal and the symmetry axis is known as the phase angle θ. α_0 And β_0 are the P-wave and S-wave velocities measured to the symmetry axis.

The magnitude of anisotropy in shale is greater than that estimated by Thomsen (Sondergeld and Rai, 2011); Sondergeld and Rai (1992) measured anisotropies as high as 42% in shear velocity and Hornby, et al. (1999) estimated P-wave anisotropy of 38%. Berryman (2008) proposed the following equations for strong anisotropy:

$$V_p(\theta) = \alpha_0\left(1 + \varepsilon \sin^2\theta - (\varepsilon - \delta)\frac{2\sin^2\theta_m \sin^2\theta \cos^2\theta}{1 - \cos 2\theta_m \cos 2\theta}\right) \text{ and} \qquad \text{Eq. 2.18}$$

$$V_{sv}(\theta) = \beta_0\left(1 + \frac{V_p^2(0)}{V_s^2(0)} - (\varepsilon - \delta)\frac{2\sin^2\theta_m \sin^2\theta \cos^2\theta}{1 - \cos 2\theta_m \cos 2\theta}\right) \text{ ,} \qquad \text{Eq. 2.19}$$

where θ_{m} is the incidence angle near which the extreme SV-wave behavior occurs (Berryman, 2008) and is given as:

$$\tan^2\theta_m = \frac{c_{22} - c_{44}}{c_{11} - c_{44}} \text{ .} \qquad \text{Eq. 2.20}$$

Any time a borehole is drilled in a transversely isotropic formation, the stresses around the wall of the borehole are not nearly as simple, almost suggesting the formation was isotropic. Aadnoy (1987) used equations to calculate the system stress around the borehole wall whenever a well is drilled in a transversely isotropic formation (Figure 2.2). The system stress calculation is split up into the components that determine the total hoop stress as show by

$$\sigma_{\theta\theta} = \sigma_{\theta\theta1} + \sigma_{\theta\theta2} + \sigma_{\theta\theta3}, \qquad \text{Eq. 2.21}$$

where $\sigma_{\theta\theta}$ the total hoop stress at the borehole wall , $\sigma_{\theta\theta1}$ is the contribution due the borehole pressure, $\sigma_{\theta\theta2}$ is the contribution of normal stresses, and $\sigma_{\theta\theta3}$ is the shear stress contribution.

$$\sigma_{\theta\theta1} = P_W \frac{E_\theta}{E_x}\left[k - n(\sin^2\theta + k\cos^2\theta) + (1-k^2)\sin^2\theta\cos^2\theta\right], \qquad \text{Eq. 2.22}$$

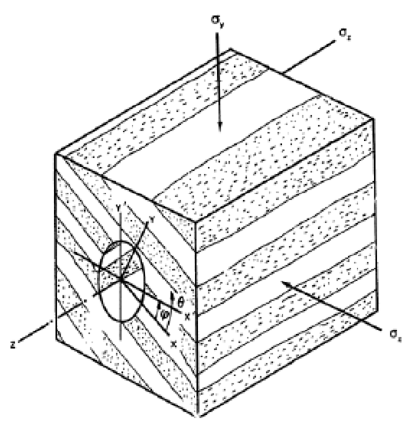

Figure 2.2 Geometry showing a borehole in a transversely isotropic medium where the X-axis is aligned with the direction of the bedding and the Y-axis is perpendicular to the bedding (Aadnoy, 1987). σx, σy, σz are the three principal stresses. σx and σy are aligned with the X'- and Y'-axis, respectively. Ɵ is the angle from the X-axis and φ is the angle measured from the bedding orientation to the horizontal axis (Castano, 2010)

where P_w is the hydrostatic pressure in the borehole, Θ is the angle from the X-axis (from the axis of isotropy), E_Θ is Young's modulus in the direction tangent to a position at a given angle, Θ, from the direction of the bedding, Ex is the Young's modulus along the X-axis (parallel to bedding). K, n are given as

$$k = \left(\frac{E_x}{E_y} \right)^{\frac{1}{2}} \quad \text{and} \qquad \text{Eq. 2.23}$$

$$n^2 = 2 + 2k \, . \qquad \text{Eq. 2.24}$$

The value E_Θ / E_x can be calculated from the following expression:

$$\frac{E_x}{E_\theta} = \sin^4\theta + 2\sin^2\theta\cos^2\theta + k^2\cos^4\theta \, . \qquad \text{Eq.2.25}$$

The contribution of normal stresses is given as

$$\sigma_{\theta\theta 2} = \sigma_x \frac{E_\theta}{E_x}\left[-\cos^2\varphi + (k+n)\sin^2\varphi\right]k\cos^2\theta + \left[(1+n)\cos^2\varphi - k\sin^2\varphi\right]$$
$$\sin^2\theta - n(1+k+n)\sin\varphi\cos\varphi\sin\theta\cos\theta) + \sigma_y \frac{E_\theta}{E_x}(\left[-\sin^2\varphi + (k+n)\cos^2\varphi\right]k\cos^2\theta +$$
$$\sigma_y \frac{E_\theta}{E_x}(\left[-\sin^2\varphi + (k+n)\cos^2\varphi\right]k\cos^2\theta + \left[(1+n)\sin^2\varphi - k\cos^2\varphi\right]\sin^2\theta - n1 + k + n)\sin\varphi\cos\varphi\sin\theta\cos\theta \qquad \text{Eq. 2.26}$$

where φ_x and φ_y are the principal stresses in the horizontal and vertical axes respectively. The angle φ is the angle measured from the bedding orientation to the horizontal axis as was shown (Figure. 2.1).The shear stress contribution is given by the following expression:

$$\sigma_{\theta\theta 3} = \tau_{xy}\frac{E_\theta}{2E_x}(1+k+n)\left(\left[-n\cos 2\varphi + (1+k)\cos 2\theta + k - 1\right]\frac{\sin 2\varphi}{\sin 2\varphi}\right) , \qquad \text{Eq. 2.27}$$

where

$$\tau_{xy} = 0.5(\sigma_y - \sigma_x)\sin 2\theta\,. \qquad \text{Eq. 2.28}$$

2.4.1 Formation permeability from microseismic data

State of the art technology has permitted using microseismic information not only for applying to hydraulic fracture but also for the evaluation of in-situ formation permeability. For this purposes two different techniques are utilized: the r method and the inversion approach (Grechka, et al., 2010).

2.4.2 R-technique for permeability estimation

The r- technique depends on the spatio-temporal dynamics characteristic of caused microseismic clouds. The volume of the injected fluid must be equal to a sum of the fluid volume stored in the fracture and the fluid volume which goes into the formation. A straight planar height-fixed fracture is considered. Under these conditions the half-length, *L*, of the hydraulic fracture is given as a function of the injection time as the following (Economides and Nolte, 2003):

$$L(t) = \frac{Q_i t}{4h_f C_L \sqrt{2t + 2h_f w}}\,, \qquad \text{Eq.2.29}$$

where Qi is the average injection rate of the treatment fluid, h_f is the average fracture height and w is the average fracture width, t is the injection time, and C_L is the fluid-loss coefficient. In the case of the hydraulic fracturing of a low permeability formation, such as tight gas sandstones, the fracture body represents the main permeable channel in the formation (Shapiro et al., 2006). The induced fracture changes the stress state in its vicinity, leading to the occurrence of microseismic events at a distance very close to the hydraulic fracture (Warpinski, 2000). Therefore, equation 2.30 can be considered as a one-dimensional approximation for the triggering front of microseismicity in the case of a penetrating hydraulic fracture (Shapiro, et al., 2006):

$$L = \sqrt{4\pi D t}\,, \qquad \text{Eq. 2.30}$$

where D is the apparent diffusivity and t is the injection time.

During hydraulic fracturing treatments the fracture growth is managed by the liquid loss effects. Generally, this means that the cumulative volume of the lost fluid is considerably larger than the volume of the hydraulic fracture. The fluid loss effects are controlled by the fluid-loss coefficient, C_L, which is characterized by the apparent diffusivity, D, (Shapiro et al., 2006):

$$C_L = \frac{Q_i}{8 h_f \sqrt{2\pi D}}\,, \qquad \text{Eq. 2.31}$$

Also, the fluid loss coefficient can be interpreted neglecting the near-surface effects (e.g., filter cake) from the pressure difference between the fracture and the far field reservoir ΔP. Economides and Nolte (2003) approximated the fluid-loss coefficient based on these assumptions to be

$$C_L = \sqrt{\frac{k_r \phi c_r}{\pi \eta_r} \Delta P}\,, \qquad \text{Eq. 2.32}$$

where k_r is the in-situ reservoir pressure, ϕ is the formation porosity, C_r and η_r are the compressibility and viscosity of the reservoir fluid and ΔP is the difference between the average injection pressure and the far-field reservoir pressure (Shapiro, et al. 2006). Substituting Equation 2.31 into Equation 2.32 and solving for the formation permeability

$$k_{r-t} = \frac{\eta_r}{128\phi c_r D}\left(\frac{Q_i}{h_f \Delta P}\right)^2 . \qquad \text{Eq. 2.33}$$

Equation 2.33 is the in-situ formation permeability calculated using the r technique. The distance from the perforation point to the event location as a function of time is shown by the r plot. Equation 2.30 symbolizes the parabolic envelope that better explains the higher limit of a lot of microseismic activity, which is reliant on the apparent diffusivity value.

CHAPTER 3: MATERIALS AND METHODS OF STUDY

CHAPTER 3.1 General Statements

The unique low flow behavior of low permeability reservoirs is due to poor utilization of reservoir pressure and to reservoir heterogeneity. Poor utilization of reservoir pressure is caused in part by depositional issues like very small grains of detrital muds (clays); other factors include diagenesis related to clay precipitation, massive cementation, pressure compaction, etc. Reservoir heterogeneity is related to depositional and post-depositional (diagenetic) events. These include the vertical/lateral heterogeneity that shows the medium and large scale geological features for turbidite deposition and fault and differential diagenesis, which include the migration and hydrocarbon generation. These characteristics show that low permeability reservoirs are simply poor conductors of fluids.

Ultra-low permeability shale reservoirs require a major fracture network to maximize well performance. Microseismic fracture mapping has revealed that huge fracture networks are typically induced in many shale reservoirs. In shale reservoirs, anywhere complex network structures in different planes are formed, the ideas about that particular fracture half-length in addition to conductivity are insufficient to portray well performance.

Thus, reservoir permeability and reservoir heterogeneity are permanent constants that we sometimes cannot change. Although this is widely known, it is possible to modify our mechanism for accessing the reservoir (i.e., the well). We may also change our development method to ensure best performance and treatment of any reservoir. The calculation of shale permeability remains problematic, particularly when considering the understanding of the end results of standard flow measurements (e.g., steady-state permeability measurements). Neuzil (1994) emphasizes less the special properties of shale permeability and more on the "regions" shown on a chart of porosity versus their logarithms of permeability. This context is important in recognizing that shales/clays have very high porosity and low permeability, which is important when considering trends. Revel and Cathles (1999) implement a power-law model for estimating permeability in shaly-sands making use of porosity and shale volume.

The influence of an in-situ stress field on a natural fracture or fault should be monitored in situ by its direction determined by that stress field. Evaluating the relationship of presented stress data to existing regional structures provides the ability to differentiate between natural fractures and new fractures being created. Although it is inconclusive to say that faulting or other geologic structures that are regularly visible on the surface near the area of a treatment well are an indication of the subsurface structure, at times surface features may work as useful signals of the valuable structural features in the subsurface. The response to an uncertainty of a new fracture, whether a new or pre-existing, was initiated has various impacts for the responsible failure mechanisms. With the utilization surface arrays and broad areal coverage laid arrays, declining mechanisms along fracture planes are often identified, giving the angle of the fault or fracture plane and also the path of slip, and details on the possible tensile area of the failure mechanism.

Microseismic monitoring surface arrays produce imaging coverage over the total stimulated volume of a treatment well. Simply because the span of areal coverage for the several channels accepting event signals deals with a massive area, it is possible to investigate the first P-wave particle motion changes across the array and determine a fault plane connected with that motion (Figure 3.1) For nearly vertical faults, the first motions across the array will have zero P-wave amplitude radiated along a line parallel to a fault, and array stations will locate positive or negative motion on specific array areas.

This technique of interpretation is performed with surface based vertical component geophones and probably will not need the use of three-component geophones. The integration of this solution with information regarding the structural style in the area provides identification of the displacement on the fault as normal or reverse dip-slip without the need to do a full source mechanism inversion.

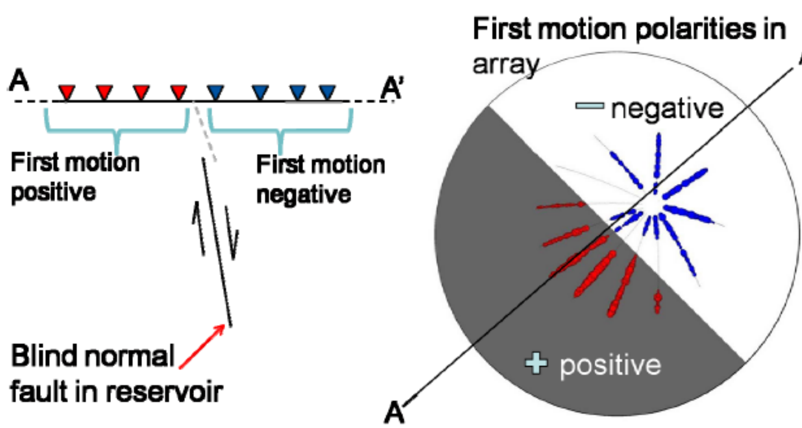

Figure 3.1. Example of surface-based microseismic geophone array configuration. The asymmetric layout of the receiver pattern optimizes signal for a horizontal well deviated to the southwest (Williams, 2009).

If perhaps a variety of strong events describe two intersecting styles about 30 degrees apart, it is clear that the treatment fluid located and reactivated two nearby fault planes (Figure 3.2.) The direction in which the fault planes slipped is not distinct from the geometry, but by combining the geologic details with the wellbore information, the final nature of the failure mechanisms and fault interactions was identified. For events describing a 120^o azimuth trend, a fault plane was described that parallels that 120^o azimuth, which signifies that the first motions of the seismic energy P-waves to the geophones in the array were positive in one area on this nodal line and negative on the other side. This kind of result can come from dip- slip motion on a steeply dipping fault in the subsurface.

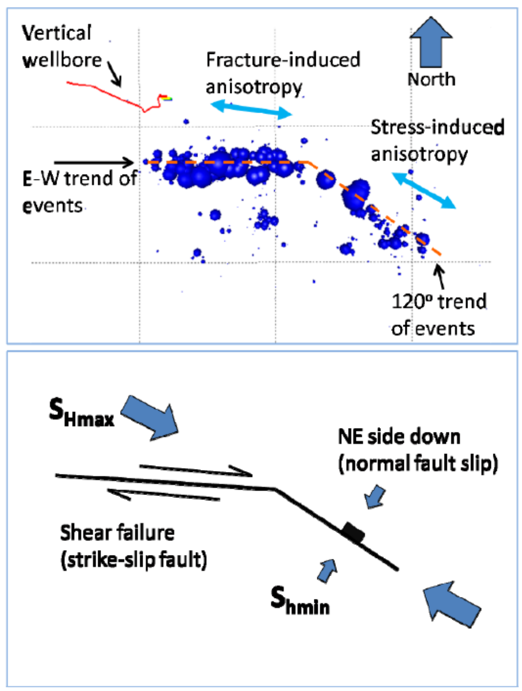

Figure 3.2 Failure mechanisms of two interacting faults reactivated by hydraulic fracture stimulation (Williams, 2009).

The events that describe the east-west pattern did not have this particular first motion of P-waves. The concept of the microseismic events is reactivation and possibly continuance of an east-west oriented fault in strike-slip motion; while it grew, it intersected a southeasterly striking fault in order for normal dip-slip motion. The analysis is in accordance with the anisotropy measurements in the wellbore that determined maximum horizontal stress parallel to the strike of the normal dip-slip fault. Figure 3.3 shows a situation of a complex fracture network activated by the microseismicity of a stimulation treatment is useful to describe the upper bounds of fracture length, and their height and dip. An assessment of the event patterns with the subsurface structure means that the microseismicity has reactivated recent structures. The largest events align parallel to the strike of major faults unidentified in the subsurface in the interpreted seismic horizons. The most significant events create a direction parallel to the faults with orientation nearby to the maximum horizontal stress direction, and a secondary trend of weaker events seems to be forming at an angle to the first trend. The two orientations exist in the subsurface, the results are interpreted to reflect reactivated existing faults and fractures. The great microseismic events describe a trend at an angle over 25 degrees from the fault trend. In this case, the effective stress in the reservoir is east-northeast (roughly sub-parallel) to the faults, so faults in this specific orientation are supposed to be critically stressed, indicating it is in an orientation that is likely to slip (Zoback, 2007). Source mechanism inversions performed for this data set demonstrate principally dip-slip normal fault displacement on the fault planes oriented approximately 80^{o} azimuth (Figure 3.3).

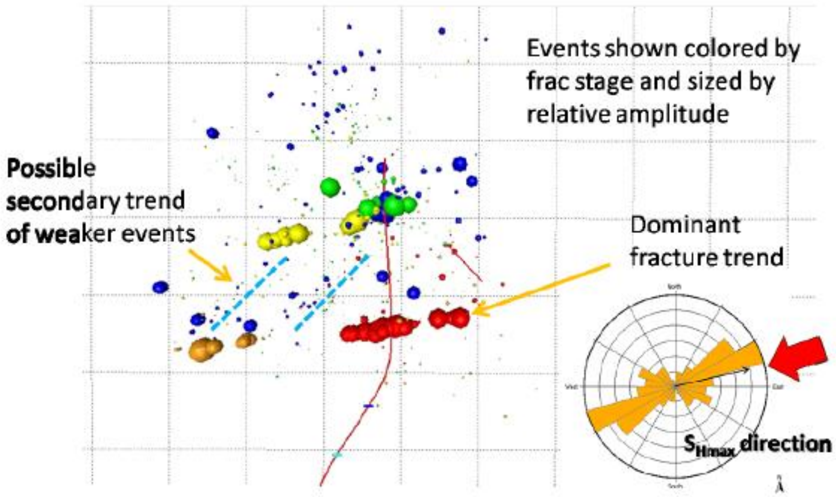

Figure 3.3 Microseismic monitoring result with some stages showing better defined trends than others. The trends are parallel to major faults mapped nearby in the subsurface. The failure mechanisms for the events are consistent with normal dip-slip motion along such faults (Williams 2009).

3.2 Microseismic Data

Data used in this study were obtained from Devon Energy Incorporated. The fracture treatment data consisted of the treating pressure, total slurry used, slurry rate, and propant concentration. The micro-seismic location data consisted of the X, Y, and Z locations of all the events east to west and from north to south, time of location in seconds, epicentral distance, and number of usable P- and, S- wave arrivals. The slurry data are the number of microseismic events and the number of microseismic cubes (See Appendixes Table 1 and Table 2).

3.3 Methodology

The main objective of this study is to calculate the volume of hydraulic fracture from micro-seismic events and compare the result with the field measured volume of slurry. Two methods are suggested. The first method is the use of a software called Surfer 6 to plot and estimate the volume of hydraulic fracture. The second method is based on the use of the excel discrete bins technique for estimating the volume of hydraulic fracture.

3.3.1 Surfer application method

The workflow of the Surfer application started by creating grid on the X, Y, and Z locations data (Figure 3.4). The first task was to use the software to create an XYZ data file, which contained three columns of data values. The first two columns were the coordinates for X and Y data points and the third column was the Z. The XYZ data were entered into column ABC in an Excel spreadsheet (Figure 3.5) Surfer 6 is powerful software that has the ability to plot, contour or make surfaces. The grid files can produce a grid-based map and a grid report. The software created a grid from the data in columns XYZ where X, Y and Z represented Easting, Northing, and Elevation, respectively (Figure 3.6). Surfaces were made from the block diagrams generated by drawing lines representing the grid X and Y lines (the grid columns and rows). At each intersection of a column and row (at each grid node), the height of the surface was proportional to the grid Z value at that point. The number of columns and rows in the grid file determines the number of X and Y lines drawn on the surface in (Figure 3.7). The volume of the hydraulic fracture can be calculated from the generated surface.

The Surfer 6 application can also plot the XYZ information from the field data into 2D and 3D in a cube without changing the location data XYZ into surfaces. Although it was assumed that the best estimation could be calculated from the 3D plot because it showed the true projection of the micro-seismic event with respect to time and space as seen in (Figure 3.8a). The procedure of plotting the events in 3D used the XY, YZ, and XZ data only, so there were three different individual plots that were needed to estimate the volume of hydraulic fracture.

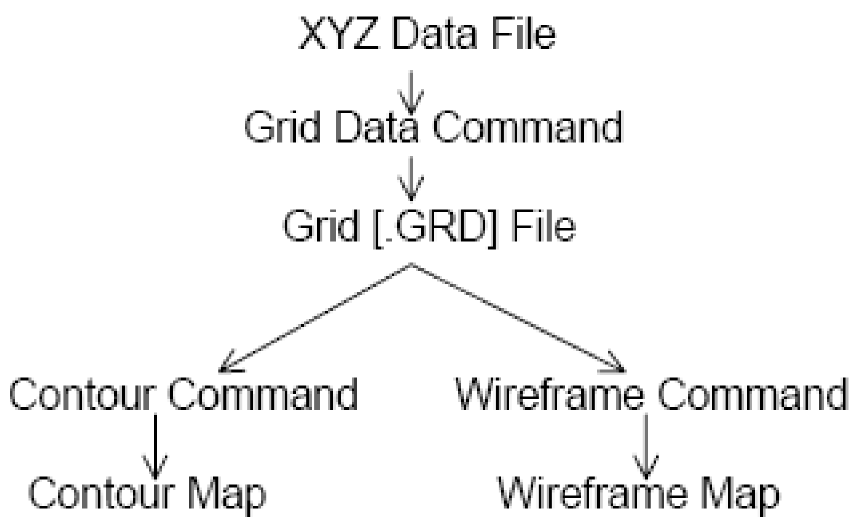

Figure 3.4.Flow chart illustrating the relationship between XYZ data, grid files, contour maps, and wireframes maps.

	A	B	C
1	X Data	Y Data	Z Data
2	0.1	0	90
3	9	3	48
4	1.3	7	52
5	4.7	1	66
6	1.7	5.6	75
7	6	1	50
8	2.5	3.6	60

Figure 3.5 The XYZ data placed in Columns A, B, and C in Surfer application.

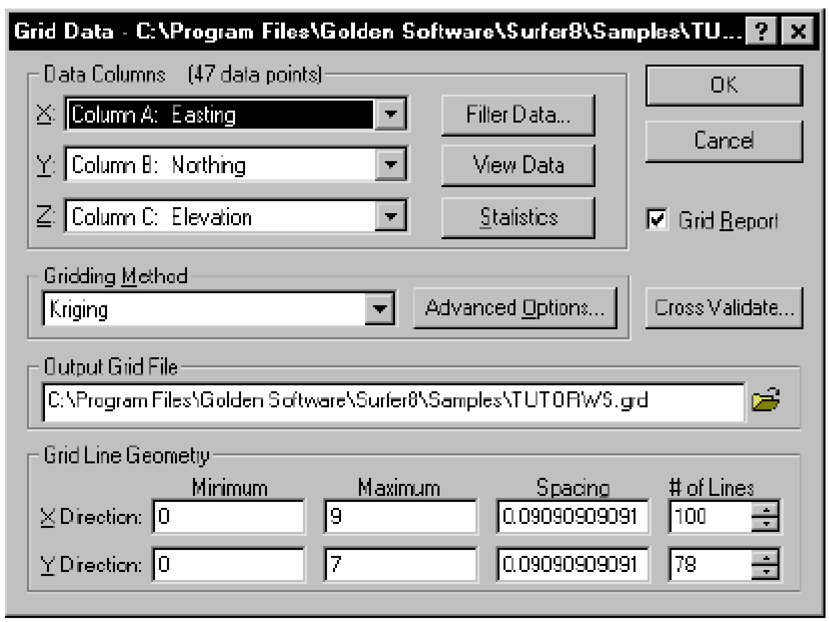

Figure 3.6 the grid data dialog box showing the gridding parameter to use when creating a grid file n Surfer application.

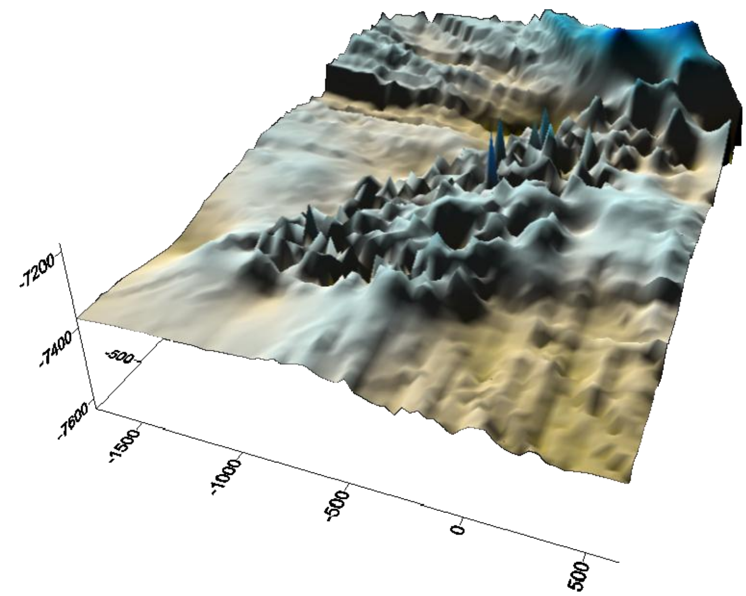

Figure 3.7 The surface from the Surfer X, Y, and Z parameters.

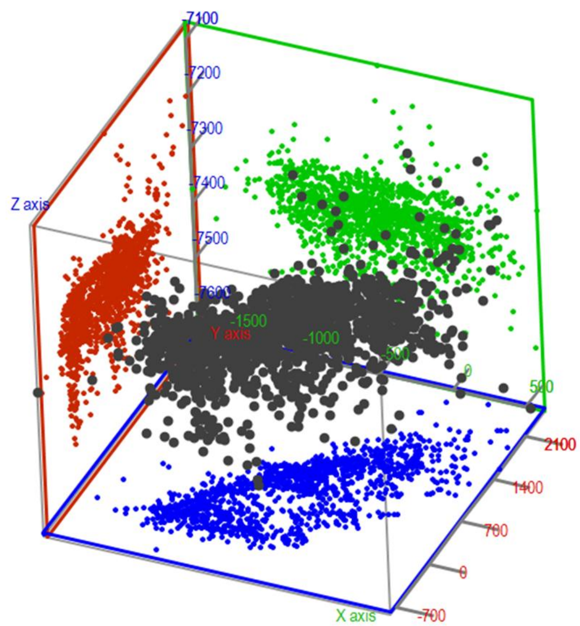

Figure3.8a Three dimensions of the micro-seismic events in Surfer.

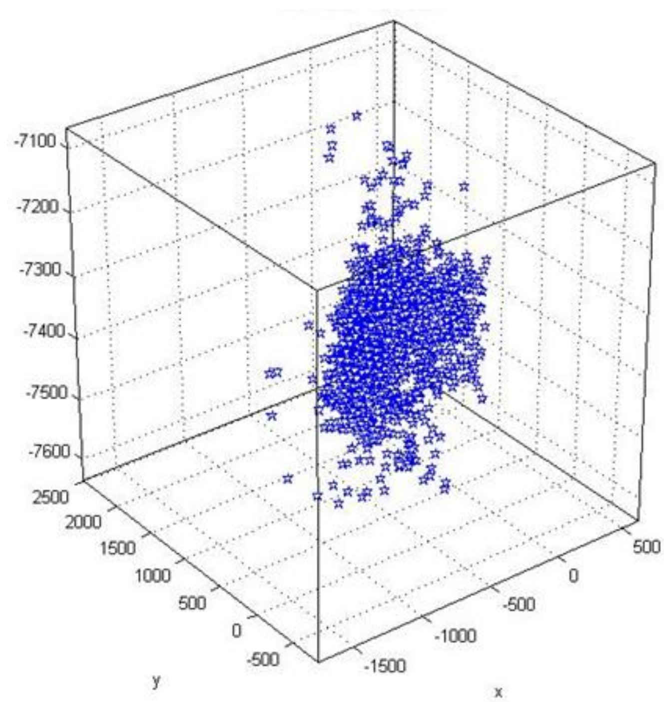

Figure 3.8b Three-dimensional projection of the all the microseismic events.

The entire Surfer plots were gridded into 100 by 100 in both axes. The volume of hydraulic fracture was estimated from the micro-seismic events by using 100 by 100 grids to form a rectangular box around the cloud. These rectangular boxes were measured from the maximum and minimum values in the x and y axes direction. The micro-seismic events were also plotted in 3D view in Surfer with the projection of the XY, XZ, and YZ at middle of the cube. Each point represented each coordinate from XYZ respectively, as show in (Figures 3.8a and Figure 3.8b). The estimated volume could be calculated from the event in the three -dimensional box of XYZ.

3.3.2 Excel Discrete Bins Method

This method is used to estimate volume of hydraulic fracture microseismic discrete bins. Constant width bins (e.g., 100ft wide) are drawn in the principal fracture direction from the borehole to the furthest event in the specific bin on both sides of the borehole either from the XY, XZ, and YZ. The individual bin areas are then summed up to approximate the total fracture area. The calculation volume of hydraulic fracture also requires an estimate of the fracture area network height in each discrete bin within the reservoir section. Figures 3.9a, 3.9b and 3.9c show the microseismic discrete bin method used for the Dollie Thorell well.

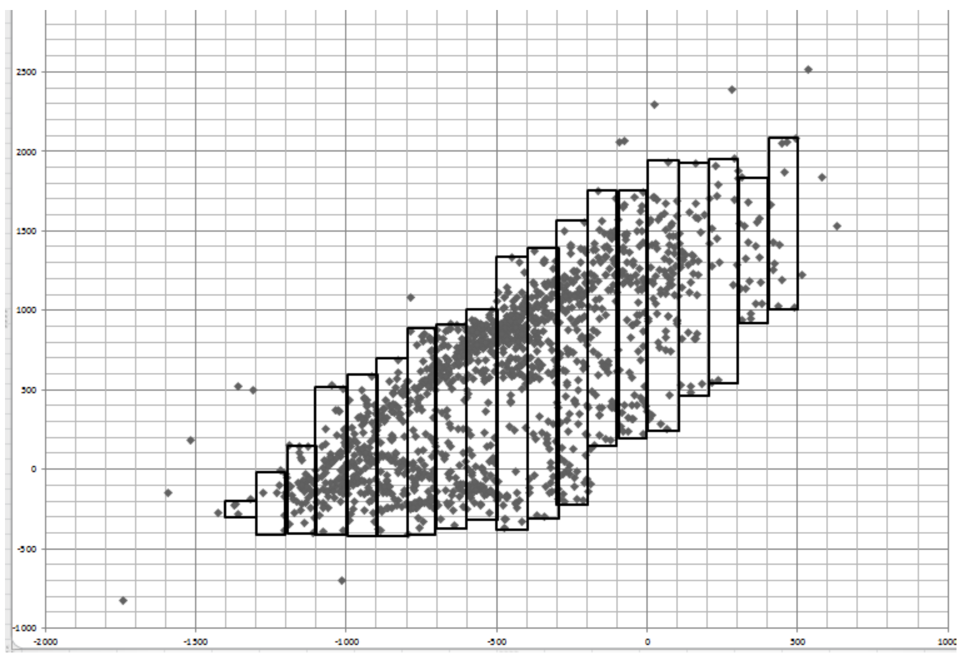

Figure 3.9a The XY axes of the micro-seismic event from the Discrete bin method.

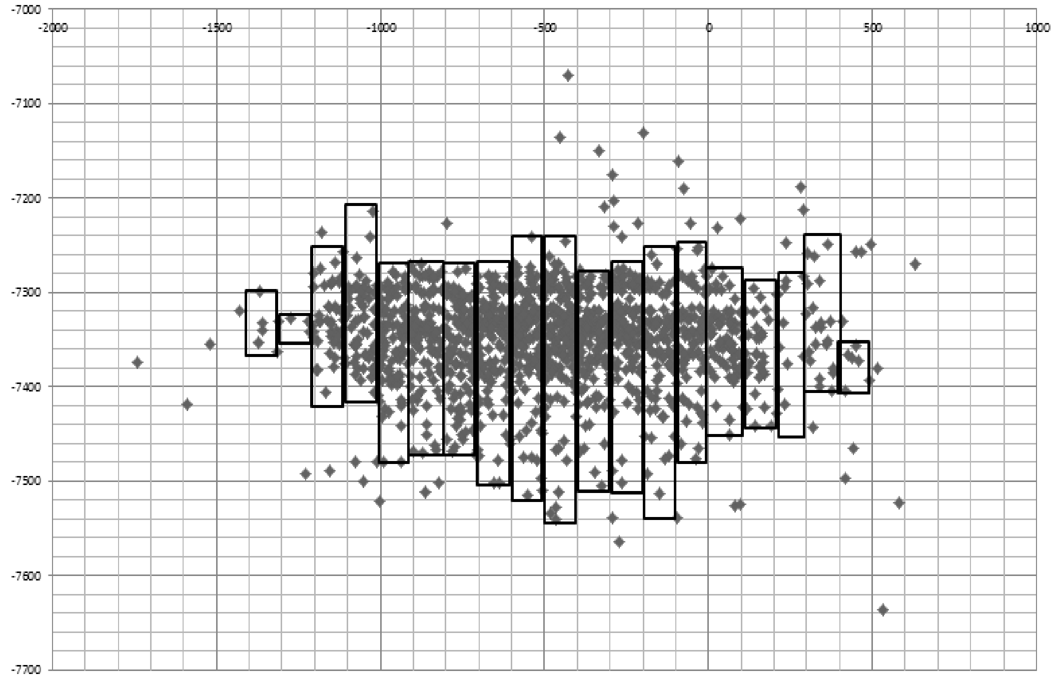

Figure 3.9b The XZ axes of the micro-seismic event from the Discrete bin method.

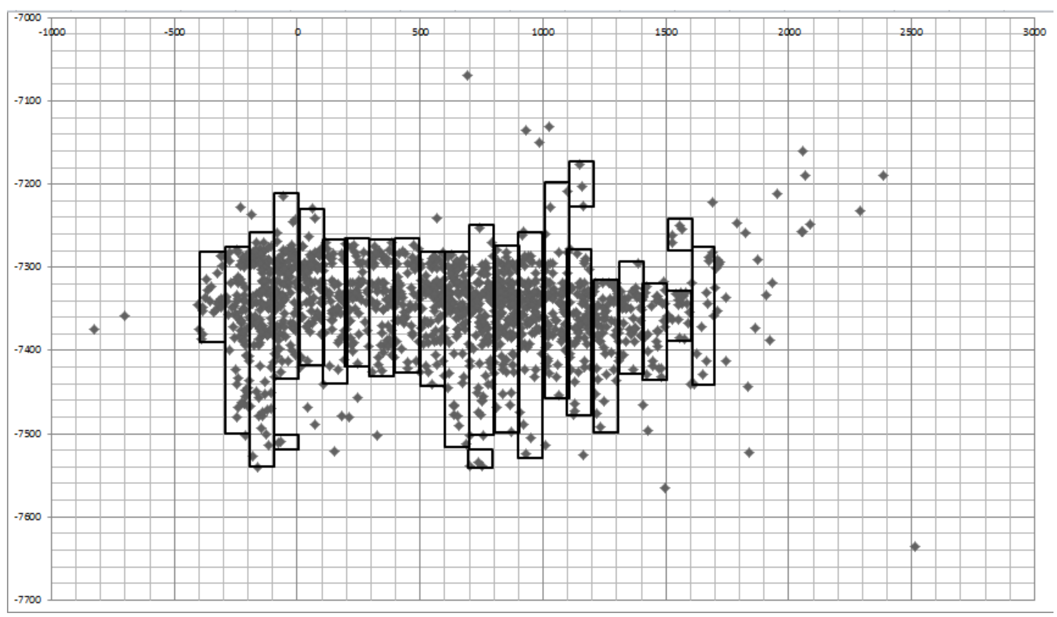

Figure 3.9c The YZ axes of the micro-seismic event Discrete bin method.

CHAPTER 4: RESULTS AND DISCUSSION

4.1 Surfer Application Result

Surfer 6 software was used for surface gridding and volume calculation. The input XYZ data (micro-seismic event data from the location) was available for the top of the Barnett Shale. No base of the interested interval was used. The way the code was written in this Surfer 6 program gridded the input XYZ data, then converted this gridded point of the XY into surfaces. The program calculated the entire area of the surface and multiplied it with the z values from the input data which is considered to be height of this event. The volume calculation thus involved the extent of the surface area and the height of the Z value of the input data. The Surfer 6 gave the output of the volume results using three rules: (i) Trapezoidal rule, (ii) Simpson's rule, and (iii) Simpson's 3/8 rules. The total volumes calculated are $6.7\text{x } 10^{10}$ cubic ft, $6.7\text{x } 10^{10}$ cubic ft and $6.7\text{x } 10^{10}$ cubic ft, respectively. The results are also presented in Figure 4.1.

4.2 Excel Discrete Bins Method Result

This is the method by which the XY data (see Columns 1 and 2 in Table 2 in the appendix) were plotted and then gridded into different bin. A total of nineteen bins were constructed with intervals of 100ft in X- axis and 100ft in Y-axis, this procedure resulted in the formation of 19 different bins .

Grid Volume Computation

Upper Surface	
Grid File Name	*C:\Users\Seun\Contacts\Desktop\MSLocation.true.12grd*
X Minimum:	-999.59
X Maximum:	1742.7
X Spacing:	$33.8x10^{12}$
Y Minimum:	-828.25
X Maximum:	2512.68
X Spacing:	$33.7x10^{12}$
Z Minimum:	$-7.631.5x10^{10}$
Z Maximum:	1742.7
Lower Surface	
Level Surface defined by Z=0	
Volumes	
Z Scale Factor:	1
Total Volumes by:	
Trapezoidal Rule:	$-6.7x10^{10}$
Simpson's Rule:	$-6.7x10^{10}$
Simpson's 3/8 Rule:	$-6.7x10^{10}$
Cut & Fill Volumes	0
Positive Volume [Cut]:	0
Negative Volume [Fill]:	$6.7x10^{10}$
Net Volume [Cut Fill]:	$6.7x10^{10}$

Figure 4.1 Calculated volumes by using Surfer software Version 6 for the Barnett Shale. The surface height was used to define a lower limit for the volume definition.

Volume was calculated from the product of area (fracture spacing) and height. The height in Figure 4.2 is the difference between the highest and the lowest values from the discrete bin in relative to the XY axes (Chesnokov, 2009).

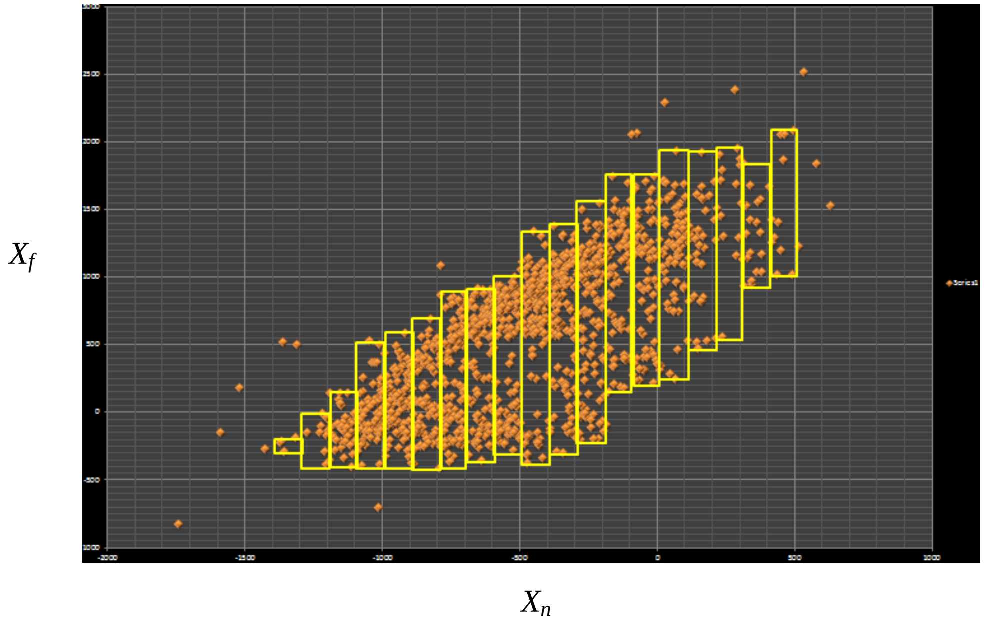

Figure 4.2 The fracture spacing of the microseismic events into different bins using the Discrete Bin method.

The volume of hydraulic fracture (V_f) calculated from this method was 6.7 10^{10} cubic ft. All calculations are shown in a spreadsheet in Table 1 in the appendix. The calculated volume of fracture (V_f) was then correlated with the volume of slurry from the field (V_i) to determine the relation fracturing crack density η.

4.3 Discussion of Results

The purpose of estimating the volume of hydraulic fracture in this study is to reflect the nature and extent of any fractures that may have been created by the over-pressurization of the well. This is related to pore pressure changes which cannot move very far from the actual fracture planes, unless natural fractures in alternate directions are opened and hydraulically enhanced as a network structure thus serving as a conduit for fluid movement. This means that a large micro-seismic event (cloud) structure must be approximately equivalent to the actual fracture network size. Thus, the microseismic event cloud structure detected by hydraulic fracturing provides a means of estimating the volume of hydraulic fractures in very tight reservoirs (Mayerhofer and Warpinski, 2008).

The total volume of the hydraulic fracture that was estimated from both methods provides details of the effectively producing fracture structure or spacing. Apart from reservoir modeling, which also provides an avenue to better evaluate the effectively producing network, the seismic signal characteristics also provide the source of the mechanical deformation that resulted in the micro-seismic event. Maxwell, et al. (2002) introduced a concept that could eventually be used to characterize fracture density. This concept was similar to the discrete bin method, which is the area of the hydraulic fracture shown in Figure 4.2. In contrast to conventional single fracture modeling using fracture half-length of the hydraulic fracture area, dimensions are given by the total fracture network length ($2x_f$) and width (x_n) (Figure 4.2). However, the key property for evaluating the volume of hydraulic fracture, is the total sum of all fracture network segments within the reservoir, which is a strong function of fracture spacing. The equation for the calculation of the total fracture length to estimate the volume of hydraulic fracture as a function of fracture network half-length x_f, width x_n and fracture spacing Δx_s is:

$$L_{ftotal} = \frac{4x_f x_n}{\Delta x_s} + 2x_f + x_n \quad . \qquad \text{Eq. 4.1}$$

The relationship between the volume of the created hydraulic fracture, (V_f), the volume of the slurry (V_i,) and the fracturing crack density (N_c) is given in Table 1 in the Appendix as:

$$N_c = V_f / V_i \qquad \text{Eq.4.2}$$

Crack density is always less than 1 due to leak-off of fracturing fluid to the reservoir pore space during the hydraulic fracturing treatment. Figure 4.1 shows that the crack density increases when the volume of the fracture increase. The crack density is a function of orientation produced by the deviatoric stress field, which led to velocity differences and anisotropy. The fracture's anisotropic elastic constants can be described in terms of a fracture-compliance matrix, which can be added to the compliance matrix of the host rock to find the equivalent-medium elastic constants (Schoenberg, 1980; Schoenberg and Sayers, 1995). Crack density and aspect ratio can be related to the fracture compliance matrix for aligned fracture sets (Hudson and Liu, 1999; Liu et al., 2000), and the compliances of multiple fracture sets can be combined (Schoenberg and Sayers,1995).

Volume of fracture ft^3

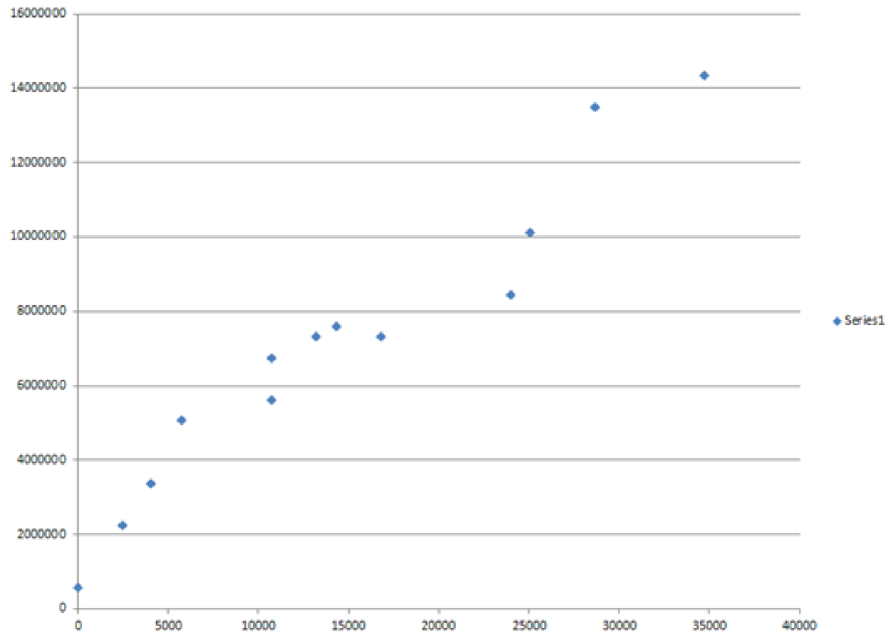

Volume of Slurry ft^3

Figure 4.3 Correlation between volume of slurry and volume of fracture from table

APPENDIX 1

Area	xmin	xmax	ymin	ymax	Number of Events	Number of Cube	Cumulative Number of the of Cube	Area	Volume	Vol of fracture(m3)	Volume Slurry (m3)	Nc=Crack Density	Time(Sec)
1	-1400	-1300	-300	-200	3	2	2	10000	3750000	562500	0	5.33333E-06	299
2	-1300	-1200	-400	0	25	8	10	40000	15000000	2250000	2475	1.66667E-06	395
3	-1200	-1100	-400	200	41	12	22	60000	22500000	3375000	4051.5	1.82222E-06	977
4	-1100	-1000	-400	550	70	18	40	90000	33750000	5062500	5737.5	2.07407E-06	1321
5	-1000	-900	-400	600	81	20	60	100000	37500000	5625000	10720.5	0.00000216	1321
6	-900	-800	-400	700	95	24	84	120000	45000000	6750000	10720.5	2.11111E-06	1473
7	-800	-700	-400	900	102	26	110	130000	48750000	7312500	13213.5	2.09231E-06	1540
8	-700	-600	-300	1000	105	27	137	135000	50625000	7593750	14311.5	2.07407E-06	1692
9	-600	-500	-300	1150	103	26	163	130000	48750000	7312500	16804.5	2.11282E-06	1758
10	-500	-400	-400	1320	93	24	187	120000	45000000	6750000	17887.5	2.06667E-06	1910
11	-400	-300	-300	1400	39	11	198	55000	20625000	3093750	20380.5	1.89091E-06	1977
12	-300	-200	-200	1590	76	22	220	110000	41250000	6187500	21478.5	1.84242E-06	2129
13	-200	-100	100	1800	98	30	250	150000	56250000	8437500	23973	1.74222E-06	2195
14	-100	0	200	1800	101	36	286	180000	67500000	10125000	25054.5	1.4963E-06	2347
15	0	100	210	1960	82	34	320	170000	63750000	9562500	27547.5	1.28627E-06	2414
16	100	200	430	1940	104	48	368	240000	90000000	13500000	28647	1.15556E-06	2566
17	200	300	510	1980	58	28	396	140000	52500000	7875000	31140	1.10476E-06	2632
18	300	400	900	1820	80	40	436	200000	75000000	11250000	32223	1.06667E-06	2784
19	400	500	1000	2100	92	51	487	255000	95625000	14343750	34717.5	9.62092E-07	2851

Table 1. Result of the values used in calculating the volume of the fracture and crack densit

Table 2. The Micro-seismic Location Data (Input Data)

X, Y, Z locations relative to Monitor Well and other parameters associated with a microseismic event, including

Rxy - Epicentral distance = sqrt(X^2 + Y^2), ft

Nsp - Number of usable P-, S-wave arrivals x 1000,

Referred to the case of "Number of geophones" = 12.

Thus the limit superior = 1000 *(2 *12) = 24000

Tm= Tc-To = Difference between start time of the current

Event file and that of the 1st event file (in seconds)

O.time - Difference (in milliseconds) between the current events

Origin time and the event file start time

E.C. - The energy class as Brigg's logarithm of relative

Seismic energy (E.C. = log10 (E / E_ref)

X, ft (W-E)	Y, ft (S-N)	Z, ft	Rxy, ft	Nsp	Tm, sec	O.time mls	E.C.
56.58	1322.37	-7348.85	1323.58	21081	2131	20.4	-3.4
-311.15	1262.99	-7345.44	1300.75	21753	2135	29.7	-3.3
-205.63	1362.94	-7379.39	1378.36	23408	2157	72.6	-2.3
-171.46	1063.61	-7454.34	1077.34	23162	2209	95.2	-3.1
-455.99	687.09	-7511.7	824.63	18121	2423	71.7	-3.8
74.13	1409.54	-7336.15	1411.49	21069	2467	13.4	-3.4
-929.54	407.26	-7364.68	1014.84	18785	2585	55	-4
-402.53	893.37	-7296.88	979.87	19354	2667	61.4	-4.1
-374.4	859.11	-7329.06	937.15	23782	2757	70.7	-3.5
-485.42	835.37	-7338.75	966.17	20349	2847	64.3	-3.8
-664.14	640.36	-7314.98	922.57	22821	2939	71.3	-3.3
-110.36	1318.88	-7329.43	1323.49	20282	2947	29.4	-3.2
-1018.92	109.6	-7378.58	1024.8	21027	3011	57.5	-3.4
-526.12	802.14	-7323.63	959.29	23532	3187	105.2	-1.9
-595.9	729.12	-7381.51	941.65	22764	3187	101.3	-2.4
-631.94	767.89	-7358.13	994.49	23578	3187	101.9	-2.3
-875.89	382.63	-7404.89	955.82	20151	3227	65.7	-3.5
-21.61	1138.05	-7332.1	1138.26	21834	3246	48	-3.1
-207.08	1383.29	-7336.44	1398.7	23009	3258	75.6	-2.6
65.52	1133.97	-7389.46	1135.86	18301	3288	44.4	-3.7
-929.9	59.38	-7343.35	931.79	20475	3360	63.4	-3.6
-738.82	559.79	-7353.08	926.94	18833	3386	61.6	-3.9
-636.48	700.4	-7501.65	946.4	22033	3486	59.8	-3.2
-253.12	944.89	-7365.06	978.21	21778	3486	67.1	-3.3
288.76	1158.36	-7367.55	1193.81	20498	3524	44.1	-3
-948.46	275.39	-7364.92	987.63	18169	3550	59.9	-3.7
-252.62	1357.18	-7349.31	1380.49	18214	3559	21.6	-2.9
-463.27	1108.28	-7277.89	1201.21	23322	3580	85.9	-1.9
-464.18	639.5	-7467.06	790.2	20287	3606	76.9	-3.5
-1067.48	252.96	-7380	1097.04	20664	3610	51.5	-2.7
-964.86	-79.53	-7397.78	968.13	20741	3626	54.3	-3.5
-927.37	353.85	-7288.42	992.58	18933	3641	61.8	-3.7
-388.95	810.91	-7369	899.36	20706	3647	269.5	-3.6
-518.43	743.55	-7365	906.44	19809	3647	70.1	-3.6
-183.69	1134.81	-7353.79	1149.58	19302	3647	40.9	-3.4
-214.26	1114.76	-7423.13	1135.16	21302	3655	48.2	-2.9
3.89	946.34	-7331.2	946.35	21978	3702	70.8	-3.1
-464.44	665.09	-7318.95	811.2	19530	3708	81	-2.9

-686.4	651.56	-7379.83	946.4	23790	3720	103.9	-2.9
-645.68	563.76	-7328.5	857.16	21262	3724	110.5	-2.5
-694.26	550.58	-7441.2	886.08	23742	3728	107	-2.5
-729.72	473.75	-7332.04	870.02	23025	3728	73.9	-3.2
113.1	1266.09	-7318.98	1271.13	21013	3760	33.6	-3.1
73.58	1167.26	-7340.07	1169.58	19519	3810	44.6	-3.1
-504.02	814.86	-7360.42	958.14	22614	3818	66.8	-3
-421.97	780.92	-7334.18	887.63	23263	3840	106	-3.4
-628.14	583.36	-7337.61	857.24	21899	3850	76	-3.5
-479.27	802.97	-7414.44	935.13	23506	3853	98.5	-2.1
-476.95	760.54	-7387.52	897.72	19718	3890	71.5	-3.8
-754.11	449.95	-7421.29	878.14	22052	3893	105.1	-1.4
-662.74	689.01	-7319	956.01	23327	3893	65.1	-2.6
-101.36	1110.43	-7342.06	1115.05	20490	3917	89.4	-2.6
-899	243.23	-7334.35	931.32	19923	3928	68.2	-3.4
-703.8	496.02	-7334.85	861.03	23282	3933	110.8	-0.6
82.94	1161.85	-7526.03	1164.81	22009	3965	41.4	-2.8
82.56	1542.42	-7332.29	1544.63	21773	3990	87.1	-2.4
-217.19	833.71	-7406.09	861.54	20465	4034	63.8	-3.6
-400.21	892.75	-7356.34	978.35	22966	4038	97.6	-2.5
-519.08	866.99	-7378.95	1010.5	20245	4042	58.8	-3.3
-112.1	1157.18	-7335.7	1162.6	22763	4047	45.7	-3.2
-764.24	497.39	-7425.14	911.84	23360	4051	103.9	-3
-737.72	222.25	-7334.98	770.47	19283	4066	87.4	-3.8
-1008.31	502.76	-7296.67	1126.7	19443	4066	42.7	-3.3
-333.11	1073.84	-7331.27	1124.32	23619	4098	92.8	-2.6
-338.44	1074.77	-7332.7	1126.8	23619	4098	-57.5	-2.6
-901.61	186.34	-7341.06	920.66	19543	4109	71.9	-2.9
-817.64	349.49	-7351.14	889.2	20109	4129	109.9	-3.6
-60.28	1362.16	-7328.29	1363.49	20346	4163	65.5	-1.4
-122.87	1258.53	-7351.81	1264.51	22316	4163	78.6	-1.2
-135.28	1337.62	-7348.75	1344.44	20535	4178	26.2	-2.9
-874.6	376.07	-7335.56	952.03	23502	4222	102	-2
-990.63	434.17	-7367.67	1081.6	20513	4222	31.2	-2.8
-65.3	936.13	-7369.22	938.4	20626	4264	67.5	-3.2
-940.41	95.92	-7342.78	945.29	20721	4294	70.5	-3.3
-271.21	1206.57	-7329.26	1236.68	19850	4311	27.7	-3.3
-731.8	538.3	-7329.25	908.46	20848	4324	71.3	-3.5
-905.21	236.82	-7349.22	935.68	19263	4327	67.6	-3.5
-694.34	-224.73	-7366.71	729.8	19340	4327	167.9	-4.2
-959.66	321.21	-7348.8	1011.99	19639	4337	60.9	-3.6
-794.49	551.59	-7294.59	967.19	23488	4351	104.7	-2.4
-713.44	567.22	-7323.26	911.45	23016	4351	67.7	-3.3
-720.47	548.62	-7323.73	905.57	23048	4371	109.2	-2.5
-901.32	240.41	-7327.97	932.83	21449	4371	68	-3.3

-291.91	922.1	-7489.48	967.2	22281	4383	61.2	-2.9
-459.72	896.67	-7333.29	1007.65	23589	4383	100.4	-2.8
-833.1	571.88	-7363.14	1010.5	22512	4392	101.1	-2.5
-423.53	959.15	-7346.84	1048.5	22769	4409	55.3	-3.2
-725.08	531.82	-7425.23	899.21	20880	4435	66.9	-3.5
-229.92	1110.04	-7404.21	1133.6	22035	4446	46.8	-3.1
-26.86	968.96	-7316.31	969.33	19285	4455	64.9	-3.2
-544.57	879.17	-7369.19	1034.16	22097	4482	58.2	-2.9
107.13	1415.43	-7383.54	1419.48	20570	4528	73.1	-2.8
-497.93	842.53	-7325.78	978.67	22231	4537	100.7	-2.7
-545.06	603.32	-7384.94	813.07	22099	4541	271.4	-3.2
-402.22	678.33	-7431.88	788.61	20482	4541	78	-3.6
-554.46	611.37	-7445.19	825.35	22127	4541	75.7	-3.2
-597.28	697.96	-7350.06	918.64	21591	4584	104.3	-3.1
-764.03	416.84	-7334.49	870.34	21402	4594	108.5	-3.2
-344.27	865.17	-7319.97	931.15	20610	4626	106.9	-3.1
-446.07	876.07	-7341.46	983.1	21968	4646	62.8	-3.1
-757.11	396.53	-7408.13	854.66	21279	4669	73.9	-3.4
-797.95	480.7	-7302.65	931.56	20588	4669	69.7	-3.6
99.21	938.23	-7320.33	943.46	21144	4675	69.4	-3.3
-207.17	1222.67	-7382.98	1240.1	22104	4679	38.1	-3.2
-392.56	811.04	-7468.79	901.05	21129	4688	68.8	-2.7
3.96	928.21	-7297.46	928.22	20800	4703	68.8	-3.3
-262.16	745.65	-7477.31	790.39	20474	4703	80	-3.5
-62.58	239.39	-7287.11	247.43	18724	4714	132.9	-5
-11.32	1190.87	-7301.9	1190.92	23076	4721	41.2	-3.1
-544.61	621.62	-7348.82	826.45	20893	4724	80.8	-3.4
-364.79	1040.21	-7306.94	1102.32	23088	4730	94.3	-2.7
489.9	1020.39	-7393.32	1131.9	21020	4734	43.6	-3.1
-561.83	763.28	-7357.61	947.76	23345	4737	106.7	-2.5
-222.9	1137.53	-7282.94	1159.16	20299	4737	40.9	-3
-104.12	1701.91	-7324.35	1705.09	22615	4753	53.1	-2.3
-1017.75	94.15	-7318.63	1022.1	23031	4771	98.7	-2.1
-432.14	843.52	-7340.77	947.77	23521	4779	102.8	-2.8
-225.17	1044.35	-7325.59	1068.35	22451	4789	58.7	-3.3
-568.54	932.32	-7331.11	1092	21614	4793	56.3	-3.1
-467.34	833.29	-7354.74	955.39	19291	4807	60.7	-3.6
289.05	1691.48	-7282.39	1716	21184	4814	55.2	-1.9
337.54	1677.48	-7288.09	1711.1	21232	4814	-95.8	-1.9
-808.12	524.08	-7383.52	963.18	19598	4862	59.9	-3.6
-296.39	387.06	-7391.96	487.51	19154	4871	107.9	-3.8
-401.77	535.98	-7390.2	669.85	19751	4871	98.4	-3.3
-276.92	-30.25	-7276.94	278.57	19130	4871	135.4	-4.4
-466.53	1142.38	-7362.05	1233.97	21475	4881	34.7	-2.9
-497.78	851.46	-7410.39	986.29	23527	4881	99.3	-2

-951.79	335.29	-7281.02	1009.12	22268	4887	99.7	-3.1
-938.72	-262.27	-7371.06	974.67	20952	4929	98.8	-2.8
-373.43	1016.81	-7334.72	1083.21	19101	4936	118.8	-2.8
-697.9	751.36	-7377.11	1025.48	18230	4936	289.5	-3.2
-666.77	630.6	-7342.08	917.74	21606	4965	107.4	-3
-343.35	1050.32	-7374.49	1105.02	23262	4977	92.4	-2.5
-270.21	1068.75	-7343.3	1102.38	20885	4986	53.1	-3.1
-259.17	350.28	-7290.51	435.74	20253	4994	347.4	-3.7
-435.41	943.71	-7367.54	1039.31	21981	4997	58	-2.9
-497.46	841.96	-7298.57	977.94	22692	5001	63.8	-3
361.68	1041.38	-7355.48	1102.4	19237	5021	49.3	-3.5
-351.21	946.08	-7391.73	1009.17	19042	5029	54.3	-3.2
-1052.78	82.82	-7302.98	1056.03	19626	5036	131	-2.6
-596.65	670.32	-7403.61	897.4	20984	5069	65.7	-3.5
-965.61	-29.26	-7393.78	966.05	21048	5073	64.1	-3.4
342.93	947.44	-7336.44	1007.59	19045	5082	62.7	-3.3
-365.12	744.34	-7416.07	829.07	22393	5082	322.8	-2.4
-719.8	585.86	-7383.69	928.09	21142	5115	98.8	-2.6
-719.16	514.08	-7392.03	884.01	20425	5124	68.4	-3.4
-903.79	259.1	-7339.43	940.2	22177	5135	104.1	-2.6
-670.05	89.47	-7282.41	676	21761	5139	122	-2.8
-272.48	1498.4	-7564.94	1522.97	22205	5139	-2.9	-2.9
-973.81	36.17	-7298.95	974.48	20073	5139	68.4	-3.3
-697.34	600.1	-7357.54	920	19481	5150	64.4	-3.6
-687.59	640.7	-7309.28	939.83	22374	5161	104.3	-2.8
233.91	1448.44	-7419.17	1467.21	21933	5171	11.1	-2.6
-863.61	327.43	-7343.85	923.6	23514	5178	106.3	-1.3
-409.18	1238.75	-7370.91	1304.58	22705	5222	80.3	-2.4
317.24	938.91	-7316.48	991.06	20979	5226	63.4	-3.1
-681.39	355.02	-7318.09	768.33	21095	5226	85.3	-3.1
-177.66	1145.12	-7425.47	1158.82	22578	5232	87.8	-2.2
-603.22	742.18	-7318.93	956.4	22412	5250	106	-2.5
-945.41	232.68	-7390.68	973.62	23393	5250	95.8	-3
-432.58	825.59	-7392.66	932.05	18065	5260	68	-3.5
-804.57	207.86	-7336.37	830.99	21136	5266	79.9	-3.4
-788.59	423.98	-7397.47	895.34	22685	5293	107.2	-3.2
-552.98	771.32	-7301.07	949.06	22661	5300	101.4	-3.7
-885.41	-383.64	-7352.29	964.95	22083	5304	59	-3.4
-285.04	1050.03	-7332.65	1088.03	23617	5304	92.1	-2.2
-1028.18	98.45	-7362.03	1032.88	23440	5309	97.5	-2.1
-784.93	869.18	-7384.45	1171.15	20927	5312	89.5	-0.7
-627.26	655.82	-7333.29	907.5	21273	5318	108.6	-0.4
72.33	1204.22	-7355.46	1206.39	20276	5343	46.5	-3.2
-509.38	736.58	-7445.28	895.55	22244	5357	104	-3
-513.03	916.47	-7338.81	1050.29	21539	5394	53.9	-3.2

-290.86	701.27	-7538.21	759.2	22116	5397	79.7	-2.8
-499.31	779.18	-7318.05	925.44	20434	5403	101.1	-2.9
-282.07	1073.63	-7380.46	1110.07	21509	5403	53.9	-3.1
-668.43	703.38	-7419.17	970.33	22669	5421	100.5	-3.1
-837.79	356.21	-7393.44	910.37	19482	5421	71.2	-3.3
-595.63	591	-7281.97	839.08	20621	5429	74.5	-3.3
-717.63	739.84	-7370.96	1030.71	21964	5435	59.1	-3.1
-977.02	34.03	-7306.76	977.61	18517	5440	101.1	-3
-1034.92	371.25	-7369.87	1099.49	21336	5469	95.3	-2.9
44.09	1595.46	-7353.83	1596.07	20904	5495	-3	-3.2
-259.68	23.91	-7274.46	260.78	18342	5495	136	-5
-750.76	522.07	-7309.72	914.44	23472	5515	105.2	-2.8
-1002.8	243.52	-7415.9	1031.94	23384	5520	57.8	-2.9
-418.31	944.85	-7340.73	1033.31	22935	5525	96.9	-2.6
-1001.46	153.4	-7521.69	1013.14	21075	5533	50.2	-3.3
-869.49	437.31	-7283.06	973.27	21014	5539	63.3	-3.4
-713.02	594.59	-7301.71	928.4	23055	5543	105.3	-2.8
-717.93	813.83	-7333.9	1085.24	22124	5556	85.1	-2.5
56.74	1608.02	-7319.25	1609.02	22733	5561	64.3	-2
63.97	1674.28	-7291.56	1675.5	21968	5561	-91.8	-2
-931.02	394.77	-7347.78	1011.26	20693	5566	61.7	-3.1
-277.56	1084	-7354.4	1118.97	22529	5570	49.4	-3
-357.56	628.65	-7344.61	723.22	19021	5576	88.6	-3.6
-535.73	562.35	-7375.29	776.69	18988	5596	80.5	-3.7
79.59	1193.94	-7378.72	1196.59	21830	5600	39.9	-3.2
-530.48	906.72	-7294.89	1050.5	20077	5604	93	-3.3
-793.23	400.24	-7326.28	888.49	23466	5618	109.7	-2.2
-950.92	-11.51	-7369.44	950.99	20678	5618	64.3	-3.1
-902.08	216.01	-7363.93	927.58	22026	5627	69.2	-3.2
-705.34	803.5	-7427.62	1069.17	21129	5649	57	-3.3
-138.69	1222.75	-7369.52	1230.59	21600	5664	78.3	-2.4
-1202.33	-147.45	-7341.54	1211.34	23590	5680	87.8	-2
-339.25	1021.75	-7366.72	1076.6	19746	5693	54	-3.1
-21.14	1627.1	-7403.75	1627.24	22776	5698	65.7	-1.9
-739.62	852.39	-7369.59	1128.54	18604	5712	9.4	-3.5
-998	109.02	-7377.37	1003.94	20301	5732	57.2	-3.4
208.4	1703.07	-7301.57	1715.77	22590	5737	48.4	-2.3
-9.55	1170.35	-7295.14	1170.39	19519	5737	45.5	-3.1
-300.3	925.54	-7392.49	973.04	22355	5754	142.7	-2.7
-297.2	917.88	-7391.42	964.8	22494	5754	-8.3	-2.7
-1105.92	-303.78	-7298	1146.88	22249	5754	85.3	-3.2
-858.09	406.61	-7333.08	949.55	22865	5761	104.8	-1.5
-1025.96	373.17	-7389.17	1091.72	23521	5771	205.1	-2.7
-1020.75	365.94	-7387.77	1084.36	23514	5771	53.9	-2.8
-180.12	1380.1	-7332.06	1391.8	22635	5779	74.5	-0.7

-172.02	1381.42	-7333.51	1392.09	22649	5779	-75.3	-0.7
-841.98	482.01	-7346.36	970.19	19895	5787	61	-3.4
-755.94	520.69	-7363.97	917.91	19795	5793	60.4	-3.9
-364.16	814.36	-7381.28	892.07	18882	5793	71.9	-3.7
-399.97	1023.94	-7318.72	1099.29	22618	5808	94.5	-1.6
-240.36	1097.18	-7306.75	1123.2	21121	5819	51.5	-2.8
-597.96	776.22	-7373.15	979.83	21945	5826	57.8	-3.3
-382.06	941.18	-7287.02	1015.77	23518	5826	100.2	-2.1
-420.86	1019.63	-7296.24	1103.07	23628	5826	-56.3	-2
-844.79	194.33	-7341.78	866.85	23564	5838	112.4	-2.5
-849.27	215.09	-7384.49	876.08	22659	5838	111.8	-2.5
-694.42	679	-7347.52	971.22	23478	5847	67.1	-3.2
-766.63	777.64	-7440.74	1091.99	22755	5859	91.5	-3.1
-1127.32	141.18	-7355.27	1136.13	20098	5864	50.8	-2.5
-991.31	23.52	-7360.38	991.59	21753	5884	100.8	-3.3
127.27	1351.63	-7374.31	1357.61	22451	5901	19.4	-2.7
143.31	1616.05	-7440.76	1622.39	18530	5912	0.6	-2.4
-223.87	949.73	-7286.48	975.76	21477	5920	64.5	-3.5
-579.33	801.43	-7328.83	988.9	20391	5920	93.2	-3.1
30.25	1212.26	-7356.75	1212.64	19140	5937	29.2	-3.4
-1050.62	37.73	-7341.83	1051.3	23473	5944	98	-2.6
-1076.86	-126.47	-7330.19	1084.26	20069	5955	56.2	-3.2
-118.76	1489.78	-7363.55	1494.51	21415	5960	6.6	-2.9
-205.97	1103.6	-7354.79	1122.66	18621	5963	51.1	-3
-464.4	966.21	-7351.91	1072.02	21532	5977	55.5	-3.2
-941.1	290.54	-7394.69	984.93	19409	5986	58.6	-3.3
161.24	1672.4	-7343.5	1680.15	22599	5997	-6.9	-2.4
-329.01	1176.45	-7356.55	1221.59	23371	5997	83.5	-2.3
-1006.46	166.95	-7320.38	1020.21	22814	6008	100.5	-2.3
-276.28	1131.55	-7392.03	1164.79	22637	6013	87.4	-2.9
-78.16	1245.55	-7318.92	1248	22569	6020	85.2	-1.4
-109.31	1291.95	-7381.93	1296.57	22953	6020	-67.3	-1.4
-377.8	635.51	-7464.76	739.33	21027	6020	81.2	-3.5
-422.12	1297.4	-7336.82	1364.34	20279	6030	26.1	-3.1
-12.85	1424.74	-7379.84	1424.8	20893	6030	305.2	-3
-599.33	824.23	-7356.67	1019.09	23436	6050	97.6	-2.1
-593.09	694.6	-7333.47	913.36	18831	6060	109.5	-3.3
-381.78	1082.71	-7351.08	1148.05	19718	6070	44.7	-3.3
-1051.14	54.07	-7315.3	1052.53	19624	6094	90.3	-3.1
-486.7	867.03	-7360.63	994.29	22125	6098	98.6	-2.6
-473.24	-312.29	-7286.09	566.99	22641	6101	166.3	-2.3
-471.67	-311.09	-7286.61	565.02	22649	6101	16.4	-2.3
-1020.15	82.04	-7356.22	1023.44	22298	6112	322	-3
-986.06	141.24	-7352.99	996.12	22785	6112	99.8	-3
-914.59	587.19	-7375.83	1086.86	19611	6119	93.7	-3.1

43.01	1251	-7359.91	1251.74	22127	6123	82.5	-2.8
25.33	1709.76	-7290.95	1709.95	20133	6168	56.6	-2.4
22.67	1712.95	-7296.41	1713.1	19760	6168	-94.4	-2.4
-658.66	597.53	-7430	889.31	21935	6188	104.7	-3
169.72	1577.44	-7386.63	1586.54	21542	6203	-4.5	-2.7
-499.98	864.18	-7306.78	998.39	21248	6211	96.7	-2.9
-1009.5	208.89	-7480.27	1030.89	21582	6214	52.6	-2.9
-606	563.7	-7324.17	827.64	23674	6222	113.7	-0.3
-1316.1	-186.04	-7362.22	1329.18	19684	6249	80.6	-3.1
-698.84	677.38	-7327.03	973.25	19762	6262	65.6	-3.6
-683	587.02	-7332.52	900.6	21879	6270	69.7	-3.2
-939.98	-75.06	-7387.31	942.97	19674	6295	67.4	-3.3
-961.23	-63.66	-7335.01	963.34	20599	6303	105	-2.8
298.36	1288.49	-7323.02	1322.58	20636	6306	22.5	-3.4
-764.13	376.37	-7278.64	851.79	20266	6340	79.6	-3.2
-1103.39	-7.78	-7375.65	1103.42	23268	6343	94.2	-2.1
-316.93	1101.46	-7209.2	1146.15	21246	6349	85.2	-2.6
-338.47	986.01	-7359.83	1042.49	21023	6352	53.1	-3.2
-553.83	804.26	-7327.06	976.5	22294	6357	103	0.5
-553.16	805.89	-7326.95	977.47	23027	6357	-47.7	0.5
324.33	1528.29	-7262.1	1562.33	18848	6399	-62.4	-2.7
-611.45	740.94	-7366.85	960.66	23391	6415	103.3	-2.9
-851.05	190.76	-7333.57	872.17	18515	6432	76.3	-3.7
-849.58	182.64	-7283.85	868.99	18198	6451	75.6	-3.7
-1742.7	-828.25	-7373.9	1929.51	22752	6469	44.2	-2.5
-974.51	-202.23	-7292.82	995.27	21482	6469	101.2	-3.4
-150.54	1561.1	-7330.52	1568.34	22079	6478	65.5	-1.4
36.83	1572.62	-7334.6	1573.05	21899	6478	-85.3	-1.4
-243.02	918.95	-7290.49	950.54	19218	6501	312.8	-3.6
-937.82	445.94	-7359.41	1038.45	20774	6508	51.2	-3.4
-834.4	509.92	-7349.1	977.88	18590	6517	105.8	-3.6
-573.92	892.95	-7347.11	1061.48	23496	6521	97.3	-2.6
-579.12	566.04	-7417.44	809.8	22731	6536	116	-2.7
-957.91	58.53	-7319.41	959.7	23259	6540	106.5	-2.8
-879.23	92.56	-7360.15	884.09	20673	6540	69.9	-3.7
-698.17	651.89	-7293.73	955.2	19741	6551	99.3	-3
-1053.49	-124.21	-7501.12	1060.79	22977	6574	89.8	-2.4
-404.9	705.69	-7397.03	813.6	19298	6588	78.9	-3.2
-1010.23	-386.39	-7379.84	1081.6	22139	6593	84.4	-3.1
-1061.53	-175.11	-7393.67	1075.88	20420	6593	-36.2	-3.5
-1059.04	-239.77	-7311.41	1085.84	21242	6601	96.4	-3
-456.58	874.51	-7382.64	986.53	23633	6612	101.3	-2.5
-1121.97	-52.3	-7318.93	1123.19	21588	6615	94.2	-2.2
-683.01	775.41	-7390.67	1033.33	23175	6622	94.5	-2.6
-864.6	-79.31	-7511.25	868.23	22686	6627	110.3	-2

-1111.36	-80.95	-7257.83	1114.3	20413	6627	49.3	-2.7
-158.42	944.35	-7333.69	957.55	19687	6641	67.2	-3.3
-484	910.32	-7373.05	1030.99	19054	6645	54.2	-3.2
-1216.11	-10.1	-7342.27	1216.15	18179	6648	41.4	-3.4
-1069.25	-84.75	-7350.35	1072.6	23267	6656	96.9	-1.2
-699.18	643.61	-7296.15	950.31	23010	6682	105	-1.8
-1096.24	-53.69	-7307.39	1097.55	20439	6691	92.5	-1.8
-1091.63	-52.14	-7299.11	1092.87	21447	6691	-54.4	-1.9
137.5	862.38	-7294.97	873.27	21794	6694	152.2	-3.3
28.61	1041.7	-7328.3	1042.09	21381	6705	57.8	-3.2
-507.61	618.91	-7390.83	800.45	21519	6709	112.9	-3.2
-961.09	123.97	-7277.35	969.05	19390	6715	60.8	-3
381.52	1042.12	-7381.08	1109.76	21828	6719	48.1	-2.9
-1140.25	-338.67	-7353.19	1189.48	21721	6725	86.4	-3
-471.2	870.87	-7336.64	990.17	21833	6749	60.9	-2.9
-429.73	869.15	-7322.18	969.58	21116	6753	59.8	-3.5
-913.68	52.9	-7294.58	915.21	21331	6758	107.9	-3
-580.9	934.79	-7347.69	1100.58	18481	6775	44.7	-3.3
-264.6	754.96	-7502.09	799.99	21188	6775	75	-3.2
-897.24	98.65	-7278.04	902.65	23252	6778	107.3	-2.2
-393.9	1014.26	-7419.03	1088.06	22048	6788	52.1	-2.7
-709.29	599.06	-7372.26	928.42	23142	6788	70.6	-2.7
107.7	1482.88	-7421	1486.79	22594	6793	75.6	-1.8
-108.2	1469.89	-7420.72	1473.87	23004	6793	-74.8	-1.8
-1020.12	-206.17	-7405.88	1040.75	20663	6800	56.4	-2.9
-550.74	911.45	-7378.3	1064.92	22846	6814	93.9	-1.7
-718.7	572.92	-7335.84	919.11	23667	6825	107	-0.5
-632.61	907.89	-7340.83	1106.55	20013	6845	52.1	-3.1
-671.98	781.24	-7414.32	1030.48	23747	6877	97.8	-2.3
-433.48	1079.86	-7326.23	1163.62	22879	6884	88	-2.6
-403.49	994.36	-7333.06	1073.11	22264	6884	-54.9	-2.7
-509.81	851.32	-7425.23	992.3	23753	6891	98.9	-2.5
-368.74	837.62	-7416.39	915.19	20549	6898	67.3	-3.2
-687.12	595.36	-7376.49	909.17	18151	6918	66.1	-3.6
-974.62	220.52	-7393.84	999.26	21400	6924	56.9	-3.5
-245.17	1176.44	-7347.21	1201.72	19768	6935	39.6	-3.2
-9.58	985.63	-7375.09	985.68	20775	6939	59.3	-3.5
-1043.4	48.46	-7366.55	1044.52	21252	6943	59.4	-3
-456.29	864.18	-7464.91	977.24	23538	6943	62	-3
-599.49	868.82	-7340.87	1055.57	23768	6949	97.5	-2.1
-1187.66	-104.34	-7330.06	1192.23	22515	6957	89.7	-1.7
-931.56	329.14	-7416.39	988	19087	6962	97.4	-3.3
-1184.72	-107.43	-7274.22	1189.58	19972	6967	76.9	-3
-177.35	876.69	-7294.74	894.45	19496	6967	60.2	-3.3
-835.74	403.71	-7342.74	928.14	23486	6970	106.9	-1.8

-1121.07	-62.02	-7284.94	1122.78	21414	6983	87.6	-2.9
-524.82	778.06	-7328.25	938.52	23574	6994	106.1	-2.1
-495.3	846.13	-7379.18	980.44	22192	7002	64.3	-3.4
-971.35	91.53	-7325.48	975.65	20037	7016	62	-3.6
-617.65	767.81	-7326.85	985.41	20956	7021	65.5	-3.2
-1086.98	-291.36	-7336.9	1125.35	21509	7037	47.8	-3.3
-665.35	332.36	-7317.83	743.74	21140	7041	65.5	-3.7
-919.12	30	-7313.34	919.61	22890	7041	102.4	-2.7
-1152.13	-101.92	-7316.56	1156.63	21876	7052	90	-2.3
-543.05	767.91	-7368.41	940.53	22490	7063	103.6	-2.8
-501.22	901.77	-7333.57	1031.7	23614	7066	95.9	-2.3
-565.27	736.19	-7474.61	928.17	22236	7066	98.7	-2.1
-573.55	837.57	-7377.08	1015.13	23715	7080	96.1	0.1
-515.38	777.61	-7387.4	932.9	23132	7105	107.2	-1.6
438.15	1023.47	-7369.38	1113.31	22652	7154	67.1	-2.6
-1150.58	-116.27	-7290.76	1156.44	22837	7163	91.1	-1.8
-1148.27	-116.12	-7291.36	1154.13	22838	7163	-58.9	-1.8
-508.62	198.4	-7337.96	545.95	19725	7173	105.7	-4.2
-372.91	791.65	-7440.98	875.08	23621	7178	72.8	-2.7
-431.48	636.93	-7477.28	769.32	23441	7188	114.4	-1.2
-997.58	40.46	-7306.73	998.4	22992	7204	103.8	-1.7
-249.95	1017.73	-7381.93	1047.97	22106	7212	100.6	-2.6
-416.49	956.79	-7379.51	1043.51	22031	7218	56	-3.3
-402.22	1033.28	-7329.73	1108.81	22628	7218	52.9	-2.7
-524.8	878.92	-7426.33	1023.68	20653	7227	60.4	-3
-293.53	1147.81	-7322.83	1184.75	23415	7235	43.7	-2.8
-611.28	793.2	-7342.83	1001.41	23067	7235	100.6	-2.7
-540.69	839.31	-7306.75	998.39	23656	7249	100.5	-2.3
-994.78	-156.83	-7393.56	1007.07	21625	7249	61.4	-2.3
-504.38	879.44	-7355	1013.81	22750	7262	61.3	-3.1
-441.2	1009.29	-7414.79	1101.51	23023	7262	46.6	-2.8
-536.78	776.89	-7328.58	944.29	23624	7268	106.1	0.5
-727.26	524.82	-7418.58	896.85	22024	7279	106.7	-2
-680.6	623.95	-7331.09	923.33	20778	7279	-9.1	-3.1
-497.01	797.8	-7321.98	939.95	23002	7297	106.8	-2.5
-553.01	812.17	-7336.65	982.57	23612	7311	103.3	-0.4
-662.09	776.92	-7381.55	1020.77	22955	7316	57.8	-1.6
-675.35	636.77	-7403.91	928.21	23048	7316	105.2	-1.3
-899.73	95.78	-7318.99	904.81	23562	7316	-20.3	-2.6
-186.98	127.56	-7287.03	226.35	20506	7347	253.8	-4.5
146.39	518.32	-7366.54	538.6	20089	7353	129.8	-3.9
-752	619.49	-7426.67	974.31	23645	7359	272.9	-2.4
-499.41	834.14	-7422.3	972.21	22894	7359	101.1	-2.4
-913.47	289.36	-7329.1	958.2	22057	7363	104	-1.2
-347.18	655.4	-7491.03	741.68	20790	7382	81.7	-3.1

-538.47	774.94	-7329.94	943.65	23230	7389	104.6	-0.7
-605.37	749.91	-7459.7	963.76	22203	7410	210.3	-2.9
-604.23	759.38	-7455.88	970.44	22216	7410	61.8	-2.9
-301.54	937.62	-7396.39	984.92	22999	7418	63.1	-2.9
-803.39	470.68	-7295.73	931.11	19275	7423	67.2	-3.4
-584.82	690.42	-7331.11	904.82	19918	7438	68.9	-3.3
-549.27	883.11	-7331.13	1039.99	20249	7455	60.2	-3
162.16	1586.05	-7343.04	1594.32	22019	7459	-2.6	-2.9
63.93	1504.57	-7357.8	1505.93	19891	7471	4.6	-3.2
-963.32	165.49	-7390.41	977.43	19464	7476	64.1	-3
-479.49	880.43	-7344.27	1002.53	19388	7500	62.3	-3.1
-554.67	809.02	-7334.08	980.9	23635	7508	103.8	-0.8
-756.71	-365.44	-7327.72	840.33	21425	7535	78.1	-3.2
-450.73	910.58	-7359.01	1016.03	20105	7546	61.4	-3.5
-12.12	221.4	-7276.33	221.73	19918	7546	91.9	-5.1
-898.87	306.92	-7425.32	949.82	19616	7558	100.2	-3.5
120.54	1314.27	-7344.82	1319.79	22397	7570	79.9	-2.1
-561.84	918.31	-7357.03	1076.55	21696	7599	56.2	-3
-667.1	650.6	-7374.02	931.83	23714	7611	107.1	-1.8
-810.95	471.02	-7379.04	937.82	21637	7611	161.3	-1.7
-666.58	651.21	-7374.47	931.88	23699	7611	-42.9	-1.8
-811.27	467.87	-7381.96	936.52	21640	7611	11.3	-1.7
-25.7	1556.06	-7384.18	1556.27	22339	7614	64.7	-2.4
-391.8	1008.11	-7304.5	1081.57	23711	7622	95.3	-2.4
-631.12	732.91	-7318.94	967.2	23178	7633	97.4	-2.6
-585.51	747.54	-7335.26	949.55	22897	7637	106.2	-2.9
-1004.68	19.5	-7408.56	1004.87	22882	7644	54.8	-3.2
-377.3	1171.22	-7329.14	1230.49	19379	7644	39.2	-3.1
-342.19	927.77	-7422.34	988.86	22184	7649	93.7	-3.4
-75.83	1664.96	-7413.24	1666.69	21312	7667	-7.8	-2.8
-660.21	613.9	-7327.09	901.53	19823	7679	74.3	-4
-267.47	-7.58	-7284.17	267.58	19956	7684	138	-4.9
-1004.58	252.26	-7322.09	1035.77	19839	7691	57.9	-3.6
-1149.74	-255.34	-7347.17	1177.75	20661	7710	89.5	-3.2
-1079.88	-49.57	-7354.88	1081.02	23087	7725	97	-0.1
-273.74	1106.23	-7322.25	1139.6	21824	7760	45.8	-3.3
-77.65	237.22	-7282.36	249.61	18589	7760	405.3	-4.9
-421.05	877.32	-7364.08	973.13	20816	7772	61.4	-3.2
-20.37	452.78	-7350.56	453.24	20285	7772	119.7	-3.9
233.69	1720.15	-7293.88	1735.95	21534	7775	56.5	-1.6
-453.28	823.17	-7378.22	939.72	23600	7779	102	-2.5
-901.66	40.81	-7469.06	902.58	21673	7804	66.6	-3.4
-193.4	1124.06	-7355.79	1140.58	20921	7839	40.6	-3.2
-624.02	654.49	-7329.57	904.3	23714	7859	72.5	-3
-658.07	632.25	-7303.74	912.58	22401	7864	105	-2.1

-575.07	744.2	-7351.36	940.5	18867	7877	367.7	-3.8
-273.72	50.71	-7285.13	278.38	19740	7892	133.1	-4.6
-907.26	402.71	-7388.4	992.62	23093	7914	98.9	-2.9
-935.85	106.59	-7440.48	941.9	22659	7930	328.1	-3.5
-1009.93	-68.99	-7370.64	1012.28	20936	7993	58.8	-2.5
-1367.73	-216.27	-7299.46	1384.72	20593	7998	76	-3.3
-369.97	957.7	-7293.06	1026.68	19157	8003	52.6	-3.4
-586.85	854.58	-7335.86	1036.68	23215	8013	92.1	-2.3
-413.37	659.97	-7298.01	778.74	19862	8054	84.9	-3.6
98.6	911.87	-7379.74	917.19	21728	8054	104.7	-3.1
-391.44	827.38	-7341.46	915.3	23359	8060	105	-2.4
-1033.98	-111.66	-7306.75	1039.99	18075	8072	59.7	-3.5
-1016.94	-100.45	-7334.66	1021.89	21353	8084	61.8	-3.2
326.6	1322.89	-7337.86	1362.61	19744	8105	25.1	-2.9
301.65	1826.46	-7258.02	1851.2	22216	8116	49.5	-1
228.9	1906.65	-7333.05	1920.34	22234	8116	-109.1	-1
-361.23	828.87	-7323.06	904.16	19265	8129	71.3	-3.4
-589.96	763.62	-7357.93	964.97	21612	8129	66.6	-2.9
-595.32	720.21	-7344.76	934.4	23661	8144	104.8	-2.8
-847.53	366.38	-7337.35	923.33	20668	8170	321.5	-3.5
-937.52	305.42	-7320.22	986.01	18832	8170	64.5	-3.4
-848.63	363.63	-7338.94	923.25	21152	8170	105	-3.5
-595.66	719.12	-7352.09	933.78	21963	8177	103.5	-2.9
44.66	1101.5	-7282.42	1102.41	20668	8177	48.5	-3
-51.4	578.6	-7290.96	580.88	18800	8191	99.6	-4.1
-403.31	879.45	-7405.35	967.52	22958	8202	103	-2.5
-313.9	1155.48	-7368.6	1197.36	23118	8208	87.8	-2.2
-600.47	670.9	-7358.78	900.37	21569	8208	104.1	-3.3
-424.69	819.16	-7356.31	922.71	18379	8212	68.7	-3.4
-161.01	1746.61	-7412.54	1754.02	22232	8216	55.2	-2.5
-924.45	95.13	-7326.31	929.33	23709	8220	107.7	-0.5
-898.11	371.73	-7346.6	972	20730	8243	134.5	-2.7
-1135.64	-82.83	-7268.6	1138.66	23279	8252	94.4	-1.1
-1034.12	-81.41	-7297.3	1037.32	22200	8259	100.7	-1.9
-402.32	1079.2	-7385.69	1151.75	22198	8265	89.6	-2.2
-469.6	833.64	-7294.61	956.81	21548	8277	99.2	-2.6
-483.19	859.87	-7316.03	986.33	21539	8277	-53.5	-2.6
344.61	977.08	-7332.45	1036.07	19525	8286	60.4	-3.4
-810.51	296.95	-7318.92	863.2	23544	8317	111	-0.9
-908.89	-276.71	-7399.58	950.08	20262	8327	65	-3.5
-404.08	903.34	-7357.2	989.6	22986	8330	101	-2.7
-404.55	828.91	-7326.74	922.36	21025	8337	71.2	-2.9
-577.51	775.01	-7387.63	966.52	22736	8337	54.3	-2.7
-572.08	765.65	-7330.41	955.77	23480	8337	105.4	-2.1
-489.89	808.56	-7366.06	945.39	22128	8355	103.3	-2

-550.79	782.37	-7331.11	956.8	22927	8365	102	-2.2
-595.56	798.55	-7325.59	996.18	22137	8365	95.6	-2.4
-960.75	-81.98	-7301	964.24	21786	8375	103.9	-1
-964.17	-84.43	-7301.53	967.86	21752	8375	-46.2	-1
-202.18	1173.17	-7289.46	1190.46	22795	8386	87.3	-2.2
-718.7	634.47	-7341.3	958.69	19543	8391	71.1	-3.2
-396.02	831.2	-7333.72	920.72	18887	8419	67.1	-3.3
-813.1	493.45	-7278.14	951.12	19473	8419	63.1	-3.5
-1110.4	-83.07	-7369.43	1113.5	18272	8435	38.2	-3.2
-1062.49	-136.82	-7281.03	1071.26	21736	8463	95.3	-1.8
-263.33	1007.37	-7323.35	1041.22	20737	8471	60.8	-3.3
-989.71	-92.97	-7333.25	994.07	21721	8481	101.8	-3.1
-1074.59	9.49	-7356.98	1074.63	22746	8492	49.4	-3.1
-655.65	537.03	-7295.31	847.51	21695	8505	67.8	-3.7
-879.74	338.46	-7282.72	942.6	20567	8509	62.8	-3.6
-884.6	312.65	-7343.7	938.23	20261	8522	67.3	-3.1
-929.53	431.48	-7336.02	1024.79	19278	8538	57.9	-3.7
-609.21	776.05	-7383.62	986.61	19910	8546	-54.9	-3
-827.42	-21.3	-7282.09	827.69	19297	8555	77	-3.8
-950.42	105.08	-7304.17	956.21	21289	8583	65	-3.3
-1109.29	-401.21	-7374.85	1179.62	21218	8595	80	-2.8
-416.02	1110.48	-7325.62	1185.85	22647	8602	79.1	-1.8
-366.02	1120.34	-7324.03	1178.61	22663	8602	-72.8	-1.8
-822.78	344.33	-7378.46	891.92	23665	8609	97.8	-2.7
-513.34	874	-7339.26	1013.6	23386	8612	99.8	-2.1
-599.64	811.24	-7294.57	1008.8	22836	8623	101.2	-1.8
-413.98	853.96	-7299.42	949.01	22085	8627	104.2	-3
-1181.34	-167.41	-7331.27	1193.14	21906	8635	89.5	-1.5
-439.23	979.78	-7330.53	1073.73	22974	8638	93.7	-2.2
-1195.41	-57.11	-7381.95	1196.77	22788	8645	81	-2.4
-150.49	1008.03	-7513.86	1019.2	23027	8661	100	-2.6
-106.93	1494.54	-7327.86	1498.36	22378	8667	5.9	-2.7
-918.23	60.19	-7295.98	920.2	20193	8676	96.9	-3.3
-614.82	701.94	-7413.22	933.13	23492	8691	104	-2.7
-1023.7	-142.35	-7381.82	1033.55	22875	8703	100.2	-2.3
-459.52	786.24	-7411.19	910.68	20599	8703	67.6	-3
-545.07	769.62	-7307.81	943.09	18685	8708	67.4	-3.5
57.94	1245.36	-7378.8	1246.71	21906	8708	30.8	-3.1
-859.12	-106.79	-7420.15	865.73	21403	8716	73.9	-3.4
-1062.04	-139.85	-7306.79	1071.21	21805	8716	54.3	-2.9
-474.26	1021.16	-7377.43	1125.92	22737	8725	50.1	-2.7
-922.98	-77.09	-7296.45	926.19	21217	8740	97.9	-3.2
-636.92	708.86	-7354.81	952.97	20458	8744	62.9	-3.4
-1202.77	-31.52	-7279.04	1203.18	22063	8751	43.7	-3
-826.83	604.5	-7341.5	1024.24	19950	8787	53.6	-3.4

-33	1177.01	-7364.3	1177.47	21125	8792	44.1	-3
-10.47	1744.37	-7336.98	1744.4	18979	8810	-23.8	-2.9
-666.62	697.21	-7391.78	964.62	22780	8815	103.4	-2.2
-749	837	-7318.95	1123.2	20333	8819	50	-3.1
-517.21	936.57	-7364.24	1069.89	19763	8819	54	-3.2
-525.55	967.36	-7319.37	1100.9	22387	8846	93.3	-2.3
-411.09	1010.97	-7397.13	1091.35	23487	8850	90.4	-0.8
-364.1	1084.51	-7331.14	1144	23235	8865	84.1	-1.6
-76.94	1646.66	-7371.53	1648.46	23027	8875	52.7	-2.2
-738.05	23.45	-7274.4	738.42	20031	8886	119.3	-3.2
-458.42	792.12	-7270.18	915.21	19984	8903	70.2	-3.1
302.33	1873.94	-7291.23	1898.17	21143	8914	48	-2.4
-455.67	923.31	-7320.34	1029.63	22377	8919	57.9	-3
-597.99	863.96	-7346.98	1050.72	20272	8924	90.2	-3
-791.75	351.87	-7402.73	866.42	22059	8929	75.7	-3
-1018.53	-3.24	-7300.15	1018.54	22589	8949	56.4	-3.3
-370.51	192.25	-7375.25	417.42	19089	8982	106	-4.7
-1135.92	-83.05	-7315.38	1138.95	21368	8987	92.1	-2.5
-445.61	901.59	-7367.13	1005.7	23193	8987	318.9	-2.7
-103.11	1212.42	-7452.94	1216.8	19329	9015	35.6	-3.5
-214.66	1081.29	-7343.3	1102.39	20404	9019	50.4	-3.3
-609.55	559.64	-7389.52	827.5	21158	9047	74.6	-3.3
-1050.84	-86.06	-7326.56	1054.36	21052	9094	98.5	-2.2
-617.7	717.38	-7398.07	946.67	23629	9094	99.5	-3
-987.47	-322.03	-7340.8	1038.65	18936	9108	57.7	-3.4
-538.15	906.21	-7473.99	1053.96	19734	9124	53.3	-3.6
-440.48	946.2	-7344.58	1043.7	23263	9132	92.8	-3
-748.4	554.39	-7319.4	931.37	22378	9142	69.5	-3.4
-1097.24	-202.61	-7294.03	1115.79	19737	9158	90.8	-3.2
-289.83	1023.52	-7427.17	1063.76	19562	9197	50.9	-3.4
-1358.21	-284.01	-7340.46	1387.59	23049	9210	75.1	-2.2
-1133.68	-33.74	-7318.12	1134.18	22985	9221	89.7	-3.1
-291.4	70.29	-7295.16	299.76	22027	9247	138.7	-4
-84.27	1224.54	-7361.05	1227.44	19363	9255	31.5	-3.4
-886.88	169.98	-7330.53	903.02	22673	9277	105.7	-3.1
-924.46	137.42	-7341.33	934.62	22991	9282	107.7	-2.5
-712.03	-184.26	-7360.23	735.49	18757	9307	85.9	-3
-138.81	630.51	-7302.61	645.61	20114	9324	61.8	-4
-525.36	48.7	-7328.58	527.61	18330	9347	109.2	-4.2
-422.79	898.58	-7329.58	993.07	23491	9360	101.6	-2
-975.1	-72.97	-7306.42	977.83	21216	9377	103.1	-2.4
-842.51	411.44	-7363.06	937.61	21041	9388	69.4	-3.4
-979.4	-79.3	-7288.69	982.61	21495	9391	103.6	-1
-452.01	703.77	-7324.49	836.42	22185	9428	75.9	-3.2
-17.78	1495.56	-7370.78	1495.67	22222	9428	12.2	-2.7

45.75	1128.53	-7373.36	1129.46	18289	9432	230.3	-3.5
581.7	1839.66	-7522.92	1929.44	22124	9447	52.9	-2.6
-219.21	1037.92	-7294.57	1060.82	21180	9487	52.1	-3.5
-912.75	66.9	-7294.6	915.2	21088	9505	104.4	-3
-497.3	1057.05	-7432.08	1168.19	21476	9514	43.4	-2.8
-76.16	1177.34	-7372.64	1179.8	22993	9514	43.2	-2.5
-933.05	71.72	-7361.65	935.8	19551	9524	59.6	-3.8
-392.54	-58.7	-7279.03	396.9	20560	9575	125	-4.5
-1070.14	157.04	-7355.47	1081.6	22860	9607	95.1	-2.3
-231.1	1243.05	-7337.19	1264.35	22555	9676	82.8	-2.3
-372.13	572.7	-7339.12	682.98	22055	9690	93.7	-3.8
-991.04	14.74	-7322.37	991.15	22478	9695	66.5	-2.2
-836.08	92.36	-7286.57	841.17	21022	9700	112.2	-3.1
-1148.03	-120.96	-7331.14	1154.38	22055	9712	90	-2
-1274.74	-146.45	-7327.23	1283.12	23010	9722	80	-1.5
-1142.43	-73.39	-7378.41	1144.78	23471	9741	50.5	-2.8
-1093.14	-139.64	-7316.88	1102.02	21993	9769	95.2	-1.6
-1051.96	98.44	-7380.81	1056.56	20555	9788	47.9	-3.2
-336.24	1150.53	-7368.46	1198.66	23478	9801	87.8	-2.5
-689.38	636.11	-7317.67	938.02	23170	9806	105.3	-1.6
-664.62	595.8	-7325.16	892.58	23805	9810	109.3	-0.5
-926.21	-138.2	-7317.08	936.46	21851	9845	106.8	-1.8
-708.94	651.62	-7321.38	962.91	23210	9850	105.8	-2.4
75.8	1464.91	-7394.42	1466.87	22299	9853	14.1	-2.8
-341.1	1164.44	-7361.1	1213.37	23621	9879	83.5	-2
-570.08	623.45	-7354.26	844.8	21592	9892	66	-3.6
-872.2	300.59	-7338.96	922.54	19361	9916	68	-3.6
-825.05	-7.03	-7404.88	825.08	21866	9928	73	-3.9
-1069.97	48.22	-7262.79	1071.06	20703	9931	54.2	-3.3
-548.33	840.25	-7330.16	1003.34	21387	9938	57.6	-3.6
-613.47	822.01	-7360.23	1025.69	22851	9946	55.5	-2.8
-1005.47	-47.18	-7336.55	1006.58	21206	9954	93	-3.1
-718.25	819.71	-7374.96	1089.87	21152	9960	51	-3.3
-342.88	1301.6	-7339.19	1346	22386	9969	78.3	-2.2
-342.98	1303.15	-7331.8	1347.53	23116	9969	-72.6	-2.2
-490.03	857.4	-7363.11	987.55	23056	9996	63.8	-3.3
-267.98	1108.76	-7327.55	1140.68	21926	10005	47.4	-3.3
-851.24	-151.29	-7278.25	864.58	22462	10016	110.7	-2.1
-1161.04	-83.01	-7328.63	1164	21922	10044	86.9	-2.8
-211.19	-197.17	-7413.18	288.92	21800	10050	139.2	-4.8
-995.99	-122.86	-7315.29	1003.54	20374	10050	62.4	-3.4
-353.83	1102.54	-7372	1157.92	23299	10069	88.6	-1.3
-375.26	1157.49	-7343.3	1216.8	22990	10069	-63.4	-1.3
-486.5	902.46	-7379.89	1025.24	20933	10080	306.5	-3.6
329.11	1139	-7355.46	1185.59	20598	10080	38.3	-3.2

-432.74	974.02	-7329.67	1065.82	20885	10088	54.2	-3
-607.22	743.12	-7344.06	959.66	21074	10113	103	-3.3
-662.21	678.07	-7288.66	947.79	21350	10137	101.1	-2.8
-741.03	542.56	-7366.06	918.42	21900	10145	105.4	-3.4
-604.69	662	-7349.57	896.6	20052	10145	5.2	-3.9
-65.16	1212.85	-7323.79	1214.6	19932	10183	39	-3.5
-935.49	10.28	-7419.85	935.55	20925	10186	62.6	-3.4
14.77	1412.09	-7325.89	1412.17	19274	10211	73.7	-1.8
107.01	1287.44	-7422.38	1291.88	20541	10221	31.7	-3
142.88	1109.74	-7408.2	1118.9	22865	10239	83.4	-2.9
-934.17	99.94	-7338.39	939.5	19782	10250	66.1	-3.6
-845.94	-153.44	-7332.34	859.74	18642	10255	71.8	-3.6
-816.9	482.82	-7412.36	948.92	22477	10287	64.3	-3.4
-814.59	491.21	-7296.92	951.23	22642	10305	104.6	-3.1
-140.17	1483.29	-7431.15	1489.9	21193	10329	11.9	-3.3
-718.76	199.47	-7375.04	745.93	23309	10376	119.4	-3.3
-257.58	1063.61	-7342.03	1094.36	23411	10384	88.9	-2.7
-747.79	369.94	-7339.46	834.29	23466	10405	112.7	-1.4
-908.06	196.22	-7272.21	929.02	19420	10465	69.8	-3.6
-252.25	1093.13	-7318.16	1121.86	23346	10465	90.5	-2.3
-173.86	1417.78	-7329.94	1428.4	23339	10472	18.1	-2.3
-641.43	652.13	-7478.2	914.72	22815	10472	62.9	-3.1
-472.89	927.93	-7348.72	1041.48	22987	10489	94.7	-2.7
-799.26	550.7	-7382.26	970.61	21466	10496	100.5	-3.5
-780.95	-54.97	-7364.87	782.88	19658	10510	79	-4.1
101.59	1468.33	-7334.37	1471.84	23062	10549	15.1	-3
-326.34	948.41	-7505.4	1002.99	22594	10553	96.4	-2.7
-888.74	-95.67	-7414.41	893.87	20937	10556	67.4	-3.5
-1007.99	-17.61	-7373.06	1008.14	21894	10571	100.7	-2.8
-1075.04	-210.88	-7294.64	1095.53	21824	10581	94.5	-2.5
-975.2	-102.11	-7379.85	980.53	20006	10601	62.1	-3.4
-892.52	280.68	-7341.73	935.61	22955	10626	108.2	-2.6
-918.23	176.24	-7337.46	934.99	23552	10626	-41.8	-2.6
-949.42	-72.24	-7398.21	952.16	22174	10629	62.8	-3.3
-939.93	143.47	-7362.72	950.82	22246	10629	102.7	-3
-1015.9	-701.24	-7358.79	1234.42	22512	10636	76.6	-2.5
77.47	1528.79	-7362.51	1530.75	22344	10639	59.2	-2.8
-891.07	-113.33	-7291.52	898.25	23244	10647	108.3	-2.3
-434.13	960.93	-7332.23	1054.45	20842	10707	59.4	-2.9
163.94	1923.15	-7387.18	1930.12	21089	10712	40.8	-2.4
-1010.26	-153.45	-7292.29	1021.85	21881	10715	97.6	-2.6
-424.43	-192.57	-7294.75	466.07	19323	10719	115.6	-4.5
118.22	1145.7	-7385.05	1151.78	19037	10719	39.8	-3.3
170.45	1220.85	-7421.61	1232.69	22638	10736	36.2	-2.4
-177.75	1298.27	-7318.92	1310.38	23269	10740	76.5	-1.9

-287.38	-37.4	-7322.71	289.8	21133	10743	135	-4.2
-624.07	710.47	-7335.81	945.64	20828	10748	69.8	-3.1
-865.91	-67.74	-7318.13	868.56	23402	10761	108	-2.1
-753.36	-24.23	-7302.39	753.75	20846	10783	88.1	-3.4
-948.83	126.11	-7333.17	957.17	21935	10807	63.9	-3.4
-1427.35	-270.88	-7319	1452.83	21883	10812	15.2	-2.7
410.9	1666.07	-7331.13	1715.99	23135	10821	56.6	-1.9
374.29	1578.64	-7331.11	1622.4	23136	10821	-88.7	-2
-264.03	1155.83	-7318.91	1185.6	23227	10834	88.8	-1.2
-275.36	1198.08	-7333.85	1229.32	23397	10834	-64.3	-1.2
-1044.84	-139.09	-7286.99	1054.06	21596	10881	98.9	-2.5
306.01	1548.93	-7362.79	1578.87	22655	10903	-0.2	-2.7
-890.45	350.26	-7318.76	956.86	20771	10909	63.7	-3.3
-777.3	43.32	-7412.08	778.51	19542	10929	81.8	-3.5
-362.91	862.79	-7294.59	936.01	19435	10934	72.2	-3.4
-700.4	375.27	-7385.46	794.6	19637	10956	239	-4.1
-1177.77	-185.23	-7235.82	1192.25	22689	10962	87.7	-2.6
-353.8	791.72	-7325.65	867.18	19497	10966	73.7	-3.5
-468.62	894.92	-7360.01	1010.19	23076	10974	92.1	-2.9
-203.08	1168.8	-7292.77	1186.31	22716	11018	86.9	-2.4
-1148.83	-215.88	-7333.58	1168.94	20029	11024	88.1	-3.4
-155.89	1303.74	-7328.94	1313.03	22399	11067	74.9	-3
-507.09	807.31	-7346.59	953.36	23802	11136	106.3	-2.6
-309.06	612.89	-7331.12	686.41	21241	11142	93.6	-3.1
-862.92	-37.49	-7312.46	863.73	20239	11156	112.1	-2.7
-242.01	1247.76	-7362.9	1271.01	23300	11159	81.7	-2.6
-571.29	756.39	-7365.33	947.89	19101	11184	353.2	-3.1
-700.2	878.23	-7416.41	1123.2	22953	11197	50	-2.9
-626	670.15	-7344.09	917.05	21208	11207	104.5	-3.2
-287.18	296.28	-7283.68	412.62	20822	11207	121.2	-4.1
-1050.69	69.18	-7293.36	1052.96	22925	11213	57.6	-2.9
-1067.97	-25.3	-7329.86	1068.27	23318	11222	95.4	-1.8
-827.96	389.99	-7342.4	915.21	21955	11237	-10	-3.3
-675.01	67.46	-7335.74	678.37	19047	11237	97.8	-4.1
-683.01	95.84	-7319.76	689.7	23569	11242	124.2	-3.1
102.55	1087.33	-7368.22	1092.16	18443	11264	53	-3
-1040.53	-183.53	-7344.24	1056.59	19139	11281	53.7	-3.5
-163.79	1181.76	-7333	1193.06	21925	11293	89	-1.7
-1157.44	100.04	-7315.51	1161.76	19526	11324	39.6	-3.4
-1154.74	143.71	-7364.07	1163.65	23426	11327	90.1	-3.1
-11.8	427.93	-7345.21	428.09	21270	11384	119.7	-4.3
40.73	761.62	-7297.45	762.71	20035	11390	86.6	-3.2
-444.9	1056.41	-7364.47	1146.27	22162	11403	45.9	-2.8
-217.8	1078.9	-7318.41	1100.66	20848	11424	91.3	-2.4
-471.05	806.19	-7322.66	933.72	23334	11482	106	-3.1

-318.93	8.57	-7345.27	319.05	19945	11497	131.1	-4.4
-438.28	920.5	-7357.28	1019.51	21165	11530	94.2	-3.1
-509.44	815.28	-7376.04	961.36	20399	11533	64.6	-3.4
-1075.39	-389.31	-7386.49	1143.69	22417	11533	81.3	-3.1
-761.54	108.42	-7297.37	769.22	20986	11546	87.9	-3.7
-216.07	946.35	-7290.16	970.7	21471	11577	63.5	-3.3
-68.68	1463.35	-7389.4	1464.96	22395	11601	21.2	-2.5
-971.74	179.01	-7382.81	988.09	23776	11612	58.8	-3
-17.23	1652.48	-7429.33	1652.57	22766	11631	49.9	-2.3
-537.3	795.62	-7285.99	960.05	18973	11662	64.6	-3.5
17.49	1185.47	-7367.83	1185.6	20829	11695	43.2	-3.4
-599.8	-247.63	-7278.72	648.91	19532	11707	97.1	-4
-560.35	875.01	-7403.35	1039.05	21438	11763	54.8	-3.6
-623.06	767.43	-7429.56	988.51	19862	11793	62.4	-3.6
-433.92	866.78	-7346.62	969.33	22780	11796	63	-3.3
-321.79	1076.12	-7331.13	1123.2	23337	11869	82.9	-2.9
-709.52	325.58	-7325.19	780.65	21127	11879	73	-3.7
-231.38	874.72	-7379.85	904.8	19436	11879	68.4	-3.6
-645.95	-255.93	-7385.13	694.8	18807	11879	218.9	-3.9
-528.01	417.68	-7329.52	673.24	22033	11895	121.8	-3.8
-638.56	-355.07	-7340.61	730.64	21450	11939	80.5	-3.7
-1072.57	-228.18	-7291.82	1096.57	19142	12014	94.9	-3.2
-938.1	-155.51	-7478.82	950.9	19842	12026	64.3	-3.6
-670.83	566.39	-7387.3	877.96	21576	12049	75.9	-3.1
-587.76	877.49	-7340.19	1056.15	22245	12099	59.6	-3.1
-332.65	1148.8	-7318.92	1195.99	21283	12129	79.5	-2.8
-1032.44	212.29	-7365.37	1054.04	21079	12140	98.9	-2.8
5.97	1401.34	-7383.04	1401.35	20833	12148	18.4	-2.8
-1048.64	39.15	-7326.02	1049.37	19222	12157	59.2	-3.3
-620.64	768.74	-7294.59	988.01	23223	12188	93.6	-2.6
22.36	1170.9	-7420.33	1171.11	20527	12211	38.9	-3.4
-1205.05	-168.72	-7294.56	1216.8	19317	12211	85.5	-3.4
-279.49	1198.95	-7326.74	1231.1	22449	12249	29.5	-3.3
-695.8	827.42	-7373.14	1081.09	23606	12302	94.8	-2.8
-1115.03	-156.01	-7329.84	1125.89	23371	12311	92.3	-2
-926.82	-114.45	-7350.04	933.86	19850	12323	106.4	-3.7
-825.49	687.48	-7365.45	1074.27	22797	12331	53.3	-3.4
-277.28	627.45	-7311.25	685.99	18388	12345	96.1	-3.3
217.89	1512.03	-7357.59	1527.65	21106	12360	2.9	-2.6
-78.74	1169.69	-7413.07	1172.34	19725	12397	35.1	-3.3
-407.69	809.24	-7395.09	906.13	21383	12426	71.4	-3.5
-1047.98	532.2	-7366.51	1175.37	22698	12463	87.2	-2.1
-1117.09	-136.6	-7318.03	1125.41	21483	12466	93.9	-2.5
-1138.32	-142.24	-7369.62	1147.17	23182	12519	90.1	-2.5
-938.1	450.83	-7413.72	1040.81	22907	12529	98.7	-1.8

-1004.97	-118.46	-7380.58	1011.93	23077	12533	99.8	-1.4
-1006.93	-123.02	-7381.31	1014.42	23092	12533	-49.5	-1.4
-443.53	950.53	-7365.45	1048.92	22938	12561	79.2	-2.4
-438.26	889.1	-7302.77	991.25	22037	12561	99.6	-2.2
-297.48	1145.41	-7375.18	1183.41	22001	12629	44.4	-3.2
-1189.33	147.15	-7351.09	1198.4	19772	12644	31.6	-3.3
-849.78	397.69	-7323.79	938.23	22968	12706	60.1	-3.3
-714.11	83.77	-7353.54	719.01	20725	12714	94.5	-3.7
-796.62	-153.83	-7456.19	811.34	22880	12774	108.1	-2.9
-888.92	329.22	-7408.35	947.93	21267	12799	61.7	-3.4
-985.11	165.61	-7423.54	998.93	23241	12831	58.6	-3.1
-1191.34	-122.49	-7382.41	1197.62	22224	12841	84.9	-2.8
63.08	1223.41	-7434.73	1225.04	19800	12878	30.6	-3
418.64	1251.88	-7404.31	1320.02	22239	12928	72.7	-2.6
-659.55	165.95	-7347.55	680.11	22044	12942	125.4	-3.3
-1000.9	-101.75	-7339.77	1006.06	18875	12964	61.4	-3.3
-610.25	-238.49	-7282.43	655.2	19563	12970	96.3	-4.4
-366.93	1029.11	-7334.31	1092.57	22470	12988	93.3	0.2
-361.36	1013.69	-7336.25	1076.17	22463	12988	-55.3	0.1
-135.54	1219.68	-7367.64	1227.19	23636	13025	81.5	-2.5
-659.42	-28.12	-7284.95	660.02	19766	13061	92.7	-4.1
-711.56	620.45	-7338.03	944.07	23611	13067	106.2	1.1
-713.38	621.25	-7331.47	945.97	23578	13067	-44.3	1.1
92.98	1095.66	-7385.27	1099.6	19675	13152	51.6	-3.2
450.68	2053.4	-7256.89	2102.28	22669	13180	38.6	-1.6
465.54	2056.44	-7256.48	2108.48	23088	13180	-110.6	-1.6
-444.16	1021.73	-7332.59	1114.1	21652	13211	44.5	-3.1
-1171.25	-275.91	-7292.03	1203.31	22957	13216	89.4	-2.4
-667.6	864.35	-7324.61	1092.15	20804	13224	95.1	-3.4
-615.73	730.66	-7450.98	955.5	20862	13247	96.7	-2.8
534.04	2512.68	-7635.66	2568.8	22232	13253	23.1	-2.2
-47.05	1286.11	-7342.6	1286.97	23147	13266	70.3	-2.6
-665.81	368.12	-7394.29	760.8	23222	13282	119	-3.2
-901.9	-62.84	-7413.29	904.09	22768	13285	109.3	-2.7
235.65	1789.64	-7247.28	1805.09	20060	13332	-21.7	-2.8
-967.24	7.07	-7294.98	967.27	22807	13337	99.6	-1.7
-118.16	1447.69	-7412.69	1452.5	20842	13366	16.2	-2.9
-972.2	-66.33	-7426.17	974.46	23260	13399	102.3	-2.3
-218.2	1093.37	-7356.88	1114.93	19031	13406	51	-3.7
-915.5	-194.84	-7294.57	936	22095	13520	106.3	-2.7
-517.42	1005.54	-7359.24	1130.86	22840	13557	341.9	-2.6
-464.6	963.22	-7379.16	1069.41	22378	13557	93.4	-2.3
-900.29	345	-7370.23	964.13	19494	13577	104.3	-3.5
-447.59	1336.04	-7389.64	1409.02	21979	13601	16.3	-3.2
-677.02	822.92	-7314.59	1065.62	20772	13626	52.3	-3.7

-598.67	708.62	-7343.52	927.66	23141	13652	289.3	-2.9
-605.41	714.79	-7344.97	936.72	22610	13652	105.2	-2.9
-702.99	593.92	-7412.53	920.29	20348	13652	62.1	-3.7
-319.01	786.76	-7420.04	848.98	18742	13660	67.7	-3.8
-466.93	815.49	-7322.55	939.71	22896	13673	98.4	-3.3
-374.74	1374.53	-7388.64	1424.7	22273	13706	17.3	-2.5
-821.4	326.68	-7501.63	883.98	23382	13706	104.9	-3.2
-296.95	1141.81	-7375.88	1179.79	21335	13749	39.9	-3.2
-980.46	51.29	-7295.98	981.8	22051	13753	103.6	-2.9
-856.98	-107.06	-7450.9	863.64	19767	13774	71.9	-3.6
-993.73	-90.52	-7430.95	997.84	23584	13814	99.5	-2.6
-761.44	449.11	-7306.65	884.02	22707	13814	71.5	-2.8
-893.02	63.6	-7295.49	895.28	23331	13829	108.6	-1.9
-230.69	563.82	-7292.6	609.19	19763	13836	102.3	-3.7
-875.89	82.88	-7300.47	879.8	21697	13842	76.7	-3
-846.07	57.63	-7352.04	848.03	18650	13855	77.6	-3.9
-233.08	1205.18	-7368.7	1227.51	19960	13930	36.2	-3.3
-270.09	983.33	-7295.4	1019.75	21841	13966	59.8	-2.7
-301.65	1307.01	-7413.16	1341.37	20415	13966	27.9	-3.1
-574.06	912.37	-7394.9	1077.94	21113	13982	45.2	-3.6
-207.56	1549.77	-7338.58	1563.61	20074	14037	58.3	-2.7
-33.72	1497.18	-7343.37	1497.56	22919	14054	64.5	-2
-999.59	143.62	-7294.64	1009.85	23576	14062	62.5	-2.6
26.45	2291.96	-7231.92	2292.11	23345	14066	-62.1	-2.4
-73.21	1472.65	-7339.01	1474.47	22634	14076	69	-0.9
-68.16	1485.63	-7343.29	1487.19	23017	14076	-80.7	-0.9
-120.2	1459.36	-7334.64	1464.3	21645	14076	8.7	-1.9
-131.19	1403.46	-7339.49	1409.58	21835	14090	75.5	-2.1
-1206.56	-292.74	-7334.98	1241.56	18277	14113	84.1	-3.1
-709.37	702.57	-7306.76	998.4	22867	14148	65.7	-1.9
-56.98	1192	-7419.28	1193.36	21109	14175	94.2	-1.6
-141.57	1397	-7347.3	1404.15	21353	14237	74.1	-0.9
-119.81	1131.63	-7473.45	1137.95	21300	14237	-55.9	-1.1
-95.81	1248.81	-7396.32	1252.48	20924	14246	35.3	-2.5
-779.16	-114.27	-7302.05	787.49	21739	14252	86.5	-3.7
-79.2	1374.98	-7372.36	1377.26	22480	14351	76.9	-1.6
-827.91	-192.74	-7466.4	850.05	20936	14363	106.7	-2.9
-505.49	719.73	-7350.26	879.51	21185	14383	68.6	-3.6
117.51	1367.48	-7423.12	1372.52	21925	14451	20.9	-2.9
-79.03	1396.2	-7381.21	1398.43	22289	14451	23.1	-2.5
-1220.76	-100.69	-7331.12	1224.91	22733	14600	83.3	-2.5
-742.76	676.61	-7320.21	1004.74	19780	14640	58.2	-3.7
-232.95	1079.2	-7379.29	1104.06	22496	14793	48.4	-2.9
-536.66	365.56	-7289.5	649.34	23193	14793	98.5	-3.7
-452.33	424.97	-7331.84	620.65	23110	14819	127	-1.7

-451.12	462.89	-7297.2	646.36	23186	14824	125.1	-2.3
-585.02	217.11	-7331.12	624.01	20917	14824	99.4	-3.3
-452.6	419.03	-7321.55	616.79	23576	14834	104.2	-3.4
-857.26	554	-7336.9	1020.69	20521	14881	57.2	-3.4
-315.37	971.53	-7353.57	1021.43	19113	14897	49.1	-3.3
-795.92	-233.12	-7227.07	829.36	20967	14919	108.9	-3.8
-307.29	1190.04	-7352.56	1229.07	19845	14949	39.7	-3
64.54	251.86	-7355.48	260	20454	14968	138.7	-4.7
-705.19	186.3	-7290.77	729.38	19376	15024	112.8	-3.1
-839.21	-190.61	-7298.63	860.58	22852	15105	109.9	-2.8
-1073.39	59.65	-7367.49	1075.05	20742	15238	48.2	-3.4
-573.59	934	-7338.89	1096.07	22969	15238	92.1	-2.6
-396.85	1029.65	-7295.09	1103.48	19378	15312	54.5	-3.3
-194.56	835.82	-7452.44	858.17	23200	15416	110.4	-2.7
-922.84	-202.3	-7282.75	944.75	19880	15450	105.9	-2.7
-978.67	-247.58	-7333.39	1009.5	20345	15450	99.7	-3
-713.55	753.37	-7392.81	1037.65	21877	15456	57.7	-3.6
-327.29	805.9	-7358.56	869.82	21884	15493	69.5	-3.4
-183.35	1171.34	-7318.9	1185.6	23019	15502	89.6	-1.1
-628.89	250.64	-7316.2	677	21612	15543	120.9	-3.8
-995.51	-95.51	-7349.09	1000.08	19331	15563	63.3	-3.4
-518.25	-140.36	-7369.54	536.92	19989	15563	109.3	-4.3
-105.11	1316.62	-7343.28	1320.81	21563	15568	81.1	-2.4
-702.04	146.66	-7283.5	717.2	19765	15581	92.8	-4.3
-201.33	1185.4	-7327.05	1202.38	23382	15613	41.3	-1.9
-163.78	1330.36	-7337.18	1340.4	19998	15634	77.3	-1.4
-241.87	1087.59	-7398.93	1114.16	22360	15640	47.8	-2.9
-342.02	988.8	-7340.1	1046.28	23522	15690	95.1	-2.6
-87.2	272.33	-7281.74	285.95	20901	15834	138.7	-4.7
-865.22	77.3	-7299.83	868.67	21182	15843	71.9	-4
-1076.71	-243.7	-7479.8	1103.94	21549	15847	87	-2.1
-456.39	887.68	-7348.57	998.13	23364	15861	102.2	-1.8
-208.33	963.19	-7341	985.46	22126	15902	62.5	-3.5
-902.46	-165.37	-7342.47	917.49	23387	15909	109	-1.5
-901.96	-164.47	-7342.53	916.83	23383	15909	-41	-1.5
-52.92	1204.53	-7362.19	1205.69	21586	15943	40.3	-3
339.81	1180.78	-7391.84	1228.7	19645	15947	33.4	-3.6
-414.98	-331.76	-7350.63	531.29	18808	15959	111.8	-4.1
-158.27	1073.45	-7376.46	1085.05	21423	15967	54.2	-3.5
-719.34	-171.08	-7366.98	739.4	21225	15974	87.3	-3.6
-796.17	-215.44	-7381.44	824.8	21701	16035	108.4	-3
-912.51	-151.11	-7342.79	924.94	21938	16045	105.6	-2.7
-951.41	-149.04	-7363.02	963.01	20662	16051	65.1	-3.6
-385.21	599.51	-7334	712.6	20337	16060	91.5	-4.1
-137.04	1332.73	-7344.63	1339.76	21011	16070	17.3	-2.8

-457.38	603.4	-7330.7	757.16	21025	16124	108.8	-3.1
165.09	1093.04	-7367.01	1105.44	21176	16152	47.6	-2.8
-1004.36	249.04	-7334.48	1034.78	23035	16159	99	-3.2
-981.07	262.93	-7318.63	1015.69	21160	16167	101.5	-2.6
-771.35	-83.42	-7407.24	775.85	23807	16186	85.6	-2.8
-991.08	179.7	-7478.8	1007.24	22700	16198	97.2	-2.9
-595.62	246.99	-7331.12	644.8	22532	16208	126.4	-1.6
-878.45	-152.08	-7390.03	891.52	22949	16211	107.8	-2.6
-24.43	1402.56	-7339.12	1402.77	23112	16244	66.1	-1.8
-220.59	1301.37	-7367.13	1319.93	23064	16244	-75.4	-1.9
-534.15	625.97	-7347.7	822.89	21608	16267	84.2	-3.6
-258.12	-31.23	-7282.42	260	22183	16304	137.9	-4.6
-793.42	-406.34	-7345.02	891.42	20645	16338	76	-3.2
-753.89	52.42	-7377.1	755.71	19114	16380	86	-4
-947.6	314.47	-7294.59	998.42	22955	16552	102.4	-3.3
114.96	1373.12	-7373.3	1377.92	23512	16655	25	-2.8
-304.24	1100.77	-7342.95	1142.04	23823	16750	86	-2.1
-436.49	-16.76	-7245.83	436.81	20362	16823	115.5	-4.8
-624.06	-118.84	-7329.66	635.27	23701	16913	124.7	-2.6
-254.42	1394.9	-7336.94	1417.91	22517	16922	73.6	-1.6
-255.6	1408.4	-7334.52	1431.41	22028	16922	-76.3	-1.6
-595.58	-150.27	-7351.63	614.24	23757	16962	128.3	-3.2
-125.86	1378.21	-7325.17	1383.94	22745	17000	70.1	-2.3
-619.74	-94.01	-7372.39	626.83	23521	17053	125.8	-3.6
-629.05	-114.23	-7325.69	639.34	23573	17059	128.9	-1.1
-618.78	-95.87	-7331.49	626.16	22082	17092	127.7	-2.4
-253.46	1193.64	-7335.05	1220.25	22959	17310	79.4	-2.2
-610.61	-144.5	-7331.22	627.47	23338	17315	127.5	-2.9
-549.12	2.59	-7324.24	549.13	21333	17315	250.8	-2.9
-587.77	-140.16	-7315.52	604.25	23742	17315	-21.5	-2.9
-581.26	-36.36	-7318.94	582.4	21385	17315	100.2	-2.8
-269.41	1087.92	-7348.12	1120.78	22925	17319	91	-2.3
-570.39	-82.37	-7335.78	576.31	22621	17452	107.4	-4.2
-592.86	-111.64	-7347.48	603.28	22288	17488	130.3	-2
-347.05	1021.58	-7412.92	1078.92	23347	17518	91	-2.5
-686.59	-312.28	-7338.11	754.27	18153	17548	136.1	-2.9
-1126.73	-179.89	-7288.54	1141	23245	17588	91.4	-2.8
-453.89	970.29	-7306.69	1071.2	23324	17592	51.7	-3.2
-473.78	1077.01	-7380.26	1176.61	20541	17604	35.3	-3.2
-378.71	224.63	-7401.49	440.32	20611	17618	117.9	-4.7
-1099.14	-210.16	-7324.86	1119.05	23736	17638	92.7	-0.7
-228.2	286.29	-7295.11	366.11	18757	17710	132.9	-4.2
-664.91	593.18	-7344.82	891.05	23706	17713	108.6	-2.1
-563.77	786.88	-7341.06	968	21640	17742	63.2	-3.5
-725.83	-194.87	-7406.35	751.53	19647	17765	118.4	-3.5

-785.21	1082.37	-7347.92	1337.19	22747	17777	30.4	-2.9
-722.94	-54.4	-7303.3	724.98	20274	17780	114.2	-2.2
-787.03	434.37	-7359.7	898.94	21178	17798	92.7	-2.5
-560.08	676.76	-7309.35	878.46	22796	17798	76.6	-2.7
-385.98	706.03	-7350.32	804.65	20094	17801	81.7	-3.1
-810.49	52.64	-7338.68	812.2	18513	17815	78.4	-3.9
-633.53	-91.91	-7382.08	640.16	22349	17827	125.2	-2.2
-595.73	711.72	-7301.96	928.14	23054	17831	108.6	-1.9
-409.58	1041.28	-7337.56	1118.94	21218	17857	92.8	-3.1
-650.96	263.56	-7305.33	702.29	23264	17865	118.5	-0.5
-837.13	36.85	-7316.31	837.94	23076	17876	112.5	-2.5
-604.63	45.07	-7295.29	606.31	21413	17919	126.7	-4
-542.08	-23.47	-7277.21	542.59	20191	17948	130.3	-4
-579.99	91.47	-7280.29	587.16	23549	18007	128.3	-3.7
-272.45	1213.3	-7318.83	1243.51	20623	18127	32.5	-3.3
-422.29	933.73	-7323.08	1024.78	21800	18199	51.1	-3.6
-438.35	691.93	-7323.88	819.1	23694	18234	113.2	-1.1
-423.8	599.73	-7314.52	734.36	21807	18291	117.6	-3.4
-422.36	647.03	-7299.74	772.68	20987	18304	85.2	-3.8
-262.19	-7.75	-7241.77	262.3	20159	18331	142.1	-4.2
192.23	1600.5	-7440.76	1612	23099	18422	-2.1	-1.9
-610.98	102.7	-7343.24	619.55	21325	18494	101.5	-4.2
-1148.38	-103.1	-7342.18	1153	21385	18559	67.4	-3.2
-609.22	254.42	-7294.47	660.21	23813	18616	122.9	-2.3
-174.32	1212.29	-7349.4	1224.76	19731	18621	39.3	-2.9
214.09	1275.8	-7402.25	1293.64	21083	18654	23	-3.5
-606.42	434.54	-7363.05	746.04	19843	18676	89.7	-3.5
-550.98	-116.71	-7514.17	563.21	20539	18696	111.5	-3.9
-861.89	86.28	-7281.53	866.2	20268	18717	74.3	-3.6
-800.18	32.45	-7294.55	800.84	23539	18762	113	-1.6
-588.42	-104.02	-7351.48	597.54	21839	18769	130.6	-3.1
-553.21	-221.28	-7349.52	595.82	20694	18793	128.8	-3.6
-569.48	-108.03	-7327.89	579.64	21315	18863	108.3	-4
-223.74	1029.87	-7317.93	1053.89	22596	18891	56.3	-2.9
-886.2	-11.76	-7355.72	886.28	22447	18931	102.4	-3.3
-776.51	23.94	-7306.27	776.88	23118	18941	117.1	-2.6
-291.58	1147.43	-7175.66	1183.9	23781	18979	93.7	-2.3
-482.04	849.45	-7287.24	976.69	22511	18983	102.1	-3.4
-742.31	-327.1	-7306.69	811.18	20872	19000	60.6	-3.8
-412.54	975.96	-7346.51	1059.57	22057	19019	48.7	-2.9
-554.48	-130.24	-7324.05	569.57	23625	19042	129	-2.4
-658.63	284.88	-7331.13	717.6	21291	19049	116.3	-3.7
-574.07	-132.98	-7451.75	589.27	23398	19062	127.8	-3.1
-339.86	1313.39	-7408.68	1356.65	22796	19080	25.6	-2.7
-522.05	575.58	-7341.32	777.06	23156	19085	113.3	-2.9

-507.24	-167.93	-7449.13	534.32	22963	19109	129.3	-2.3
-499.41	654.31	-7294.25	823.12	21305	19139	79.2	-3.7
-634.48	-55.39	-7293.36	636.89	19111	19170	121.9	-3.9
214.16	548.48	-7301.15	588.81	18450	19201	81.2	-4.4
-567.02	-130.59	-7316.43	581.86	22073	19274	128.4	-3.4
-794.1	35.22	-7372.12	794.88	22495	19330	113.9	-1.5
-539.41	-166.74	-7290.8	564.59	21908	19359	132.3	-3.7
-531.46	-153.65	-7371.34	553.23	20657	19359	312.3	-3.4
-709.71	-241.47	-7319.39	749.66	19039	19431	82.6	-4.1
64.3	1100.76	-7322.38	1102.64	21972	19508	36.1	-3.3
-591.57	117.85	-7270.19	603.19	18205	19530	128.3	-4.1
105.99	1326.33	-7347.86	1330.56	19832	19568	76.9	-3.3
-577.93	-99.78	-7339.32	586.48	22473	19574	105.6	-2.4
-545.35	-119.36	-7347.71	558.26	21331	19574	132.5	-2.1
-554.82	-100.99	-7366.77	563.94	19809	19579	130.8	-2.1
-373.2	868.3	-7335.78	945.1	21559	19610	106.2	-3
-507.72	-66.21	-7509.8	512.02	20432	19617	106.3	-3.8
-395.98	835.87	-7303.33	924.92	19508	19670	67	-4
-776.49	244.19	-7293.2	813.98	18128	19670	82.8	-3.8
-567.42	845.1	-7339.36	1017.92	21027	19674	52.2	-3.6
-573.96	-214.64	-7340.98	612.78	19106	19874	100.6	-4
-654.67	-55.7	-7333.61	657.04	20445	19889	101.9	-3.5
-546.42	-105.82	-7329.55	556.57	21529	19901	132.4	-2.6
-975.87	-47.62	-7383.69	977.03	20734	19908	65.9	-3.9
-597.21	499.77	-7300.44	778.74	22067	19971	86.5	-3.9
-660.41	-230.83	-7296.05	699.59	19122	20018	95.6	-4
-584.95	-180.17	-7335.03	612.07	21232	20028	126.7	-3.9
-1146.2	54.73	-7287.87	1147.51	20230	20133	90.7	-3.1
-760.01	-38.11	-7317.96	760.96	22464	20187	117.8	-2.4
-575.53	-81.35	-7345.52	581.25	21428	20208	107.8	-3.8
-895.07	-375.77	-7335.93	970.75	21781	20263	63.3	-3.8
-478.71	579.35	-7343.55	751.54	18941	20267	82.2	-4.1
-625.16	-173.87	-7296.96	648.89	19552	20297	121.7	-4.5
-486.68	913.91	-7262.11	1035.42	20029	20304	58.2	-3.1
-436.84	-212.44	-7350.39	485.76	20411	20331	117.1	-4.7
18.81	1075.61	-7389.7	1075.77	18737	20346	52.2	-3.6
-611.53	-96.03	-7349.95	619.02	20828	20513	127.6	-3.8
-458.86	916.39	-7318.15	1024.85	23214	20540	95	-2.4
-30.92	1049.78	-7363.18	1050.24	23020	20592	97.3	-3.1
312.25	1134.78	-7372.68	1176.96	20282	20608	84.8	-3.1
-510.63	74.5	-7317.17	516.04	20992	20682	115.5	-4.2
-839.33	71.76	-7282.37	842.39	23360	20745	113	-2.2
-335.79	989.67	-7341.28	1045.08	22163	20795	57.3	-3.2
-1132.73	-214.27	-7339.53	1152.82	21973	20802	46.4	-3.3
-39.13	1220.59	-7476.16	1221.22	23463	20866	88.2	-1.7

-82.8	1248.16	-7460.32	1250.9	23540	20866	-62.4	-1.7
-582.21	-19.81	-7273.38	582.55	21198	20985	128	-4.6
317.07	1835.55	-7443.41	1862.73	22230	21039	-29.4	-2.1
-385.42	972.71	-7362.23	1046.29	21847	21083	99.5	-2.9
291.68	1955.08	-7211.7	1976.72	23625	21122	40.6	-1.9
69.97	1932.09	-7318.83	1933.36	23662	21122	-109.2	-1.9
-1060.43	14.88	-7299.11	1060.53	22712	21129	54.3	-3.5
154.96	1307.4	-7379.02	1316.55	21862	21145	33.1	-3.2
-864.97	-148.91	-7373.86	877.69	22529	21209	104.4	-3.6
-646.08	-139.58	-7328.11	660.99	19855	21223	125.8	-2.1
-904.31	-325.93	-7343.35	961.25	20913	21238	103.5	-3.4
-411.37	753.92	-7296.21	858.85	23624	21238	107.9	-3
-260.12	877.45	-7294.56	915.19	20427	21284	70.7	-3.6
-986.25	-279.82	-7356.22	1025.18	22927	21311	97.9	-2.9
-1373.03	-225.14	-7353.08	1391.37	18673	21316	23.2	-3.2
-72.48	1442.35	-7346.97	1444.17	21883	21337	14.2	-2.8
-887.18	-249.84	-7355.85	921.69	21403	21457	64.8	-3.9
-334.25	985.27	-7149.29	1040.42	23792	21489	100.4	-2.6
11.91	1565.87	-7344.2	1565.92	22311	21553	64.7	-1.1
-1004.18	-131.21	-7376.09	1012.72	21646	21623	60.4	-3.7
-492.69	1114.51	-7392.24	1218.55	19506	21665	-43.2	-3.5
-452.98	929.34	-7135.93	1033.86	23358	21686	64.6	-3
-473.13	-369.2	-7314.06	600.13	19308	21698	124.3	-3.6
-275.11	-207.12	-7373.97	344.36	20352	21701	195.2	-4.3
-663.64	-209.67	-7394.17	695.97	21671	21722	120.8	-3.1
-52.97	1166.43	-7226.62	1167.63	20511	21733	44.9	-3.2
-370.88	581.27	-7319.71	689.51	23504	21733	115.7	-3.3
-397.47	566.02	-7315.76	691.64	21729	21741	94.1	-3.9
-837.15	106.2	-7295.95	843.86	22249	21747	108.5	-3
-597.96	450.72	-7294.58	748.8	20361	21757	111	-4
-261.96	728.18	-7330.67	773.87	19241	21764	79.8	-4
-441.59	813.13	-7278.71	925.3	21005	21764	67.7	-3.6
-186.6	1232.9	-7491.54	1246.94	22924	21764	83.5	-2.5
-1518.33	178.55	-7355.46	1528.79	23116	21828	63	-2.2
-448.85	625.16	-7306.71	769.6	22235	21831	86.1	-3.9
-722.07	828.78	-7335.57	1099.21	22025	21838	94.7	-2.9
-400.69	1024.23	-7381.41	1099.82	22625	21858	52.4	-3.4
-386.6	559.94	-7348.48	680.44	18471	21883	91.7	-4
-653.61	880.11	-7382.41	1096.27	20497	21953	48.5	-3.5
-709.18	-25.6	-7299.95	709.64	22505	22060	124.5	-2.2
-73.11	1372.57	-7374.79	1374.52	20851	22210	22.8	-2.8
6.03	1183.5	-7360.35	1183.52	23554	22255	85	-2.6
-540.16	-129.13	-7437.31	555.38	21039	22290	131.1	-3.7
-449.13	580.98	-7388.5	734.34	20157	22428	111.8	-3.7
-196.92	1023.93	-7130.11	1042.69	23423	22524	99.6	-2.8

-171.56	1018.13	-7410.16	1032.48	21089	22608	53.6	-3.2
69.65	962.4	-7359.84	964.92	22513	22627	61.1	-4
-298.74	650.26	-7353.1	715.6	23602	22673	119.7	-2.9
-205.59	809.68	-7384.59	835.37	23040	22701	109.4	-2.5
-709.84	-65.01	-7346.23	712.81	21845	22725	119.5	-3.9
79	744.6	-7306.77	748.78	20987	22725	87.4	-4.4
-479.15	737.59	-7534.73	879.56	23045	22735	98.5	-3.5
-778.93	-242.47	-7467.96	815.8	22989	22951	111	-2.3
-130.84	1124.81	-7477.07	1132.39	20094	22990	45.1	-3.2
-16.45	1129.65	-7437.89	1129.77	21940	23013	88.4	-3.4
-549.23	6.73	-7298.88	549.27	20917	23040	127.4	-2.9
-75.38	2068.42	-7190.1	2069.79	22012	23130	-48.7	-2.3
-755.67	-196.32	-7435.36	780.76	23622	23135	114.9	-1.5
-390.26	-116.37	-7275.94	407.24	20720	23241	127.9	-4.6
-478.79	1011.01	-7383.37	1118.65	18696	23275	48.9	-3.3
-357.35	570.28	-7301.26	672.99	19662	23284	96	-4.3
-854.13	-109.51	-7374.76	861.12	23473	23301	76.4	-3.4
-416.24	655.94	-7360.31	776.86	21447	23347	111.8	-3.9
-6.87	1142.07	-7378.98	1142.09	22226	23355	38.6	-2.8
-541.69	231.36	-7273.25	589.03	21411	23385	125.5	-4.2
-746.03	116.97	-7326.82	755.14	19455	23543	88.5	-4.6
-754.87	-220.7	-7388.76	786.47	23475	23600	116.4	-0.8
-54.73	825.8	-7328.28	827.61	20367	23662	48.8	-3.7
-624.22	26.57	-7295.59	624.79	19559	23662	102.9	-2.8
-390.26	-150.04	-7373.56	418.11	19883	23716	125	-4.4
-231.38	675.02	-7321.39	713.57	23127	23716	90.5	-3.6
-760.21	0.6	-7315.35	760.21	23195	23747	119.3	-1.2
-797.75	-16.61	-7301.44	797.92	23329	23874	116.3	-2
-434.82	757.69	-7306.79	873.59	23287	23943	107.6	-3.3
-288.57	1159	-7202.56	1194.38	20392	24082	53.5	-3
161.96	821.83	-7346.35	837.64	19152	24158	40.8	-4
-414.62	502.05	-7316.28	651.13	21879	24182	89.6	-4.1
-842.26	474.57	-7297.49	966.76	19994	24197	89.2	-2.8
-284.38	131.57	-7288.29	313.34	18859	24302	111.8	-4.8
-1030.67	69.65	-7240.73	1033.02	19783	24314	50.9	-3.4
283.85	2384.98	-7188.98	2401.81	22276	24534	15.7	-0.7
458.32	1865.5	-7372.87	1920.98	22421	24534	-43.4	-1.8
-252.43	738.11	-7316.56	780.08	22578	24562	83.2	-3.7
-510.1	871.39	-7497.06	1009.71	22787	24572	52.6	-3.3
-1080.54	143.33	-7374.26	1090	20362	24610	51.1	-3.3
-600.67	563.56	-7405.51	823.65	22562	24615	78.4	-3.7
-670.15	584.64	-7358.89	889.33	20741	24619	70.8	-4
-11.21	1196.81	-7369.89	1196.86	22936	24689	87.1	-2.3
-732.46	634.09	-7343.84	968.8	20522	24721	105.2	-3.4
-66.74	1297.65	-7435.83	1299.37	20844	24721	79.2	-3.3

-155.86	1311.57	-7404.2	1320.8	21352	24752	20.7	-3.1
-220.78	1386.22	-7295.15	1403.69	22700	24756	19.8	-3.1
-427.1	694.79	-7069.38	815.57	23010	24831	115.6	-2.3
-219.14	816.66	-7292.39	845.55	23271	24870	75.7	-3.6
-746.26	-211.06	-7455	775.53	23319	24877	116.3	-0.2
-582.7	873.96	-7318.89	1050.4	22452	24977	97.8	-2.2
-606.58	903.21	-7317.38	1087.99	21864	24982	93.4	-2.7
-1129.35	-105.6	-7347.36	1134.28	19251	25118	47.8	-3.4
-30.25	744.15	-7252.71	744.76	22075	25155	85.8	-4
425.91	1294.08	-7365.75	1362.37	20026	25174	25.8	-2.9
-850.75	55.54	-7301.24	852.56	22375	25184	109.7	-3.2
-1359.55	524.78	-7332.06	1457.32	23006	25259	72.3	-2
-1310.61	498.62	-7331.02	1402.26	22680	25283	77.4	-2.4
-517.51	-133	-7377.95	534.33	20056	25357	111.6	-4.4
-93.6	753.39	-7538.19	759.18	23271	25425	75.9	-3.4
-105.97	1059.1	-7416.91	1064.39	21076	25440	96.4	-3.1
-301.69	606.61	-7336.4	677.49	23418	25623	117	-3.6
-565.73	863.15	-7298.84	1032.03	19444	25627	101	-0.7
-651.95	911.58	-7317.52	1120.72	21309	25631	89.1	-1.7
-600.9	893.08	-7297.54	1076.42	22805	25631	97.3	-1.1
-530.4	141.87	-7315.33	549.05	21811	25759	114.7	-2.4
-534.89	-58.82	-7319.82	538.11	20949	25759	248.5	-2.2
-520.08	153.28	-7321.28	542.2	20145	25759	98.4	-2.2
237.79	559.1	-7287.65	607.57	23695	25793	125.7	-3
496.59	2084.92	-7248.49	2143.24	22344	25818	-56.8	-2.4
-804.75	-27.1	-7367.8	805.21	23266	25828	111.4	-3.6
-820.91	43.75	-7318.26	822.07	22000	25876	113.7	-2.8
-42.12	1707.55	-7352.34	1708.07	23052	25919	53.7	-1.4
32.45	1695.8	-7358.04	1696.11	23116	25919	-98.9	-1.4
101.36	1591.24	-7366.5	1594.46	22021	25921	-15.6	-1.1
-315.99	592.48	-7283.85	671.48	21312	26026	95.2	-4.1
-423.58	814.04	-7313.08	917.65	21881	26112	105.7	-2.7
-383.99	649.94	-7383.16	754.9	23169	26123	114.6	-3.2
-330.17	609.29	-7332.95	693	22317	26221	86.2	-3.8
-584.55	-14.85	-7366.55	584.74	21044	26238	130.3	-3.6
-156.3	1502.74	-7364.6	1510.85	22218	26275	5.5	-2.9
-659.89	878	-7336.74	1098.33	21063	26290	49.4	-3.6
-750.84	-203.19	-7451.31	777.85	21750	26327	112.1	-3.6
515.94	1225.74	-7380.95	1329.9	19348	26356	27.7	-3
-1165.35	-205.42	-7406.18	1183.32	23135	26359	90.4	-2.8
-703.84	-202.09	-7466.33	732.28	22255	26365	83.2	-3.5
-137.54	967.64	-7431.73	977.37	23084	26389	49	-3.7
-168.11	860.45	-7363.92	876.72	20359	26439	66.5	-3.4
-1152.08	73.21	-7489.52	1154.4	22539	26472	42.3	-3
-433.21	773.69	-7372.75	886.72	22608	26533	72.6	-3.1

-651.09	139.54	-7289.61	665.88	18868	26554	98.1	-3.6
-247.12	130.85	-7417.88	279.62	18535	26660	115.5	-5.4
-1590.56	-149.29	-7419.07	1597.55	22801	26767	63.4	-1.9
-769.74	206.47	-7352.1	796.95	23557	26928	76.5	-3.6
-518.22	-37.48	-7412.5	519.57	18269	27012	134.8	-4.7
-422.92	650.17	-7291.96	775.62	22983	27029	110.6	-3.7
-89.64	2057.28	-7160.61	2059.23	19055	27051	-41.3	-2.4
-724.42	-227.21	-7318.95	759.22	23145	27113	119.5	-3.4
-769.96	-246.07	-7314.23	808.32	21908	27170	68.8	-3.3
-571.32	-133.13	-7295.16	586.63	18320	27208	104.7	-4.7
-315.52	753.08	-7460.66	816.51	20342	27384	78.4	-2.3
-427.58	801.85	-7334.48	908.73	21156	27446	75	-2.9
-806.33	-130.89	-7296.14	816.88	20170	27646	80.8	-4.2
-598.22	8.24	-7296.61	598.28	21517	27716	106.7	-3.7
-670.22	-135.64	-7280.46	683.81	22568	27807	120.1	-3.4
-479.42	-231.33	-7297.69	532.31	20573	27948	113.5	-4.4
-654.88	-25.79	-7311.86	655.39	23378	27959	121.9	-1.7
-50	910.87	-7340.09	912.24	22479	27981	67.7	-3.4
-536.35	689.57	-7318.94	873.6	22527	27989	107.1	-3
-770.46	-215.15	-7463.36	799.94	21525	28170	113.1	-1.1
-816.66	-234.08	-7383.77	849.55	18332	28193	79.2	-3.5
-198.7	403.72	-7297.04	449.97	22648	28389	120	-4.4
-159.37	343.61	-7423.8	378.77	18428	28398	141.4	-4.3
-717.32	-200.14	-7445.4	744.72	23424	28408	116.9	-1.1
-597.41	817.81	-7322.13	1012.77	23204	28433	62.8	-3.3
-464.72	-162.6	-7540.07	492.34	20095	28458	98.9	-4.4
-711.26	-119.71	-7471.37	721.26	21898	28484	118	-3.7
167.68	854.74	-7383.29	871.03	21264	28650	75.2	-3.4
-654.58	-14.29	-7290.41	654.74	23374	28838	99.8	-3.9
-246.9	1245.7	-7348.19	1269.93	22370	28891	39.8	-2.7
-753.88	-214.82	-7387.88	783.89	22931	29093	118.5	-0.2
-652.81	-212.07	-7501.64	686.39	23376	29173	118.7	-3.7
159.66	817.93	-7305.21	833.37	21247	29204	107.5	-3.7
-493.35	-183.53	-7281.31	526.38	21491	29269	116.5	-2.4
-764.77	-59.91	-7332.94	767.11	22579	29293	114	-1.4
-301.97	171.41	-7387.49	347.23	18735	29305	142.4	-4.3
-739.81	-20.71	-7398.89	740.1	22061	29325	115.6	-2
-727.15	-35.22	-7306.76	728	20714	29349	119.6	-1.2
-726.05	-143.8	-7376.76	740.15	21639	29371	115.3	-2.2
-265.53	311.77	-7298.51	409.52	21707	29441	141.9	-4.6
-739.85	-212.05	-7447.12	769.64	23846	29498	115.9	-0.4
-161.96	590.88	-7296.17	612.67	20732	29574	102.7	-4
-201.37	212.52	-7352.24	292.77	20805	29621	138.2	-4.7
-310.13	287.23	-7375.93	422.71	20359	29693	127.4	-3.7
-483.55	660.94	-7344.87	818.94	23426	29754	321.4	-3.9

-106.38	1326.92	-7367.6	1331.18	22876	29782	79	-1.9
-585.71	-163.65	-7290.77	608.14	20926	29946	127.8	-4.2
-287.31	729.77	-7339.42	784.29	21766	30007	115.1	-3.5
-224.77	350.98	-7351.21	416.78	18898	30046	233.5	-5.2
-873.77	-134.07	-7270.18	884	20788	30074	74.7	-3.6
-628.33	873.97	-7342.95	1076.39	22915	30314	94.1	-2.1
-404.65	263.84	-7316.39	483.07	21927	30365	115.4	-4.1
-242.67	436.84	-7353.37	499.72	21368	30401	110.4	-4.5
-361.85	926.64	-7285.84	994.78	21934	30439	100.9	-3.1
-369.32	913.33	-7336.37	985.17	20714	30540	166.7	-3.9
-109.43	1225.17	-7345.45	1230.05	18474	30577	35.9	-3.6
-150.47	672.86	-7289.38	689.48	21225	30651	119.8	-3.2
-210.53	670.74	-7297.01	703	23736	30692	123.1	-3.2
-387.93	995.04	-7403.73	1067.99	19685	30761	46.4	-3.6
-404.27	1064.08	-7282.27	1138.29	22446	30766	89.9	-1.5
-13.82	868.99	-7327.43	869.1	19407	30848	51.1	-4.2
-299.37	416.32	-7283.78	512.78	23667	30899	132.5	-3.7
11.39	1270.76	-7338.29	1270.81	20174	30919	29.9	-3.7
63.24	871.39	-7450.04	873.68	19772	30925	69.4	-4
-269.36	613.21	-7329.15	669.76	19869	30942	87.7	-4.6
-421.35	603.55	-7328.82	736.08	21121	30942	89.4	-4.2
-479.25	605.65	-7336.21	772.33	20919	30946	78	-4.3
-815.89	16.06	-7359.41	816.05	19643	30962	80.1	-3.9
-409.61	585.85	-7335.21	714.84	19676	30977	95.8	-3.9
-496.11	-155.37	-7291.9	519.87	22943	30986	135.6	-2.2
-785.96	-230.43	-7364.58	819.04	23568	31109	113.7	-2
-767.31	-100	-7375.26	773.8	23050	31109	225.8	-1.9
-787.04	-227.62	-7364.52	819.29	23572	31109	-36.3	-2
-768.3	-103.32	-7374.81	775.22	23047	31109	75.8	-1.9
-859.84	-246.92	-7440.15	894.59	22817	31119	104.5	-3.5
-522.97	-143.52	-7478.08	542.31	21675	31144	126.7	-3.4
30.65	1421.79	-7323.68	1422.12	22614	31151	71.5	-2.3
86.76	1463.58	-7340.67	1466.15	22594	31151	-83.6	-2.2
88.73	1227.63	-7387.9	1230.83	19809	31190	36	-3.4
-441.62	244.67	-7456.59	504.87	22387	31220	132.6	-3.6
-108.35	390.72	-7328.14	405.46	23025	31242	141.4	-1.2
-374.39	-37.39	-7292.18	376.25	20477	31280	129.2	-5
-102.56	398.49	-7330.37	411.48	22301	31286	141.1	-2.5
-99.43	401.93	-7338.88	414.05	21597	31302	128.2	-3.5
-118.39	429.64	-7361.88	445.65	22854	31313	138.2	-3.3
-238.27	413.21	-7319.19	476.99	18291	31313	118.3	-3.4
-95.2	1566.62	-7253.95	1569.51	22896	31353	53.9	-2.1
-162.78	718.52	-7332.46	736.73	22091	31357	91.8	-3.9
-28.36	1130.86	-7464.63	1131.22	20738	31370	249.1	-3.4
-649.11	-165.42	-7283.21	669.86	22404	31479	124.1	-3.5

146.43	1174.88	-7364.45	1183.97	20507	31484	37.4	-3.6
-146.79	649.97	-7360.92	666.34	20924	31538	122.8	-3.7
-784.78	-249.6	-7423.22	823.52	22827	31542	106.8	-3.7
-356.86	657.2	-7301.04	747.84	21432	31559	82.2	-4.4
-205.17	647.08	-7317.31	678.83	20982	31624	94.4	-4.5
-348.21	227.58	-7318.96	415.98	19612	31628	410.7	-3.7
-331.79	214.69	-7318.96	395.19	20434	31628	142.2	-3.7
-40.71	464.63	-7325.19	466.41	18269	31683	118.3	-4.7
92.24	1394.97	-7364.73	1398.02	20402	31683	11.2	-3.7
-49.04	406.31	-7315.59	409.26	20672	31717	124.1	-4.9
-177.31	740.99	-7359.71	761.91	19650	31800	113.1	-4
-467.59	-168.61	-7269.73	497.06	23431	31829	136.5	-2
-769.4	-233.18	-7375.49	803.96	23090	31855	114.7	-0.4
72.86	462.08	-7370.7	467.79	21234	31926	113.7	-4.7
-872.67	-105.33	-7470.38	879	23423	31931	70.7	-3.4
-1204.96	-383.28	-7348.02	1264.45	23155	32004	77.2	-2.7
-1116.73	-244.65	-7340.55	1143.21	23178	32004	-64.3	-2.8
138.29	1284.23	-7321.05	1291.65	22926	32008	35.4	-3.3
376.08	1329.9	-7405	1382.05	22143	32011	21.3	-3.4
176.72	1489.74	-7317.39	1500.19	21067	32011	66.9	-3.2
-881.36	-264.95	-7348.1	920.32	21732	32053	109.4	-3
-765.08	-239.68	-7433.8	801.74	23134	32068	113.6	-0.8
-362.09	671.95	-7438.9	763.3	22128	32140	84.7	-4.1
-413.07	671.02	-7300.16	787.97	18849	32184	78	-4.5
71.83	1366.42	-7361.92	1368.31	20333	32238	24.1	-3.4
116.26	820.1	-7379.04	828.3	19741	32254	52	-4.4
-492.91	-78.98	-7294.59	499.2	19646	32310	116.7	-4.3
-963.3	-53.21	-7371.85	964.77	21599	32361	61.7	-4.1
-21.52	686.07	-7331.13	686.41	21471	32409	94.6	-3.9
99.15	928.78	-7524.36	934.06	20278	32519	55.1	-4.2
-73.52	401.52	-7364.13	408.2	22003	32526	139.6	-3.8
16.69	343.59	-7319.36	344	19159	32558	131.2	-4.6
-777.53	0.51	-7349.86	777.53	22613	32580	115.7	-3.4
-523.67	-277.82	-7282.36	592.8	20369	32686	128.4	-4.1
-809.15	-157.68	-7386.18	824.37	20653	32787	112.8	-4.3
-194.85	390.95	-7331.11	436.82	20439	32887	140.9	-2.5
-268.71	459.41	-7344.47	532.22	21845	32890	133.3	-3.8
-114.37	384.68	-7376.28	401.32	22739	33039	143.5	-4.7
-281.24	1011.94	-7315.17	1050.29	23445	33112	98.6	-1.2
-279.04	1005.04	-7314	1043.06	23454	33112	-51.7	-1.2
77.93	1256.04	-7371.24	1258.46	23297	33145	82.7	-2.7
153.11	1342.53	-7348.22	1351.23	23615	33154	73.5	-3.2
-705.6	165.46	-7349.9	724.74	20165	33258	84.6	-4.5
207.47	1420.71	-7428.24	1435.78	21876	33292	15.9	-3.4
-46.05	1306.6	-7365.82	1307.41	18992	33292	33.1	-3

-295.94	-127.91	-7294.58	322.4	20523	33330	140	-4.2
-181.92	487.73	-7290.38	520.55	22392	33339	395.3	-4.6
-171.49	468.73	-7288.45	499.12	21866	33339	115.1	-4.7
-538.8	568.24	-7241.31	783.07	18172	33403	85.8	-4.3
168.59	1305.62	-7374.04	1316.46	22533	33409	28.6	-3.4
148.44	1349.95	-7336.69	1358.09	22269	33677	74.1	-3.5
-150.01	385.76	-7388.78	413.9	19551	33707	109.1	-5.2
31.18	1388.99	-7334.59	1389.34	18542	33732	17.2	-3.7
-332	167.89	-7335.19	372.04	20643	33767	138.6	-3.7
-332.84	161.82	-7350.02	370.09	21760	33778	148.2	-2.9
-323.89	130.31	-7329.96	349.12	19368	33806	145.1	-4.1
-267.73	543.73	-7329.08	606.07	22577	33822	126.8	-3
-307.32	684.56	-7374.18	750.38	21614	33905	118	-3.4
76.58	1310.2	-7389.31	1312.44	19372	33919	23	-3.7
-287.78	63.15	-7229.18	294.63	19350	33942	134.4	-5.3
34.51	974.19	-7372.97	974.8	20689	34201	100.2	-3.6
69.5	963.91	-7328.58	966.41	18101	34231	64.9	-4.2
-702.29	108.98	-7329.15	710.7	18883	34313	92.5	-4.2
-173.28	149.45	-7319	228.83	20622	34342	155.1	-5
-135.42	188.81	-7342.5	232.35	22957	34472	349.8	-4.8
-157.53	213.44	-7350	265.28	22153	34477	151.1	-4
-121.21	185.7	-7333.31	221.76	21898	34477	148	-5
-364.79	-288.27	-7288.51	464.94	18325	34511	117.5	-5.1
-362.87	682.56	-7354.34	773.02	23109	34630	116.3	-3.5
-440.78	592.24	-7340.38	738.27	20942	34634	90.4	-4.3
-832.62	-224.36	-7461.94	862.32	23332	34694	103	-2.9
242.18	1297.71	-7375.63	1320.11	20891	34727	29.6	-3.5
-465.39	-182.36	-7527.65	499.84	21321	34786	130.7	-4.4
-1187.94	-349.46	-7323.55	1238.27	22823	34843	83.1	-2.5
-205.68	84.58	-7285.57	222.39	18119	35033	238.6	-5.5
418.51	1425.82	-7496.47	1485.97	19270	35119	-6	-3.7
-194.69	-138.97	-7343.32	239.2	19941	35148	143.9	-5.2
-215.19	1031.71	-7227.33	1053.91	23503	35156	60.9	-3
-312.91	597.27	-7326.52	674.27	21063	35178	95.3	-4.2
-696.98	-140.1	-7473.88	710.92	21116	35195	109.7	-3.4
-301.37	546.14	-7289.05	623.77	22437	35203	121.5	-4
-862.9	-243.88	-7314.42	896.7	22536	35313	108.4	-3.5
93.03	1356.88	-7379.97	1360.07	19088	35382	-16.5	-4
-173.38	1009.29	-7259.69	1024.07	22867	35510	60.9	-3.6
-187.15	829.64	-7347.05	850.49	23589	35513	78.4	-3.3
-35.35	969.45	-7422.33	970.09	22666	35630	101.8	-3.8
94.76	1279.55	-7364.14	1283.05	22085	35876	33.2	-3.6
9.43	316.8	-7275.26	316.94	18058	35902	147.4	-4
450.54	1194.23	-7356.96	1276.39	19487	35911	35.4	-3.7
-211.93	629.65	-7285.36	664.36	21061	35998	95.4	-4.2

-127.83	610.78	-7297.97	624.01	21137	36159	102.9	-3.8
-186.45	-90.76	-7403.63	207.37	21535	36202	149.9	-4
155.08	1233.52	-7389.49	1243.23	19213	36246	35	-3.8
-46.03	903.63	-7355.47	904.8	22093	36347	74.5	-3.7
-135.54	651.2	-7317.64	665.16	23600	36570	123.6	-3.4
-363.29	671.22	-7368.69	763.23	22275	36667	113.9	-3.9
-101.65	613.62	-7287.9	621.98	21295	36694	101.1	-4.5
-947.1	495.72	-7388.57	1068.99	18250	36711	52.9	-4
6.22	351.66	-7328.61	351.72	19156	36753	132.1	-1.6
-239.65	-108.98	-7361.59	263.27	23066	36898	140.7	-4.2
-202.33	224.46	-7338.36	302.19	22634	36903	148.7	-4.3
-127.18	652.6	-7302	664.88	21078	36927	93.4	-4.1
-553.09	-228.26	-7313.74	598.34	21424	36951	127	-3.7
-498.2	-194.52	-7359.56	534.83	20411	37087	128.1	-3
-848.13	-246.25	-7357.58	883.16	22403	37090	110	-1.9
-432.2	-242.01	-7338.46	495.34	21872	37209	118.3	-4.3
-773.36	-214.85	-7375.78	802.65	23742	37236	114.7	-2.1
-775.2	-246.53	-7359.34	813.46	23651	37353	117	-2
-759.56	-309.45	-7348.07	820.18	20485	37379	113.5	-4.3
-32.8	920.48	-7256.31	921.06	21333	37402	71.8	-2.5
-743.97	803.12	-7317.98	1094.76	20437	37632	95.3	-3.7
-84.5	357.97	-7326.81	367.81	19759	37820	130.9	-1.3
-247.03	733.98	-7346.65	774.44	21322	37852	89.5	-4.1
-92.48	620.45	-7323.49	627.3	23028	37875	107.3	-4
-23.56	1258.17	-7428.56	1258.39	20123	37912	29.5	-3.7
37.31	799.82	-7351.92	800.69	19350	37925	85.1	-4
63.16	750.73	-7332.13	753.38	20904	37925	117.8	-4.3
-12.68	776.72	-7335.58	776.82	19280	37930	87.5	-4.3
63.37	830.33	-7353.76	832.74	20572	37990	80.7	-4.2
-127.25	680.77	-7331.06	692.56	20226	38012	121	-4.4
-749.62	-50.93	-7301.52	751.35	21916	38321	88.9	-3.9
-1229.52	-148.22	-7493.05	1238.42	22081	38399	82.8	-2.7
-1022.62	-57	-7213.79	1024.21	23421	38732	99.3	-3.2
-58.5	608.88	-7347.01	611.68	22727	17274	128.1	-4.3
-314.38	-144.25	-7377.33	345.89	19435	17601	131.3	-4.1
-544.93	761	-7306.79	935.99	21577	17616	65	-3.9
-267.01	529.24	-7318.96	592.78	18839	17637	121.3	-4.7
-491.76	-173.56	-7359.02	521.49	21489	17794	131.7	-3.9
-710.6	-7.78	-7318.52	710.64	21484	17858	117.8	-2.2
-156.29	385.53	-7270.18	416	21711	17913	125.2	-3.2
-230.39	494.41	-7290.5	545.45	21676	17923	109.2	-3.9
-199.43	-62.58	-7341.56	209.02	20401	17923	158.1	-4.4
440.25	1409.64	-7465.11	1476.79	21119	18134	74.1	-3
-240.01	428.01	-7280.22	490.71	23186	18152	137.2	-4.3
-207	-85.88	-7329.96	224.11	21559	18227	156.1	-2.5

-311.04	-45.15	-7280.54	314.3	18930	18669	138	-3.6
-507.75	38.95	-7304.07	509.24	23568	18964	135.1	-2.4
-200.14	777.71	-7317.99	803.05	21148	19048	84.5	-4.2
-261.22	235.31	-7330.77	351.58	20421	19063	132.4	-5
-157.79	340.94	-7393.21	375.68	21093	19152	142.6	-4.3
-542.13	556.07	-7285.7	776.61	21071	19172	81.7	-4
-358.9	331.84	-7282.41	488.8	22259	19343	114.5	-4.7
-45.05	316.23	-7288.38	319.42	19139	41278	134.4	-5.1
98.68	1688.32	-7222.21	1691.2	22375	41597	59	-1.9
-294.73	-189.02	-7369.49	350.13	18066	41616	119.3	-5.4
-10.38	520.05	-7323.23	520.15	23138	41828	136.1	-2.9
362.61	1403.56	-7351.33	1449.64	21587	41974	13.7	-3.3
-549.9	909.55	-7381.54	1062.86	18636	42168	56.6	-4
-432.91	-144.96	-7283.58	456.54	21317	42551	135.8	-3.7
-594.32	473.79	-7272.6	760.06	23121	42573	116.4	-3.4
113.07	527.3	-7365.09	539.29	21004	42608	133	-4.6
632.22	1527.98	-7270.22	1653.61	22120	42879	57.8	-2.7
337.75	1424.88	-7400.18	1464.36	20537	42885	14.8	-3.5
364.76	1555.59	-7249.77	1597.78	22267	43028	1.7	-3
-331.85	189.08	-7410.52	381.94	21448	43303	144.8	-4.7
-49.37	318.6	-7282.37	322.4	21810	43740	148.1	-2.9
-470.31	-173.44	-7279.29	501.27	21103	43830	132.6	-4.1
147.47	478.38	-7348.64	500.59	20885	44270	117.4	-4.3
-737.47	559.36	-7332.32	925.61	23121	44281	108	-3.3
-774.25	510.44	-7327.3	927.37	20854	44356	107.6	-3.7
-62.71	326.69	-7329.37	332.65	18205	44799	145.7	-4.3
182.22	533.31	-7329.37	563.58	22338	44910	131.7	-3.6
-341.79	-299.36	-7342.53	454.35	19861	45050	121.8	-4.5
-517.21	56.8	-7296.81	520.32	18064	45107	109.8	-4.8
-435.8	-223.02	-7288.46	489.55	18993	45253	112.5	-4.8
-570.05	14.89	-7326.44	570.24	19118	45562	109.5	-4
-773.26	-133.86	-7299.22	784.76	22197	45709	110.5	-3.3
-96.96	1249.3	-7355.56	1253.06	18854	45984	35	-3.6
-458.53	266.75	-7293.38	530.48	23019	46343	115.1	-4.2
-289.28	-184.67	-7343.31	343.2	22476	46701	137.7	-3.2
379.14	1171.17	-7385.06	1231.01	18866	46930	33.6	-3.5
-322.66	-146.44	-7302.21	354.34	19397	47415	132.7	-4.4
-232.93	-189.53	-7342.9	300.3	19658	48084	134.8	-5.3
-320.66	-89.1	-7295.24	332.81	19038	48592	127.3	-4.9
-335.12	-111.61	-7341.98	353.22	19624	49852	131.7	-4.3
6.55	1550.54	-7344.54	1550.55	23658	50489	67	-2
-119.84	1469.04	-7377.81	1473.92	20812	51161	70.5	-2.2
-119.88	1466.49	-7376.1	1471.38	20817	51161	138.2	-2.2
-648.89	503.28	-7372.92	821.19	19916	53803	78.6	-3.4
-318.89	41.36	-7370.49	321.56	19703	54458	133.7	-4.9

-543.76	852.67	-7281.94	1011.3	19232	55986	56.6	-3.8
-327.74	300.7	-7293.79	444.79	21512	56886	137.8	-3.6
-796.91	501	-7337.97	941.31	18826	57111	71.8	-4
-98.51	407.89	-7311.02	419.62	22895	57345	144	-3.8
-119.03	396.32	-7291.87	413.81	21489	57550	143.5	-3.4
-241.9	-52.58	-7338.93	247.55	22721	62018	143.2	-3.8
-523.32	953.2	-7345.49	1087.41	20688	63064	94.3	-3.7
-280.22	-152.72	-7295.66	319.13	21151	63409	146.6	-3.7
-232.71	-18.03	-7373.42	233.41	20219	63667	145	-5
-34.46	406.01	-7295.64	407.47	23028	64543	142.2	-3.2
-4.17	393.61	-7282.91	393.63	23321	64547	145.2	-2.8
1.53	365.23	-7295.81	365.23	20985	64758	145.4	-4.4
45.29	286.17	-7328.09	289.73	20126	66710	139.7	-2.2
-565	781.52	-7323.14	964.36	22616	68485	104.3	-2.3
-229.59	936.65	-7323.03	964.38	22606	69264	101.7	-3.7

BIBLIOGRAPHY

Aadnoy, B.S., 1987, Stresses Around Horizontal Boreholes Drilled in Sedimentary Rocks, SPE Journal 17119: 219-526

Albright, J.N. and Pearson, C.F., 1982, Acoustic Emissions as a Tool for Hydraulic Fracture Location: Experience at the Fenton Hill Hot Dry Rock Site, SPE Journal, V. 22 (4): 523-530.

Annual Report, 1978,– 1977, Hot Dry Rock Geothermal Energy Development Project, Los Alamos Scientific Laboratory Progress Report LA-7109-PR, Los Alamos, New Mexico, February 1978.

Barron, K., 1969, The Fracture of Brittle Rocks Around Mine Excavations, Internal Report MR 69/25 LD, Mining Research Center, Department of Energy, Mines and Resources, Ottawa.

Barron, K., 1970, Detection of Fracture Initiation in Rock Specimens by the Use of a Simple Ultrasonic Listening Device, International Journal of Rock Mechanics and Mining Sciences, V. 8: 55-59.

Barzilai, A., VanZandt, T. and Kenny, T., 1998, Improving the Performance of a Geophone Through Capacitive Position Sensing and Feedback, ASME Dynamite Systems and Control Division, V. 64: 629-636.

Bawker, 2008, Barnett Shale—Unfolded: Sedimentology, Sequence Stratigraphy, and Regional Mapping, Gulf Coast Association of Geological Societies Transactions Vol. 58, 777-795

Berryman, J.G., 2008, Exact Seismic Velocities for Transversely Isotropic Media and Extended Thomsen Formulas for Stronger Anisotropies, Geophysics, V. 73 (1): D1-D10.

Byerlee, J.D. and Lockner, D., 1977, Acoustic Emission During Fluid Injection, Proceedings First Conference on Acoustic Emission/Microseismic Activity in Geologic Structures and Materials, Pennsylvania State University, June 1975, Trans Tech Publications, Clausthal, Germany.

Castano, A.F., 2010, Estimation of Uncertainty in Microseismic Event Location Associated with Hydraulic Fracturing, Master's Thesis, University of Oklahoma.

Cipolla, C.L., Lolon, E.P., Mayerhofer, M.J. and Warpinski, N.R., 2009, Fracture Design Considerations in Horizontal Wells Drilled in Unconventional Gas Reservoirs, SPE Hydraulic Fracturing Technology Conference, 19-21 January, The Woodlands, Texas, USA.

Cipolla, C.L., Warpinski, N.R., Mayerhofer, M.J. and Lolon, E.P., 2010, The Relationship Between Fracture Complexity, Reservoir Properties, and Fracture-Treatment Design, SPE Productions and Operations, V. 25 (4): 438-452.

Charlotte Sullivan, Kurt J. Marfurt, Alfred Lacazette, and Mike Ammerman Walper, 1982 Application of New Seismic Attributes to Collapse Chimneys in the Fort Worth Basin. Society of Exploration Geophysics, Vol. 71. No 4: 111-119

Cheung, L.S. and Haimson, B., 1989, Hydrofracturing Stress Measurements in Fractured Rock: A Laboratory Study, The 30th U.S. Symposium on Rock Mechanics, June 19-22, 1989, Morgantown, WV.

Chitrala, Y., Moreno, C., Sondergeld, C.H. and Rai, C., 2010, Microseismic Mapping of Laboratory Induced Hydraulic Fractures in Anisotropic Reservoirs, SPE Tight Gas Conference, 2-3 November 2010, San Antonio, Texas, USA.

Chitrala, Y., 2011, Microseismic Analysis of Laboratory Induced Fractures, Master's Thesis, University of Oklahoma.

Clark, J.B., 1949, A Hydraulic Process for Increasing the Productivity of Wells, Journal of Petroleum Technology – Transactions, V. 1 (3): 1-6.

De Pater, C.J. and Dong, Y., 2007, Experimental Study of Hydraulic Fracturing in Sands as a Function of Stress and Fluid Rheology, SPE-Hydraulic Fracturing Technology Conference, 87-96.

Detournay, E. and Cheng, A.H., 1992, Influence of pressurization rate on the magnitude of the breakdown pressure, Proceedings of the 33rd U.S. Symposium on Rock Mechanics, Santa Fe, eds. J.R. Tillerson and W.R. Wawersik, Balkema, pp. 325-333, June 8-10, 1992.

Dinske, C., Shapiro, S.A. and Rutledge, J.T., 2010, Interpretation of Microseismicity Resulting from Gel and Water Fracturing of Tight Gas Reservoirs, Pure Applied Geophysics, V. 167 (1-2): 169-182.

Durham, S., 2007, Barnett Hits do not Rule out misses; Still a 'Statistical Play': AAPG Explorer, v. 28, no. 10, p. 51.

Dozier, G., Elbel, J., Fielder, E., Hoover, R., Lemp, S., Reeves, S., Siebrits, E., Wisler, D. and Wolhart, S., 2003 Refracturing Works, Schlumberger Oilfield Review Article 38-53

Economides, M.J. and Nolte, K.G., 2003, Reservoir Stimulation, Wiley, NY and Chichester, Third Edition, 750pp.

Faber, K. and Maxwell, P.W., 1996, Geophone Spurious Frequency: What is It and How Does It Affect Seismic Data Quality? SEG International Exposition and 66th Annual Meeting, November 10-15 1996, Denver, Colorado.

Fall, S.D., Young, R.P., Carlson, S.R. and Chow, T., 1992, Ultrasonic Tomography and Acoustic Emission of Hydraulically Fractured Lac du Bonnet Grey Granite, Journal of Geophysical Research, V. 97 (B5): 6867-6884.

Frantz, J.K. and Jochen. V., 2005 An Overview of Modern Shale Gas Development In The United States. Natural Gas1998: Issues and Trends. Shale Gas White Paper. 05OF299. 2-11.

Fisher, M.K, Maxwell, S.C and C. Urbancic, 2002., Imaging Seismic Deformation Induced by Hydraulic Fracture Complexity, Journal of Petroleum Technology, v. 59, (3), 54-57.

Fisher, M.K., Wright, C.A., Davidson, B.M., Goodwin, A.K., Fielder, E.O., Buckler, W.S. and Steinsberger, N.P., 2002, Integrating Fracture Mapping Technologies to Optimize Stimulations in the Barnett Shale, SPE Production and Facilities, V. 20 (2): 85-93.

Gidley, J.L, Holditch, S.A., Nierode, D.E. and Veatch Jr., W., 1989, Recent Advances in Hydraulic Fracturing, SPE Monograph Series, V. 12.

Goodman, R.E., 1963, Subaudible Noise During Compression of Rocks, Geological Society of America Bulletin, V. 74: 487-490.

Grechka, V., Mazumdar, P. and Shapiro, S.A., 2010, Predicting Permeability and Gas Production of Hydraulically Fractured Tight Sands form Microseismic Data, Geophysics, V. 75 (1): B1-B10.

Groenenboom, J., van Dam, D.B. and de Pater, C.J., 1999, Time Lapse Ultrasonic Measurements of Laboratory Hydraulic Fracture Growth: Widt Profile and Tip Behaviour, SPE Annual Technical Conference and Exhibition, 3-6 October 1999, Houston, Texas USA.6(1).14-21.

Ground Water Protection Council, 2009, Modern Shale Gas – Development in the United States: A Premier, Prepared for U.S Department of Energy, Office of Fossil Energy and National Technology Laboratory.

Haimson, B. and Fairhurst, C., 1969, Hydraulic Fracturing in Porous-Permeable Materials, Journal of Petroleum Technology, V. 21 (7): 811-817.

Haimson, B.C. and Kim, K., 1977, Acoustic Emission and Fatigue Mechanisms in Rock, Proceedings First Conference on Acoustic Emission/Microseismic Activity in Geologic Structures and Materials, Pennsylvania State University, June 1975, Trans Tech Publications, Clausthal, Germany. 35-56

Haimson, B.C. and Zhao, Z., 1991, Effect of Borehole Size and Pressurization Rate on Hydraulic Fracturing Breakdown Pressure, The 32th U.S. Symposium on Rock Mechanics, 191-199, Norman, Oklahoma.

Hassebroek, W.E. and Waters, A.B., 1964, Advancements Through 15 Years of Fracturing, Journal of Petroleum Technology, V. 16 (7): 760-764.

Heydarabadi, F.R., Moghadasi, J., Safian, G. and Ashena, R., 2010, Criteria for Selecting A Candidate Well for Hydraulic Fracturing, 34th Annual SPE International Conference and Exhibition, 31 July-7 August 2010, Tinapa-Calabar, Nigeria. pp 59

Hoffma, F. L., Hodge, V. F., Folsom, T R. (1974). Polonium 210 radioactivity in certain mid-water fish of the Eastern Temporal Pacific. Health Physics 26: 412-856

Holcomb, D.J., 1993, General Theory of the Kaiser Effect, International Journal of Rock Mechanics and Mining Science & Geomechanics Abstracts, V.30 (7): 929-935.

Hornby, B.E., Howie, J.M. and Ince, D.W., 1999, Anisotropy Correction for Deviated Well Sonic Logs: Application to Seismic Well Tie, Extended Abstracts, SEG 69th Annual Meeting: 112-115.

Hsu, N. N. and Breckenridge, F. R., 1981, Characterization and Calibration of Acoustic Emission Sensors, Materials Evaluation, V. 39 (1): 60-68.

Isaac, J.H. and Lawton, D.C., 1999, Image Mispositioning Due to Dipping TI Media: a Physical Seismic Modeling Study, Geophysics, V. 64 (4): 1230-1238.

Jarvie D.M., 2005, Shale Gas Potential of Source Rocks along the Ouachita Thrust Front, Barnett Shale Symposium III. 3-4.

Karastathis, A., 2007, Petrophysical Measurements on Tight Gas Shale, M.S. Thesis, University of Oklahoma. 117pp.

Khair, A.W., 1977, A Study of Acoustic Emission During Laboratory Fatigue Tests on Tennessee Sandstone, Proceedings First Conference on Acoustic Emission/Microseismic Activity in Geologic Structures and Materials, Pennsylvania State University, June 1975, Trans Tech Publications, Clausthal, Germany. pp.45-66

Kranz, R.L., Satoh, T., Nishizawa, O., Kusunose, K., Takahashi, M., Masuda, K. and Hirata, A., 1990, Laboratory Study of Fluid Pressure Diffusion in Rock Using Acoustic Emissions, Journal of Geophysical Research, V. 95 (B13): 21-593, 21-607.

Lhomme, T.P., de Pater, C.J. and Helfferich, P.H., 2002, Experimental study of hydraulic fracture initiation incolton sandstone, SPE Paper 78187, Proc. SPE/ISRM Rock Mechanics Conference, Irving TX, 20-23.

Lockner, D. and Byerlee, J.D., 1977(a), Hydrofracture in Weber Sandstone at High Confining Pressure and Differential Stress, Journal of Geophysical Research, V. 82 (14): 2018-2026.

Lockner, D. and Byerlee, J.D., 1977(b), Acoustic Emission and Fault Location in Rocks, Proceedings First Conference on Acoustic Emission/Microseismic Activity in Geologic Structures and Materials, Pennsylvania State University, Trans Tech Publications, Clausthal, Germany: 99-107.

Lockner, D., 1993, The Role of Acoustic Emission in the Study of Rock Fracture, 1993, International Journal of Rock Mechanics and Mining Sciences and Geomechanics Abstracts, V. 30 (7): 883-899.

Mae, I. and Nakao, K., 1968, Characteristics in the Generation of Microseismic Noises Under Under Uniaxial Compressive Load, Journal of the Society of Materials Science, V. 17 (181): 62-67.

Majer, E.L. and Doe, T.W., 1986, Studying Hydrofractures by High Frequency Seismic Monitorin, International Journal of Rock Mechanics and Mining Sciences and Geomechanics Abstracts, V. 23 (3): 185-199.

Margesson, R.W. and Sondergeld, C.H., 1998, Anisotropy And AVO: A Case History from West of Shetlands, Petroleum Geology of Northwest Europe, Proceedings of the 5th Conference, Ed. Fleet and Boldy. Geological Society, London, 634-643.

Masuda, K., Nishizawa, O., Kusunose, K. and Satoh, t., 1993, Laboratory Study of Effects of In Situ Stress State and Strength on Fluid-induced Seismicity, International Journal of Rock Mechanics and Mining Sciences and Geomechanics Abstracts, V. 30 (1): 1- 10.

Matsunaga, I., Kobayashi, H., Sasaki, S. and Ishida, T., 1993, Studying Hydraulic Fracturing Mechanism by Laboratory Experiments with Acoustic Emission Monitoring, The 34th U.S. Symposium on Rock Mechanics, June 28-30 1993, Madison, WI. V.30, pp. 909-912

Matthews, H.L., Schein, G. and Malone, M., 2007 Stimulation of Gas Shales: SPE Paper106070, SPE Hydraulic Fracturing Technology Conference, 29-31.

Mavko, G., Mukerji, T. and Dvorkin, J., 2003, The Rock Physics Handbook, Cambridge University Press, Cambridge, UK., 329pp.

Maxwell, S.C., and Urbancic, T.I. 2002, Source Parameters of Hydraulic Fracture Induced Microseismicity, SPE Paper 77439. Annual Technical Conference and Exhibition, San Antonio, Texas USA.

Mayerhofer, M.J., Lolon, E.P., Youngblood, J.E. and Heinze, J.R., 2006, Integrations of Microseismic Fracture Mapping Results with Numerical Fracture Network Production Modeling in the Barnett Shale, SPE Paper 102103. Annual Technical Conference and Exhibition, San Antonio, Texas, USA.

Meckel, L.D., Jr., Smith, D.G., and Wells, L.A., 1992, Ouachita Foredeep Basins: Regional Paleogeography and Habitat of Hydrocarbons in Ouachita, American Association of Petroleum Geologists, Memoir 55., 427-444.

Medlin, W.L. and Masse, L., 1979, Laboratory Investigation of Fracture Initiation Pressure and Orientation, Society of Petroleum Engineers of AIME Journal, V. 19 (2): 129-144.

Medlin, W.L. and Masse, L., 1984, Laboratory Experiments in Fracture Propagation, SPE Journal, V. 24 (3): 256-268.

Mckee, Thomas H. Anderson, Jonathan A. Nourse, James W. and Maureen B. Steiner., 1992, The Mojave-Sonora Megashear Hypothesis: Development, Assessment, and Alternatives GSA, Special Paper 393, 199-208.

Mogi, K., 1962, Study of the Elastic Shocks Caused by the Fracture of Heterogeneous Materials and its Relation to Earthquake Phenomena, Bulletin of Earthquake Research Institute, V. 40: 125-173.

Nordgren, R.P., 1972, Propagation of a Vertical Hydraulic Fracture, SPE Journal, V. 12 (4): 306-314.

Obert, L. and Duvall, W.I., 1942, Use of Subaudible Noise for Prediction of Rock Bursts, Part II, U.S. Bureau of Mines, RI 3654, 1215pp.

Obert, L. and Duvall, W.I., 1945(a), Microseismic Method of Predicting Rock Failure in Underground Mining, Part I. General Method, U.S. Bureau of Mines, RI 3797, 986.

Obert, L. and Duvall, W.I., 1945(b), Microseismic Method of Predicting Rock Failure in Underground Mining, Part II. Laboratory Experiments, U.S. Bureau of Mines, RI 3803, 1374pp.

Obert, L., 1975, The Microseismic Method: Discovery and Early History, Proceedings First Conference on Acoustic Emission/Microseismic Activity in Geologic Structures and Materials. The Pennsylvania State University, Trans Technical Publications, Clausthal, Germany,. 11-12.

Parker, M.A., Vitthal, S., Rahimi, A., McGowen, J.M. and Martch Jr., W.E., 1994, Hydraulic Fracturing of High-Permeability Formations to Overcome Damage, SPE Paper 27378 International Symposium on Formation Damage Control, Lafayette, Louisiana, USA. 329-344.

Patterson Jr., B.F., 1957, Hydraulic Fracturing in the Caddo-Pine Island Field, Journal of Petroleum Technology, V. 9 (1): 11-16.

Perkins, T.K. and Kern, L.R., 1961, Widths of Hydraulic Fractures, Journal of Petroleum Technology, V. 13 (9): 937-949.

Pollastro R.M., Jarvie D.M., Hill R.J. and Adams C.W., 2007, Geologic Framework of the Mississippian Barnett Shale, Barnett Paleozoic Total Petroleum System, Bend Arch – Fort Worth Basin, Texas, AAPG Bulletin, V.91(4): 405-436.

Roberts. J, Britton, T., 1996, West Texas Shale Gas Play; Challenges to Commerciality, West Texas Geological Society, v. 06-117, p. 937-959.

Rutledge, J. and Phillips, W.S., 2001, Hydraulic Stimulation of Natural Fractures as Revealed by Induced Microearthquakes, Carthage Cotton Valley Gas Field, East Texas, Los Alamos National Laboratory. 153-169.

Sachse, W. and Ruoff, A.L., 1975, Elastic Moduli of Precompressed Pyrophyllite used in Ultralight-pressure Research, Journal of Applied Physics, V. 46 (9): 3725-3730.

Sayers, C., and A. Tura 2005, Introduction to this special section: Rocks under stress, The Leading Edge, v. 24, 1213.

Schoenberg, M., and C. M. Sayers 1995, Seismic Anisotropy of Fractured Rock, Society of Exploration Geophysics v. 60, 204–211.

Schoenberg, M. 1980, Elastic wave behavior across linear slip interfaces, Journal Acoustic, Society of America. v. 68, 1516–1521.

Scholz, C.H., 1968(a), Experimental Study of the Fracturing Process in Brittle rock, Journal of Geophysical Research, V. 73 (4): 1447-1454.

Scholz, C.H., 1968(b), Microfracturing and the Inelastic Deformation of Rock in Compression, Journal of Geophysical Research, V. 73 (4): 1417-1432.

Scott, L., Montgomery, B., Daniel, M., Jarvie, A., Kent, A., and Pollastro M., 2005, Mississippian Barnett Shale, Fort Worth Basin, North-Central Texas: Gas-shale Play with Multi–Trillion Cubic Foot Potential, AAPG Bulletin, v. 89, no. 2, 155–175.

Shapiro, S.A., Dinske, C. and Rothert, E., 2006, Hydraulic-fracturing Controlled Dynamics of Microseismic Clouds, Geophysical Research Letters, V. 33 (14): L14312.

Sleefe, G.E., Warpinski, N.R. and Engler, B.P., 1995, The Use of Broadband Microseisms for Hydraulic-Fracture Mapping, SPE Formation Evaluation, V. 10 (4): 233-240.

Solberg, P., Lockner, D. and Byerlee, J., 1977, Shear and Tension Hydraulic Fractures in Low Permeability Rocks, Pure and Applied Geophysics, V. 115 (1-2): 191-198.

Sondergeld, C.H., Getting, I.C., Spetzler, H.A. and Sobolev, G.A., 1980, Velocity Changes Associated with Generalized Triaxial Deformation of Pyrophyllite, Pure and Applied Geophysics, V. 118 (4): 975-989.

Sondergeld, C.H. and Estey, L.H., 1982, Source Mechanisms and Microfracturing during Uniaxial Cycling of Rock, Pure Applied Geophysics, V. 120 (1): 151-166.

Sondergeld, C.H. and Rai, C.S., 1992, Laboratory Observations of Shear Wave Propagation in Anisotropic Media, The Leading Edge, V. 11: 38-43.

Sondergeld, C.H. and Rai, C.S., 2011, Elastic Anisotropy of Shales, The Leading Edge, V. 30 (3): 324-331.

Song, I. and Haimson, B.C., 2001, Effect of Pressurization Rate and Initial Pore Pressure on the Magnitude of Hydrofracturing Breakdown Pressure in Tablerock Sandstone, The 38th U.S. Symposium on Rock Mechanics, Washington D.C. A.A. Balkema Publishers, Lisse, The Netherlands, 235-242.

Song, I., Suh, M., Won, K.S. and Haimson, B., 2001, A Laboratory Study of Hydraulic Fracturing Breakdown Pressure in Table Rock Sandstone, Geosciences Journal, V.5 (3): 263-271.

Stein, S. and Wysession, M., 2003, An Introduction to Seismology, Earthquakes, and Earth Structure, Blackwell Publishing Ltd., Malden, MA, USA. 498pp

Surdi, A.A., Ekart, D.D., Duran, P. and Suarez-Rivera, R., 2010, Possible Sources of Acoustic Emission Events During Hydraulic Fracturing, ARMA Paper 10-478. 44th U.S. Rock Mechanics Symposium and 5th U.S.- Canada Rock Mechanics Symposium, Salt Lake City, Utah, June 27-30, 2010. 323-478.

Suzuki, T., Sasaki, K. and Hirota, T., 1964, A New Approach to the Prediction of Failure by Rock Noise, Proceedings Fourth International Conference on Strata Contro and Rock Mechanics, Columbia University, New York: 1-9.

Talebi, S. and Boone, T., 1998, Source parameters of injection-induced microseismicity, Pure Applied Geophysics, V153,:113-130.

Tam, M. T., and Weng, C. C. (1995). Acoustic-Emission Kaiser Effect in Fly-Ash Cement Mortarunder Compression. Journal of Materials in Civil Engineering, 7(4): 212-217.

Thomsen, L., 1986, Weak Elastic Anisotropy, Geophysics, V. 51 (10): 1954-1966.

Urbancic, T.I. and Maxwell, S.C., 2002, Source Parameters of Hydraulic Fracture Induced Microseismicity, SPE Paper 77439. Annual Technical Conference and Exhibition, 29 September-2 October 2002, San Antonio, Texas USA. 1444-1448.

Van Dam, D.B., de Pater, C.J. and Romijn, R., 1998, Analysis of Hydrualic Fracture Closure in Laboratory Experiments, Proceedings of the SPE/ISRM Rock Mechanics in Petroleum Engineering Conference, V. 2: 365-374.

Veatch Jr., R.W., 1983, Overview of Current Hydraulic Fracturing Design and Treatment Technology-Part 1, Journal of Petroleum Technology, V. 35 (4): 677-687.

Verdon, J., Kendall, J.M. and Maxwell, S.C., 2010, A Comparison of Passive Seismic Monitoring of Fracture Stimulation from Water and CO_2 Injection, Geophysics, V. 75 (3): MA1-MA7.

Vestrum, R.W., Lawton, D.C. and Schmid R., 1999, Imaging Structures Below Dipping TI Media, Geophysics, V. 64 (4): 1239-1246.

Vinegar, H.J., Wills, P.B. and Shlyapobersky, J., 1992, Active and Passive Seismic Imaging of a Hydraulic Fracture in a Diatomite, Journal of Petroleum Technology, V. 44 (1): 28-34.

Walker, R.N., Hunter, J.L., Brake, A.C., Fagin, P.A. and Steinsberger, N., 1998, Proppants, We Still don't Need no Proppants – A Perspective of Several Operators, SPE Paper 49106 Annual Technical Conference and Exhibition, 27-30, New Orleans, Louisiana USA.

Walper J.L.,1977, Paleozoic Tectonics of the Southern Margin of North America, Gulf Coast Association Geological Societies v. 27,. 230-241.

Walper, Jack L., 1982 Petroleum Geology of the Fort Worth Basin and Bend Arch Area, AAPG Conference. 237-251.

Walter, W.R. and Brune, J.N., 1993, Spectra of Seismic Radiation from a Tensile Crack, Journal of Geophysical Research, V. 98 (B3): 4449-4459.

Wang, Z., 2002, Seismic Anisotropy in Sedimentary Rocks, Part 2: Laboratory Data, Geophysics, V. 67 (5): 1423-1440.

Warembourg, P.A., Klingensmith, E.A., Flopetrol Johnston, Hodges Jr., J.E., Dowell ; Erdle, J.E., 1985 Fracture Stimulation Design and Evaluation. SPE Paper 14379. Society of Petroleum Engineers 22-25.

Warpinski, N.R., Uhl, J.E. and Engler, B.P., 1997, Review of Hydraulic Fracture Mapping Using Advanced Accelerometer-Based Receiver Systems, Sandia National Laboratories. V. 4: 242-250.

Warpinski, N.R., Branagan, P.T., Peterson, R.E., Wolhart, S.L. and Uhl, J.E., 1998, Mapping Hydraulic Fracture Growth and Geometry Using Microseismic Events Detected by Wireline Retrievable Accelerometer Array, SPE Paper 40014. Gas Technology Symposium, Calgary, Alberta, Canada. 579-589

Warpinski, N.R., 2000, Analytic Crack Solutions for Tilt Fields Around Hydraulic Fractures, Journal of Geophysical Research, V. 105 (23): 463–478.

Warpinski, N.R., Waltman, C.K., Du, J. and Ma, Q., 2009, Anisotropy Effects on Microseismic Mapping, Annual Technical Conference and Exhibition, New Orleans, Louisiana, USA. SPE Paper 124-208.

Warpinski, N.R., 1998 Development of Stimulation Diagnostic Technology, GRI Annual Report GRI-97/1327., 100pp.

Warpinski, N.R., and Pinnacle, J. Du., 2009 Source-Mechanism Studies on Microseismicity Induced by Hydraulic Fracturing SPE Paper 135254 Annual Technical Conference and Exhibition, Italy, 19-22.

Williams, S., 2009. Geological Microseismic Fracture Mapping – Methodologies for Improved Interpretations Based on Seismology and Geologic Context, 2009 Convention, CSPG CSEG SWLS, Expanded Abstracts, 501-504.

Wyss, M. and Brune, J.N., 1968, Seismic Moment, Stress and Source Dimensions for Earthquakes in the California-Nevada Region, Journal of Geophysical Research, V. 73 (14): 4681-4694.

Zoback, M.D., Rummel, F., Jung, R. and Raleigh, C.B., 1977, Laboratory Hydraulic Fracturing Experiments in Intact and Pre-Fractured Rock, International Journal of Rock Mechanics and Mining Sciences and Geomechanics Abstracts, V. 14 (2): 49-56.